MODELING AEROSOL – WATER INTERACTIONS IN SUBSATURATED AND SUPERSATURATED ENVIRONMENTS

A Dissertation
Presented to
The Academic Faculty

By

Christos Fountoukis

In Partial Fulfillment
Of the Requirements for the Degree
Doctor of Philosophy in the
School of Chemical and Biomolecular Engineering

Georgia Institute of Technology

August 2007

MODELING AEROSOL – WATER INTERACTIONS IN SUBSATURATED AND SUPERSATURATED ENVIRONMENTS

Approved by:

Dr. Athanasios Nenes, Advisor
School of Chemical & Biomolecular Engineering and Earth and Atmospheric Sciences
Georgia Institute of Technology

Dr. Rodney Weber
School of Earth and Atmospheric Sciences
Georgia Institute of Technology

Dr. Amyn Teja
School of Chemical & Biomolecular Engineering
Georgia Institute of Technology

Dr. Rong Fu
School of Earth and Atmospheric Sciences
Georgia Institute of Technology

Dr. Joseph Schork
School of Chemical & Biomolecular Engineering
Georgia Institute of Technology

Date Approved: June 04, 2007

“Look and you will find it – what is unsought will go undetected.”

Sophocles (495-406 B.C.)

To my parents, Yiannis and Katy,
and to Christina.

ACKNOWLEDGMENTS

First, I would like to thank my advisor, Thanos Nenes, for his expert guidance and most valuable support. He provided me with the opportunity to work on different and exciting projects. I would like to particularly thank him for being so understanding and supportive during my first year when I was juggling the demands of classes, research and adjusting to the United States. I was very fortunate to have such a wonderful person as an advisor.

I would like to thank my friend and colleague Nikolaos Pratikakis for all the fun we had from the first day we arrived together in the United States. I will never forget his extraordinary sense of humor. Likewise, I thank Kevin Doyle, a great friend and colleague whom I feel very lucky to have met. Many thanks to Charlene Rincon, Eduardo Vazquez and Paul Wissmann for their friendship, help, and support during all these years. I would also like to thank all the members of the Nenes group whom I enjoyed working with.

I would never make it without the constant support and love of my family. My parents, Yiannis and Katy, my brother Kostas, and my sister Evi were always there for me, even from thousands of kilometers away.

I would like to greatly thank Christina whose love and support was my major source of inspiration. This journey would never have been so successful without her.

Finally, I would like to thank the School of Chemical and Biomolecular Engineering of Georgia Institute of Technology for giving me the unique opportunity to pursue advanced graduate studies.

This research was supported by a NASA EOS-IDS, a NASA New Investigator Award, the National Science Foundation under award ATM-0340832, an NSF CAREER award, a Gerondelis Foundation Fellowship, the National Oceanic and Atmospheric Administration under contract NMRAC000-5-04017 and by Georgia Institute of Technology faculty startup funds.

TABLE OF CONTENTS

LIST OF TABLES

LIST OF FIGURES

LIST OF SYMBOLS AND ABBREVIATIONS

a_i	Activity of species *i*
CF	Completeness factor
c_p	Heat capacity of air
c	Weighting factor
D	*C*oncentration dissolved species
D_c	Critical Diameter
$D_{g,i}$	Geometric mean diameter of mode *i*
D_p	Particle diameter
$D_{p,big}$	Upper particle size bound
$D_{p,low}$	Lower particle size bound
$D_{p(\tau)}$	Size of a CCN when $s = s_c$
D_v	Diffusivity of water vapor in air
D_v'	Corrected diffusivity of water vapor in air
DRH	Deliquescence relative humidity
$F^s(s)$	CCN spectrum
G	Concentration of gaseous species
I	Ionic strength of the solution
K_j	Equilibrium constant of the *j*-th reaction
K_o	Equilibrium constant at T_o

k_a'	Thermal conductivity of air
L	Latent heat of condensation of water
L_s	Latent heat of fusion for the salt from a saturated solution
M_i	Molar concentration of species i
M_s	Solute molecular weight
M_w	Molecular weight of water
MDRH	Mutual deliquescence relative humidity
MDR	Mutual deliquescence region
m_i	Molality of cations
m_j	Molality of anions
$m_{oi}(a_w)$	Molality of an aqueous binary solution of the i-th electrolyte with the same a_w as in the multicomponent solution
m_s	Molality of the saturated solution at temperature T_o
N_{ap}	Total number of particles
N_d	Activated droplet number
N_i	Aerosol number concentration of mode i
NME	Normalized mean error
NMB	Normalized mean bias
$n^d(D_p)$	Size distribution
n_m	Number of modes in the distribution
$n^s(s)$	Supersaturation distribution
$PM_{2.5}$	Mass concentration of particulate matter with diameter less than 2.5 μm

p	Ambient pressure
p^s	Water vapor pressure
p_v^*	Saturation vapor pressure of water
$p(w)$	Vertical velocity probability density function
R	Universal gas constant
R_1	Sulfate ratio
R_2	Crustal and sodium ratio
R_3	Crustal ratio
R^2	Correlation coefficient
RH	Relative humidity
RH_{wet}	DRH of the salt with the lowest DRH in the mixture
S	Concentration of solid species
s	Supersaturation
s_c	Critical supersaturation
$s_{g,i}$	Critical supersaturation of particle with diameter $D_{g,i}$
s_{max}	Maximum parcel supersaturation
s_{part}	Partitioning critical supersaturation
T	Parcel temperature
T_0	reference temperature (typically at 298.15 K)
t_{max}	Time of maximum supersaturation
V	Cloud parcel updraft velocity
V_{ins}	Insoluble volume fraction

V_{sul}	Volume fraction of ammonium sulfate
V_{total}	Total aerosol volume
w_+	Average cloud updraft velocity (at cloud base)
W	Mass concentration of aerosol water
z_i	Absolute charge of ionic species *i*

Greek letters

A_γ	Debye-Hückel constant
a_c	Mass accommodation (or condensation) coefficient
γ_{ij}	Activity coefficient of an electrolyte species *ij* in water
γ_{ij}^o	Binary activity coefficient computed at the ionic strength of the multicomponent solution
γ_{12}	Mean activity coefficient of cation 1 and anion 2 at 298.15K
Δ	Descriminant
$\Delta c_P^o(T)$	Change of molar heat capacity of products minus reactants
$\Delta H^o(T)$	Enthalpy change of the reaction at temperature *T*
ΔH_{cr}	Molar enthalpy of formation of the crystalline phase
ΔH_{aq}	Molar enthalpy of the species in aqueous solution
Δx	% change of the mean predicted value of each species compared to the base case prediction
$\mu_i^o(T)$	Standard chemical potential of species *i* at 1 atm pressure
v	Effective Van't Hoff factor

ν_{ij}	Stoichiometric coefficient of species *i* participating in the reaction *j*
ν_I	moles of cations
ν_j	moles of anions
$\rho_{org.}$	Density of organics
ρ_s	Density of the solute
$\rho_{sul.}$	Density of ammonium sulfate
ρ_w	Density of water
σ	Droplet surface tension
σ_i	Geometric standard deviation of mode *i*
σ_+	Standard deviation of w_+
$\sigma_{(TD-LIF\ nitrate)}$	Uncertainty in the measurement of volatile nitrate
$\sigma_{(PILS\ nitrate)}$	Uncertainty in the measurement of aerosol nitrate
$\sigma_{HNO_{3(g)}}$	Uncertainty in the measurement of gas-phase nitrate
τ	Time needed for activation
ψ_w	Standard deviation for a Gaussian probability density function

SUMMARY

The current dissertation is motivated by the need for an improved understanding of aerosol – water interactions both in subsaturated and supersaturated atmospheric conditions with a strong emphasis on air pollution and climate change modeling. A cloud droplet formation parameterization was developed to *i)* predict droplet formation from a lognormal representation of aerosol size distribution and composition, and, *ii)* include a size-dependant mass transfer coefficient for the growth of water droplets which explicitly accounts for the impact of organics on droplet growth kinetics. The parameterization unravels most of the physics of droplet formation and is in remarkable agreement with detailed numerical parcel model simulations, even for low values of the accommodation coefficient. The parameterization offers a much needed rigorous and computationally inexpensive framework for directly linking complex chemical effects on aerosol activation in global climate models.

The new aerosol activation parameterization was also tested against observations from highly polluted clouds (within the vicinity of power plant plumes). Remarkable closure was achieved (much less than the 20% measurement uncertainty). The error in predicted cloud droplet concentration was mostly sensitive to updraft velocity. Optimal closure is obtained if the water vapor uptake coefficient is equal to 0.06. These findings can serve as much needed constraints in modeling of aerosol-cloud interactions in the North America.

Aerosol – water interactions in ambient relative humidities less than 100% were studied using a thermodynamic equilibrium model for inorganic aerosol and a three dimensional

air quality model. We developed a new thermodynamic equilibrium model, ISORROPIA-II, which predicts the partitioning of semi-volatiles and the phase state of $K^+/Ca^{2+}/Mg^{2+}/NH_4^+/Na^+/SO_4^{2-}/NO_3^-/Cl^-/H_2O$ aerosols. A comprehensive evaluation of its performance was conducted against the thermodynamic module SCAPE2 over a wide range of atmospherically relevant conditions. Based on its computational rigor and performance, ISORROPIA-II appears to be a highly attractive alternative for use in large scale air quality and atmospheric transport models.

The new equilibrium model was also used to thermodynamically characterize aerosols measured at a highly polluted area. In the ammonia-rich environment of Mexico City, nitrate and chloride primarily partition in the aerosol phase with a 20-min equilibrium timescale; $PM_{2.5}$ is insensitive to changes in ammonia but is to acidic semivolatile species. When RH is below 50%, predictions improve substantially if the aerosol follows a deliquescent behavior.

The impact of including crustal species (Ca^{2+}, K^+, M^{2+}) in equilibrium calculations within a three dimensional air quality model was also studied. A significant change in aerosol water (-19.8%) and ammonium (-27.5%) concentrations was predicted when crustals are explicitly included in the calculations even though they contributed, on average, only a few percent of the total $PM_{2.5}$ mass, highlighting the need for comprehensive thermodynamic calculations in the presence of dust.

CHAPTER 1

PREFACE

1.1 Introduction

Anthropogenic airborne particles (aerosols) have increased over the past century, and are believed to play a central role in processes responsible for the deleterious effects on the environment and society, such as visibility (Altshuller, 1984), health degradation in polluted areas (e.g. Ramachandran and Vincent, 1999; Zanobetti *et al.*, 2000; Brauer and Brook, 1997), acid rain and climate change (IPCC, 2001). Therefore, interactions of aerosols with water are very important and need to be well understood both for subsaturated (where ambient relative humidity, RH, is below 100%) and supersaturated atmospheric conditions (RH > 100%).

1.2 Aerosols and air quality

A large part of the particle mass is inorganic. They are also composed of water, insoluble materials (dust, crustal material), organics (soot, VOC) and trace metals. The size of these particles cover a broad range, and the compositions and mechanism that generate them differ for each size section. Knowledge of the physical state and composition of atmospheric aerosols is of great importance. Within aerosols, the inorganic components may be in the form of aqueous ions (NH_4^+, SO_4^{-2}, NO_3^-, etc.), or in the form of precipitated solids (ammonium nitrate, $NH_4NO_{3(s)}$, ammonium sulfate, $(NH_4)_2SO_{4(s)}$,

letovicite $(NH_4)_3(SO_4)_{2(s)}$, etc.) and may be in equilibrium with atmospheric gases (HCL, HNO_3, NH_3). Inorganic salts comprise 25 – 50% of dry total fine aerosol mass (Heintzenberg, 1989) and together with water comprise a significant portion of the total aerosol mass, especially in high relative humidity environments. The equilibrium partitioning between these condensed and gas – phases is complex, requiring consideration of both physical and thermodynamic processes. Thermodynamic equilibrium calculations are required in every aerosol model because mass transport of volatile species (e.g. water) between gas and aerosol phases is driven from the difference between ambient and equilibrium concentrations. Thus, a thermodynamic equilibrium module is an essential component of any aerosol model and to a large extent determines the characteristics and efficiency of it.

1.3 Aerosols and climate change

At steady state, the Earth's energy balance requires that the flux of incoming energy from the sun, most of which is in the visible part of the spectrum, must be balanced by an equal outgoing flux of infrared radiation. Any deviation on either side of this balance, incoming or outgoing, drives the earth's climate to a new warmer or cooler equilibrium state so that the requirement for energy balance will again be satisfied. Greenhouse gases intercept some of the outgoing longwave radiation and thereby act to force the earth's surface to come to a higher equilibrium temperature. In contrast to greenhouse gases, which interact with infrared radiation, aerosols can influence both sides of the energy balance. They reflect a significant amount of radiation back to space, thus enhancing the planetary albedo (also known as the aerosol "direct" radiative effect). By acting as cloud

condensation nuclei (CCN), they also have a strong impact on cloud optical properties, the latter of which play a profound role on climate. For a given Liquid Water Content (LWC), an increase in the number concentration of aerosol particles, which results in an increase of CCN, will lead to larger droplet concentrations; this means the cloud will have droplets with smaller effective radius, thus increasing the cloud shortwave reflectivity (also known as the "1_{st} aerosol indirect radiative effect"), (*Twomey*, 1977; *Charlson et al*., 2001). The decrease in droplet size also may decrease the precipitation efficiency of clouds, thus producing longer-lived clouds (this is known as the "2_{nd} aerosol indirect radiative effect"), (*Albrecht*, 1989; *Rosenfeld*, 2000). Figure 1.1 represents the first and second aerosol indirect effect showing two clouds with similar LWC under clean and polluted aerosol conditions.

Figure 1.2 shows global-average radiative forcing estimates and ranges in 2005 for anthropogenic carbon dioxide (CO_2), methane (CH_4), nitrous oxide (N_2O) and other important agents and mechanisms, as well as the net anthropogenic radiative forcing and its range. Estimates show that tropospheric aerosols have a total global cooling effect of -1.2 W m^{-2} with a large uncertainty ranging from -0.4 to -2.7 W m^{-2}. This highlights the strong need for a better understanding of the indirect climatic effect of aerosols. What is necessary is a better understanding of the relation between changes in atmospheric aerosol properties and changes in cloud radiative properties. Key parameters affecting this relation are aerosol and cloud droplet properties such as size, number, composition, and liquid water content.

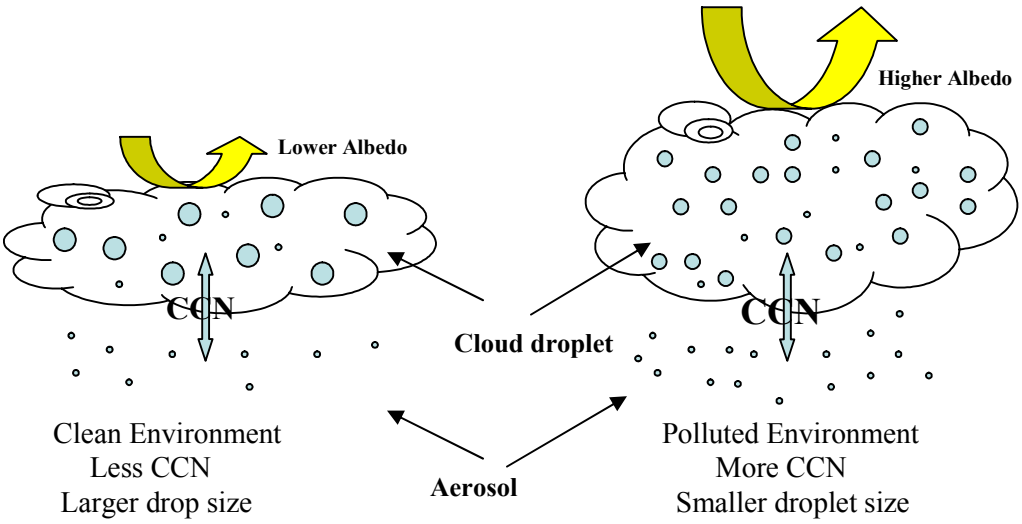

Figure 1.1: “First” and “Second” aerosol indirect radiative effects.

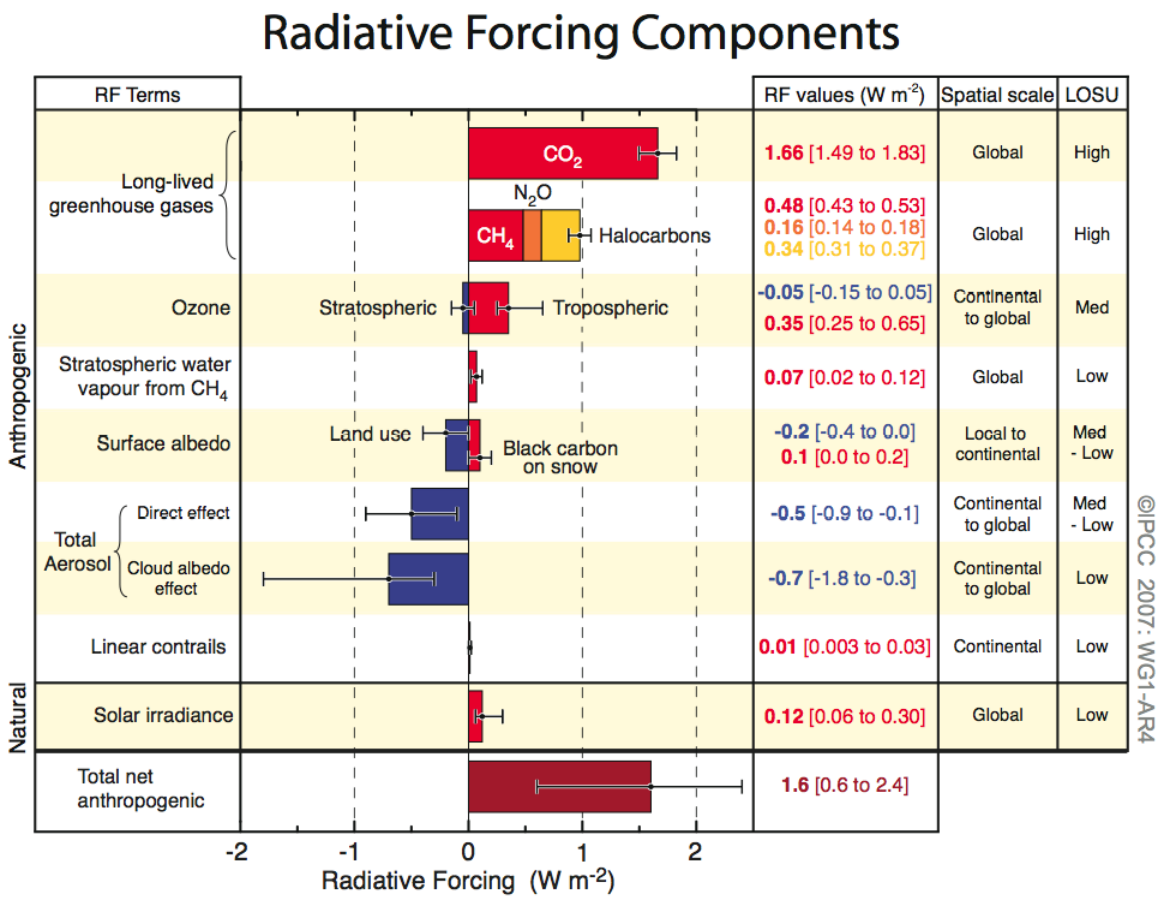

Figure 1.2: Global-average radiative forcing estimates and ranges in 2005 for anthropogenic carbon dioxide (CO_2), methane (CH_4), nitrous oxide (N_2O) and other important agents and mechanisms, together with the typical geographical extent (spatial scale) of the forcing and the assessed level of scientific understanding. The net anthropogenic radiative forcing and its range are also shown.

1.4 References

Altshüller, A.P.: Atmospheric particle sulfur and sulfur dioxide relationships at urban and nonurban locations, Atmos. Environ., 18, 1421 - 1431, 1984.

Brauer, M., and Brook, J.R.: Ozone personal exposures and health effects for selected groups residing in the Fraser Valley, Atmos. Environ., 31, 2113 - 2122, 1997.

Ramachandran, G., and Vincent, J.H.: A Bayesian approach to retrospective exposure assessment, Applied Occupational and Environmental Hygiene, 14, 547 - 558, 1999.

Zanobetti, A., Schwartz, J., and Dockery, D.W.: Airborne particles are a risk factor for hospital admissions for heart and lung disease, Environmental Health Perspective, 108, 1071 - 1082, 2000.

Intergovernmental Panel on Climate Change: The scientific Basis, Cambridge Univ. Press, New York, 2001.

.

CHAPTER 2

A CLOUD DROPLET FORMATION PARAMETERIZATION FOR GLOBAL CLIMATE MODELS[I]

2.1 Abstract

This study presents continued development of the Nenes and Seinfeld (2003) cloud droplet activation parameterization. First, we expanded the formulation to *i)* allow for a lognormal representation of aerosol size distribution, and, *ii)* include a size-dependant mass transfer coefficient for the growth of water droplets to accommodate the effect of size (and potentially organic films) on the droplet growth rate. The performance of the new scheme is evaluated by comparing the parameterized cloud droplet number concentration with that of a detailed numerical activation cloud parcel model. The resulting modified parameterization robustly and closely tracks the parcel model simulations, even for low values of the accommodation coefficient (average error 4.1±1.3%). The modifications to include the effect of accommodation coefficient do not increase the computational cost but substantially improves the parameterization performance. This work offers a robust, computationally efficient and first-principles approach for directly linking complex chemical effects (e.g., surface tension depression, changes in water vapor accommodation, solute contribution from partial solubility) on aerosol activation within a global climate modeling framework.

[I] Appeared in publication: Fountoukis, C., and A. Nenes, Continued development of a cloud droplet formation parameterization for global climate models, J. Geophys. Res., 110, D11212, doi:10.1029/2004JD005591, 2005.

2.2 Introduction

Of the most uncertain of anthropogenic climate forcings is the effect of aerosols on clouds (IPCC, 2001). Calculation of cloud properties from precursor aerosol in general circulation models (GCMs) has often relied on empirical (phenomenological) correlations (e.g. Boucher and Lohmann, 1995; Gultepe and Isaac, 1996), which are subject to significant uncertainty. To address this limitation, first-principle approaches (e.g., Ghan *et al*., 1997; Lohmann *et al*., 1999) have been proposed, which require setting up a cloud droplet number balance in each GCM grid cell; processes such as the activation of aerosol into cloud droplets, evaporation and collision/coalescence affect droplet number concentration. Explicitly resolving each of these processes is far beyond anything computationally feasible for GCMs, so, a prognostic GCM estimate of the aerosol indirect effect must rely on parameterizations of aerosol-cloud interactions.

The chemical complexity and heterogeneity of global aerosol can have an important effect on activation and must be included in aerosol-cloud interaction studies (e.g., Nenes *et al*., 2001; Rissman *et al*., 2002; Lance *et al*., 2004). Incorporating such complexity into extant parameterizations is not a trivial task. For example, the presence of surface active species may facilitate the activation of cloud condensation nuclei (CCN) into cloud droplets (Facchini *et al*., 1999). The influence of surfactants depends on their concentration (e.g., Shulman *et al*., 1996; Charlson *et al*., 2001) which varies considerably with CCN dry size (e.g., Charlson *et al*., 2001; Rissman *et al.*, 2004). Because of this, an explicit relationship between the critical supersaturation, s_c (the supersaturation required to activate a CCN into cloud droplet) and the critical diameter,

D_c is not possible (Li *et al*., 1998; Rissman *et al*., 2004), and becomes challenging to incorporate into mechanistic parameterizations (Rissman *et al*., 2004). Furthermore, the droplet growth rate may be influenced by the presence of organic films (Feingold and Chuang, 2002; Chuang, 2003; Nenes *et al*., 2002; Medina and Nenes, 2004; Lance *et al.*, 2004) and slightly soluble substances (Shantz *et al.*, 2003; Shulman *et al.,* 1996) both of which could have an impact on cloud droplet number (Nenes *et al.*, 2002).

One of the most comprehensive parameterizations developed to date is by Nenes and Seinfeld (2003) (hereafter referred to as "NS"). NS can treat internally or externally mixed aerosol with size-varying composition and can include the depression of surface tension from the presence of surfactants, insoluble species and slightly soluble species within a framework in which minimal amount of empirical information is used (e.g., of all 200 cases tested by NS, only 20% required a correlation derived from a numerical parcel model). Despite the significant improvement in droplet number prediction compared to other parameterizations, NS may underestimate the droplet number concentration, and cannot, as most other mechanistic parameterizations, explicitly consider the potential delays in droplet growth from the presence of film forming compounds. Furthermore, NS employs a sectional representation of aerosol size, which may impose an unnecessary computational burden for global climate models using lognormal aerosol size distributions. These shortcomings are addressed in this study.

The research presented here extends the NS parameterization by i) providing a formulation of the parameterization for a lognormal description of the aerosol size distribution, and, ii) including explicit size-dependence of water vapor diffusivity. The latter overcomes the underprediction tendency of the original formulation, and, allows to

explicitly include the effect of organics that may affect the condensational growth of CCN.

2.3 The NS Parameterization

NS is based on a generalized sectional representation of aerosol size and composition (internally or externally mixed), with size-varying composition. The NS methodology involves two steps: The first involves calculation of CCN concentration as a function of supersaturation (the "CCN spectrum") using the appropriate form of Köhler theory (e.g., Seinfeld and Pandis, 1998). In the second step, the CCN spectrum is included within the dynamical framework of an adiabatic parcel with a constant updraft velocity (or cooling rate), to compute the maximum supersaturation, s_{max}, achieved during the cloud parcel ascent. Calculation of s_{max} is based on a balance between water vapor availability from cooling and water vapor depletion from the condensational growth of the CCN. CCN with $s_c \leq s_{max}$ will then be activated into droplets.

NS introduce the concept of "population splitting" to obtain an analytical expression for the water vapor condensation rate; an integro-differential equation is reduced to an algebraic equation which can be numerically solved. Population splitting entails division of the CCN into two separate populations: those which have a size close to their critical diameter (the diameter a CCN must grow to before experiencing unstable growth), and those that do not. As a result of this approach, kinetic limitations on droplet growth are explicitly considered, and, (compared with other mechanistic parameterizations), the reliance on empirical information or correlations is significantly reduced. A comparison of NS with extant parameterizations is done in Nenes and Seinfeld (2003) and will not be

repeated here.

2.4 NS Formulation for Lognormal Aerosol

The sectional representation of aerosol size and composition gives the most general description of aerosol size distribution. However, if such a representation is not available in a host model, it may be unnecessarily costly to implement. Instead, a formulation using a lognormal description of the aerosol may be preferred and is derived here.

2.4.1 Representation of the CCN Spectrum

Using the nomenclature of Nenes and Seinfeld (2003), size distributions, $n^d(D_p)$, are taken to be of the single or multiple lognormal form,

$$n^d(D_p) = \frac{dN}{d\ln D_p} = \sum_{i=1}^{n_m} \frac{N_i}{\sqrt{2\pi}\ln\sigma_i} \exp\left[-\frac{\ln^2(D_p/D_{g,i})}{2\ln^2\sigma_i}\right] \tag{2.1}$$

where D_p is particle diameter, N_i is the aerosol number concentration, $D_{g,i}$ is the geometric mean diameter of mode i, σ_i is the geometric standard deviation for mode i, and n_m is the number of modes in the distribution.

If the chemical composition of an aerosol mode does not vary with size, then $n^d(D_p)$ can be mapped to supersaturation space and the critical supersaturation distribution, $n^s(s)$, can be obtained as follows:

$$n^s(s) = \frac{dN}{ds} = -\frac{dN}{d\ln D_p} \cdot \frac{d\ln D_p}{ds} \tag{2.2}$$

where

$$\frac{dN}{d\ln D_p} = \sum_{i=1}^{n_m} \frac{N_i}{\sqrt{2\pi}\ln\sigma_i} \exp\left[-\frac{\ln^2(D_p / D_{g,i})}{2\ln^2\sigma_i}\right] \tag{2.3}$$

The critical supersaturation of a particle with diameter D_p is

$$s = \frac{2}{\sqrt{B}} \cdot \left(\frac{A}{3D_p}\right)^{3/2} \tag{2.4}$$

where $A = \frac{4\sigma M_w}{\rho_w}$ and $B = \frac{\nu\rho_s M_w}{\rho_w M_s}$ (Seinfeld and Pandis, 1998), ρ_s is the solute density, M_s the solute molecular weight, ν is the number of ions resulting from the dissociation of one solute molecule. From Eq. (2.4) we obtain,

$$\frac{d\ln D_p}{ds} = -\frac{2}{3s} \tag{2.5}$$

and

$$\frac{D_p}{D_g} = \left(\frac{s_g}{s}\right)^{2/3} \tag{2.6}$$

Substitution of Eq.s (2.1), (2.3), (2.5) and (2.6) into (2.2) yields the critical supersaturation distribution,

$$n^s(s) = \sum_{i=1}^{n_m} \frac{2N_i}{3s\sqrt{2\pi}\ln\sigma_i} \exp\left[-\frac{\ln^2(s_{g,i}/s)^{2/3}}{2\ln^2\sigma_i}\right] \tag{2.7}$$

where $s_{g,i}$ is the critical supersaturation of a particle with diameter $D_{g,i}$.

From Eq. (2.7), the CCN spectrum (concentration of particles with $s_c \le s$), $F^s(s)$, is given by

$$F^s(s) = \int_0^s n^s(s)ds = \sum_{i=1}^{n_m} \frac{N_i}{2} erfc\left[\frac{2\ln(s_{g,i}/s)}{3\sqrt{2}\ln\sigma_i}\right] \tag{2.8}$$

If the maximum parcel supersaturation, s_{max}, is known, the activated droplet number, N_d,

can be calculated from Eq. (2.8), as

$$N_d = F^s(s_{\max}) \tag{2.9}$$

2.4.2 Calculating s_{max} and Droplet Number Concentration

The maximum supersaturation, s_{max}, is calculated from an Eq. that expresses the water vapor balance (Nenes and Seinfeld, 2003):

$$\frac{2aV}{\pi\gamma\rho_w} - Gs_{\max} I(0, s_{\max}) = 0 \tag{2.10}$$

where,

$$a = \frac{gM_w L}{c_p RT^2} - \frac{gM_a}{RT}, \qquad \gamma = \frac{pM_a}{p^s M_w} + \frac{M_w L^2}{c_p RT^2} \tag{2.11}$$

and V is the cloud parcel updraft velocity, ρ_w is the density of water, T is the parcel temperature, M_w is the molecular weight of water, L is the latent heat of condensation of water, p^s is the water vapor pressure, c_p is the heat capacity of air, p is the ambient pressure and R is the universal gas constant. G in Eq. (2.10) is given by

$$G = \frac{1}{\dfrac{\rho_w RT}{p_v^* D_v' M_w} + \dfrac{L\rho_w[(LM_w/RT)-1]}{k_a' T}} \tag{2.12}$$

where p_v^* is the saturation vapor pressure of water, D_v' is the diffusivity of water vapor in air and k_a' is the thermal conductivity of air.

The quantity $I(0,s_{max})$ in Eq. (2.10) is defined as,

$$I(0, s_{\max}) = \int_0^{S_{\max}} [D_p^2(\tau) + \frac{G}{aV}(s_{\max}^2 - s(\tau)^2)]^{1/2} n(s) ds \tag{2.13}$$

$D_p(\tau)$ denotes the size of a CCN when it is exposed to $s = s_c$; τ is the time needed (above

cloud base) to develop the supersaturation needed for its activation. A common assumption (e.g., used by *Ghan et al*., 1993) is that CCN instantaneously activate, i.e., $D_p(\tau)$ is equal to the CCN critical diameter, $D_c=8M_w\sigma/3RT\rho_w s$, (where σ is the droplet surface tension at the point of activation). Evaluation of $I(0,s_{max})$ and substitution into Eq. (2.10) results in an algebraic equation that can be solved for s_{max}.

2.4.3 Calculation of Integral $I(0,s_{max})$

We can approximate $I(0,s_{max})$ by employing the "population splitting" concept of NS:

$$I(0,s_{\max}) = I_1(0,s_{part}) + I_2(s_{part},s_{\max}) \tag{2.14}$$

where s_{part} is the "partitioning critical supersaturation" (Nenes and Seinfeld, 2003), that defines the boundary between the CCN populations. In Eq. (2.14), $I_1(0,s_{part})$ represents the growth of CCN for which $D_p^2(\tau) << 2G\int_{\tau}^{t_{\max}} s\,dt$, or those that experience significant growth beyond the point where they are exposed to $s > s_c$. $I_2(s_{part},s_{max})$ expresses the growth of CCN that do not strictly activate, or do not experience significant growth beyond their critical diameter for which we assume $D_p^2(\tau) >> 2G\int_{\tau}^{t_{\max}} s\,dt$. With these simplifications, $I_1(0, s_{part})$ and $I_2(s_{part}, s_{max})$ (using Eq. 2.8) become,

$$I_1(0,s_{part}) = \int_0^{S_{part}} \left(\frac{G}{aV}\right)^{1/2} \left(s_{\max}^2 - s^2\right)^{1/2} \frac{2N_i}{3s\sqrt{2\pi}\ln\sigma_i} \exp\left\{\frac{-\ln^2\left[\left(s_{g,i}/s\right)^{2/3}\right]}{2\ln^2\sigma_i}\right\} ds \tag{2.15}$$

$$I_2(s_{part},s_{\max}) = \int_{S_{part}}^{S_{\max}} \frac{2A}{3s}\frac{2N_i}{3s\sqrt{2\pi}\ln\sigma_i} \exp\left\{\frac{-\ln^2\left[\left(s_{g,i}/s\right)^{2/3}\right]}{2\ln^2\sigma_i}\right\} ds \tag{2.16}$$

where $s_{g,i}$ is given by

$$s_{g,i} = \sqrt{\frac{4A^3 \rho_w M_s}{27 \nu \rho_s M_w D_{p,g}^3}} \tag{2.17}$$

M_s is the solute molecular weight, ν is the effective Van't Hoff factor and ρ_s is the density of the solute and $A=4M_w\sigma/RT\rho_w$. Eq. (2.17) assumes that the CCN are completely soluble; appropriate modifications should be used if the CCN contain a slightly soluble (Laaksonen *et al*., 1998), insoluble (e.g., Seinfeld and Pandis, 1998) or surfactant fraction (Rissman *et al*., 2004).

The integration of Eq.s (2.15) and (2.16) can be done with the help of the transformation coefficient $u = \dfrac{\ln\left(s_{g,i}/s\right)^2}{3\sqrt{2}\ln\sigma_i}$, and by approximating $\left(1-\dfrac{s_{g,i}}{s_{\max}}\right)^{1/2}$ in Eq. (2.15) with $1-\dfrac{1}{2}\dfrac{s_{g,i}}{s_{\max}}$,

$$I_1(0,s_{part}) = \frac{N_i}{2}\left(\frac{G}{aV}\right)^{1/2} s_{\max}\left\{erfc\left(u_{part}\right) - \frac{1}{2}\left(\frac{s_{g,i}}{s_{\max}}\right)^2 \exp\left(\frac{9\ln^2\sigma_i}{2}\right)\cdot erfc\left(u_{part}+\frac{3\ln\sigma_i}{\sqrt{2}}\right)\right\} \tag{2.18}$$

$$I_2(s_{part},s_{\max}) = \frac{AN_i}{3s_{g,i}}\exp\left(\frac{9\ln^2\sigma_i}{8}\right)\left[erf\left(u_{part}-\frac{3\ln\sigma_i}{2\sqrt{2}}\right) - erf\left(u_{\max}-\frac{3\ln\sigma_i}{2\sqrt{2}}\right)\right] \tag{2.19}$$

where

$$u_{part} = \frac{\ln\left(s_{g,i}/s_{part}\right)^2}{3\sqrt{2}\ln\sigma_i}\ , \quad u_{\max} = \frac{\ln\left(s_{g,i}/s_{\max}\right)^2}{3\sqrt{2}\ln\sigma_i} \tag{2.20}$$

It should be noted that the integrals in Eqs (2.18) through (2.20) bears some similarity with the formulations of Abdul-Razzak *et al.* (1998); this similarity arises from the usage of lognormal distributions. However, our formulations are distinctly different, as, *i*) they arise from the application of population splitting and thus use the integrals in a distinct manner, and, *ii*) lack the post-integration modifications applied by Abdul-Razzak *et al.*

(1998).

2.4.4 Using the Parameterization

The procedure for using the modal formulation is similar to the sectional aerosol formulation (Nenes and Seinfeld, 2003). Figure 2.1 displays the solution algorithm for the lognormal aerosol formulation. s_{part} is calculated using the "descriminant criterion", or the sign of the quantity $\Delta = \left(s_{\max}^4 - \frac{16A^2\alpha V}{9G} \right)$. Δ expresses the extent of kinetic limitations throughout the droplet population; $\Delta = 0$ marks a boundary between two droplet growth regimes, one where most CCN are free from kinetic limitations $(\Delta > 0)$ and one in which kinetic limitations are dominant $(\Delta < 0)$. When $\Delta > 0$, s_{part} is given by an analytical expression as $s_{part} = s_{\max} \left\{ \frac{1}{2} \left[1 + \left(1 - \frac{16A^2 aV}{9Gs_{\max}^4} \right)^{1/2} \right] \right\}^{1/2}$; when $\Delta < 0$, s_{part} is determined by an empirical correlation, $s_{part} = s_{\max} \min \left\{ \frac{2 \cdot 10^7 A}{3} s_{\max}^{-0.3824}, 1.0 \right\}$. After determining s_{part}, Eqs (2.18) and (2.19) are substituted into Eq. (2.10), and solved for s_{max} using the bisection method. The number of droplets is computed from Eq. (2.9). An evaluation of the modal formulation is provided in section 2.6.

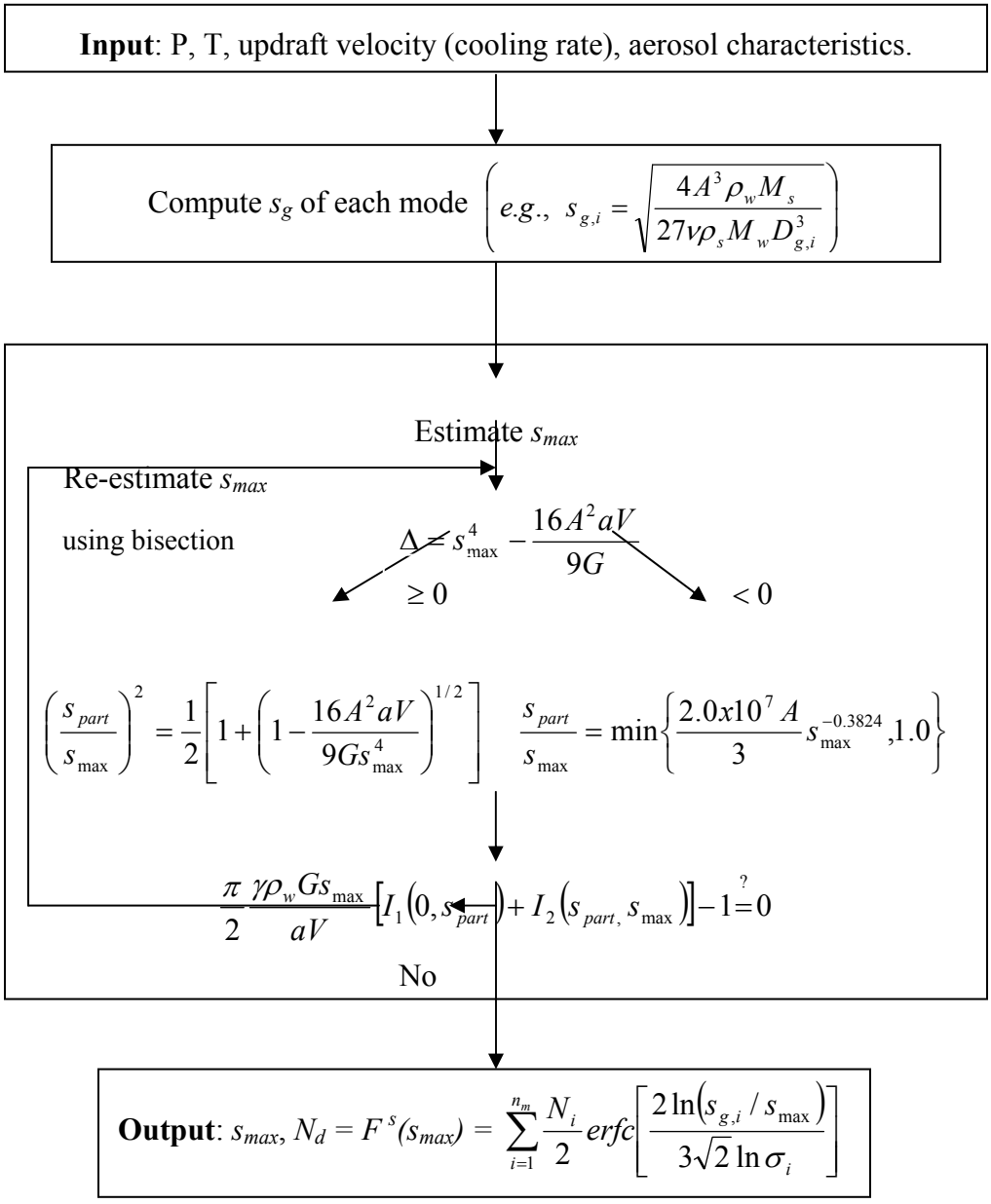

Figure 2.1: Parameterization algorithm (lognormal formulation)

2.5 Including Size-Dependant Growth Kinetics into NS

In developing the sectional and modal formulations of NS, we have assumed that the diffusivity of water vapor onto the droplets, $D_v^{'}$, is independent of their size. Although a good approximation for water droplets larger than 10μm (Seinfeld and Pandis, 1998), it substantially decreases for smaller and potentially multicomponent drops (Seinfeld and Pandis, 1998). As a result, water vapor condensation in the initial stages of cloud formation is overestimated and the stronger competition for water vapor biases the parcel supersaturation low. This results in an underestimation of cloud droplet concentration, which worsens if the presence of film-forming compounds further impedes the growth rate. It is important to note that other mechanistic parameterizations (e.g., Ghan *et al*., 1993; Abdul-Razzak *et al*., 1998; Rissman *et al*., 2004) also neglect size-dependence of the diffusivity coefficient and also tend to underestimate N_d (Nenes and Seinfeld, 2003). Size effects on water vapor diffusivity can be introduced by the following relationship (Fukuta and Walter, 1970),

$$D_v^{'} = \frac{D_v}{1 + \frac{2D_v}{a_c D_p}\sqrt{\frac{2\pi M_w}{RT}}} \tag{2.21}$$

where a_c is the accommodation coefficient, a fundamental parameter that expresses the probability of a water vapor molecule remaining in the droplet phase upon collision (Seinfeld and Pandis, 1998),

$$a_c = \frac{\text{number of molecules entering the liquid phase}}{\text{number of molecular collisions with the droplet surface}}$$

For pure water, a_c ranges between 0.1 and 0.3 (Li *et al.,* 2001) but an aged atmospheric droplet tends to have a lower accommodation coefficient, typically between 0.04 and

0.06 (Pruppacher and Klett, 2000; Shaw and Lamb, 1999; Conant *et al.*, 2004). The presence of organic films can further decrease the accommodation coefficient; although still controversial, there are indications that such compounds exist in the atmosphere (e.g., Chuang, 2003).

For typical droplet sizes, D_v' depends strongly on a_c (Eq. 2.21). For a value of a_c close to unity, the difference between D_v' and D_v is less than 25% for particles larger than 1 μm and less than 5% for droplet diameters larger than 5μm. However, D_v' becomes significantly lower than D_v if $a_c<1$ (Seinfeld and Pandis, 1998). Therefore, introducing the dependence of D_v' on size and a_c is important to eliminate biases in droplet activation. The thermal conductivity of air, k_a' (Eq. 2.12), also has a dependence on size, which is rather weak for the droplet sizes of interest. Simulations (not shown here) confirm that introducing a size-dependant thermal conductivity is not necessary.

2.5.1 Implementing Size-Dependant D_v into NS

Eq. (2.21) could be substituted into Eq. (2.12) in order to account for the size-dependence on D_v'. However, in such a case, Eq. (2.13) becomes impractical in its implementation. An alternate approach is needed.

Two approaches can be used to introduce corrections to D_v: i) using an average value for the diffusivity, $D_{v,ave}$, for those CCN that activate, and, ii) calculating D_v' for each CCN section. We choose to adopt the first approach because it can be used in both sectional and modal formulations of the NS parameterization (while the second approach cannot), and, the second approach adds upon the computational burden. For simplicity, we adopt a size-averaged diffusion coefficient, $D_{v,ave}$,

$$D_{v,ave} = \frac{\int_{D_{p,low}}^{D_{p,big}} D_v' dD_p}{\int_{D_{p,low}}^{D_{p,big}} dD_p} \tag{2.22}$$

where $D_{p,big}$ and $D_{p,low}$ are the upper and lower size bounds used for calculating the average. Substituting Eq. (2.21) into (2.22) and integrating yields:

$$D_{v,ave} = \frac{D_v}{D_{p,big} - D_{p,low}} \left[\left(D_{p,big} - D_{p,low} \right) - B \cdot \ln\left(\frac{D_{p,big} + B}{D_{p,low} + B} \right) \right] \tag{2.23}$$

where $B = \frac{2D_v}{a_c} \cdot \left(\frac{2\pi M_w}{RT} \right)^{1/2}$. In deriving Eq. (2.23), we assume that a_c remains constant throughout the activation process.

If $D_{p,big}$ and $D_{p,low}$ and a_c are known, Eq. (2.23) can be used to calculate $D_{v,ave}$, and substituted into the G term (Eq. 2.13) of NS. a_c is usually constrained from observations (e.g., Chuang *et al.,* 2003; Conant *et al.*, 2004). What remains is the determination of the $D_{p,big}$ and $D_{p,low}$.

Table 2.1: Simulations considered for empirically determining $D_{p,big}$ and $D_{p,low}$ of $D_{v,ave}$

Property	**Value / Range**
Cloud height (m)	500
N_i (cm^{-3})	100, 500, 1000, 5000, 10000
σ_i	1.1, 1.2, 1.5, 1.5, 2.0, 2.5
$D_{p,g}$ (μm)	0.025, 0.05, 0.75, 0.5, 0.25
V (ms^{-1})	0.1, 0.3, 1.0, 3.0
Chemical composition	$(NH_4)_2SO_4$:100%, $(NH_4)_2SO_4$:50% - insoluble:50%, NaCl:100%, NaCl:25% - insoluble:75%
Accommodation coefficient	0.001, 0.005, 0.042, 0.01, 0.1, 1.0
Pressure (mbar)	100, 500, 800, 1000
Relative humidity	90%, 98%
Temperature (K)	273, 293, 303, 310

2.5.2 Determination of $D_{p,big}$ and $D_{p,low}$

We have evaluated two methods for calculating $D_{p,big}$ and $D_{p,low}$:

Empirical determination of $D_{p,big}$ and $D_{p,low}$.

A set of numerical parcel model simulations were used to determine $D_{p,big}$ and $D_{p,low}$ that, after substitution into Eq. (2.23) (and subsequently into NS), would give a parameterized N_d in agreement with the numerical parcel predictions. Published literature suggests values for a_c as low as 10^{-5} (e.g., Chuang, 2003) during the initial stages of particle growth; if true, such CCN would experience a "slow growth" phase (with a very low a_c) followed by a "fast growth" phase with much higher a_c.

Simulations with the Nenes *et al.* (1998) parcel model (not shown) suggests that CCN with a constant $a_c \sim 10^{-3}$ experiences roughly the same growth as a "film-breaking" CCN with a slow-growth phase $a_c \sim 10^{-5}$ and a rapid-growth phase $a_c \sim 0.042$. Therefore, a_c is assumed to vary between 0.001 and 1.0.

$D_{p,big}$ and $D_{p,low}$ were determined for the wide set of conditions and a_c listed in Table 2.1.

Optimization criteria were the minimization of error and standard deviation between parameterized and parcel model N_d. The optimum $D_{p,big}$ was found to be 5 μm, while the optimum $D_{p,low}$ was found to vary with a_c; a correlation that relates the optimum $D_{p,low}$ and a_c was then derived,

$$D_{p,low} = \min\left\{0.207683 \cdot a_c^{-0.33048}, 5.0\right\} \tag{2.24}$$

where $D_{p,low}$ is given in μm.

From Eq. (2.24), a_c increases with decreasing $D_{p,low}$. This is expected; for large a_c, small

CCN experience less kinetic limitations, and therefore can activate into droplets (Nenes *et al.*, 2001). As a result, a wider range of CCN sizes need to be considered in the calculation of $D_{v,ave}$, so $D_{p,low}$ should decrease. When a_c decreases, only the largest of CCN (with low s_c) have enough time to activate; hence a narrow range of CCN sizes can contribute to droplet number concentration, thus increasing $D_{p,low}$.

Theoretical determination of $D_{p,big}$ and $D_{p,low}$.

$D_{p,big}$ and $D_{p,low}$ may also be determined using theoretical arguments. One can be derived from the Eq. that describes the diffusional growth of a droplet from time τ (when the parcel supersaturation is equal to the CCN critical supersaturation, s_c), to the time of maximum supersaturation, t_{max} (Nenes and Seinfeld, 2003),

$$D_p^2 = D_p^2(\tau) + 2\int_{\tau}^{t_{\max}} G\, s\, dt \tag{2.25}$$

$D_p(\tau)$, like in Eq. (2.13), is assumed to be equal to the critical diameter $D_c=8M_w\sigma/3RT\rho_w s_c$, while the supersaturation integral in Eq. (2.25) can be evaluated using the lower bound of Twomey (1959):

$$\int_{\tau}^{t_{\max}} s\, dt \approx \frac{1}{2aV}[s_{\max}^2 - s(\tau)^2] \tag{2.26}$$

where $s(\tau)$ is the parcel supersaturation at time τ. Substituting Eq. (2.26) into (2.25), we eventually obtain

$$D_p = \sqrt{\left(\frac{2A}{3s_{c,\min}}\right)^2 + \frac{G}{aV}\left[s_{\max}^2 - s_{c,\min}^2\right]} \tag{2.27}$$

where $s_{c,min}$ is the critical supersaturation of the largest CCN that exceeds its critical

diameter. Eq. (2.27) can be used as an estimate for the upper limit, $D_{p,big}$. The lower limit, $D_{p,low}$, can be estimated by the smallest CCN that can theoretically activate:

$$D_{p,low} = \frac{2A}{3s_{\max}} \tag{2.28}$$

It is notable that in this method, $D_{p,big}$ depends on a_c as opposed to the empirical method where $D_{p,low}$ depends on a_c.

Assessment of $D_{p,big}$ and $D_{p,low}$ calculation methods

Both methods of calculating $D_{v,ave}$ were introduced into the NS parameterization; N_d predictions were then compared with parcel model simulations.

The comparisons were done for the activation of single mode lognormal aerosol with $D_{p,g}$ ranging between 0.025 to 0.25μm, σ_i between 1.1 to 2.5, and for updraft conditions ranging between V = 0.1 to 3.0 ms^{-1}. Ambient P and T were set to 800 mbar and 283 K, respectively. Figure 1.2 shows the parameterized droplet number concentration (using the two different methods of estimating $D_{v,ave}$) against the parcel model simulations. The 1:1 line represents a perfect agreement between the parameterization and the parcel model. Results are presented for two values of the accommodation coefficient (a_c = 0.042, a_c = 0.1). An average error of 6% (±1%) was observed for the theoretical method, which slightly underperforms against the empirical method (average error=2%, ±0.9%). We thus choose to use the empirical method until an alternate theoretical criterion is derived.

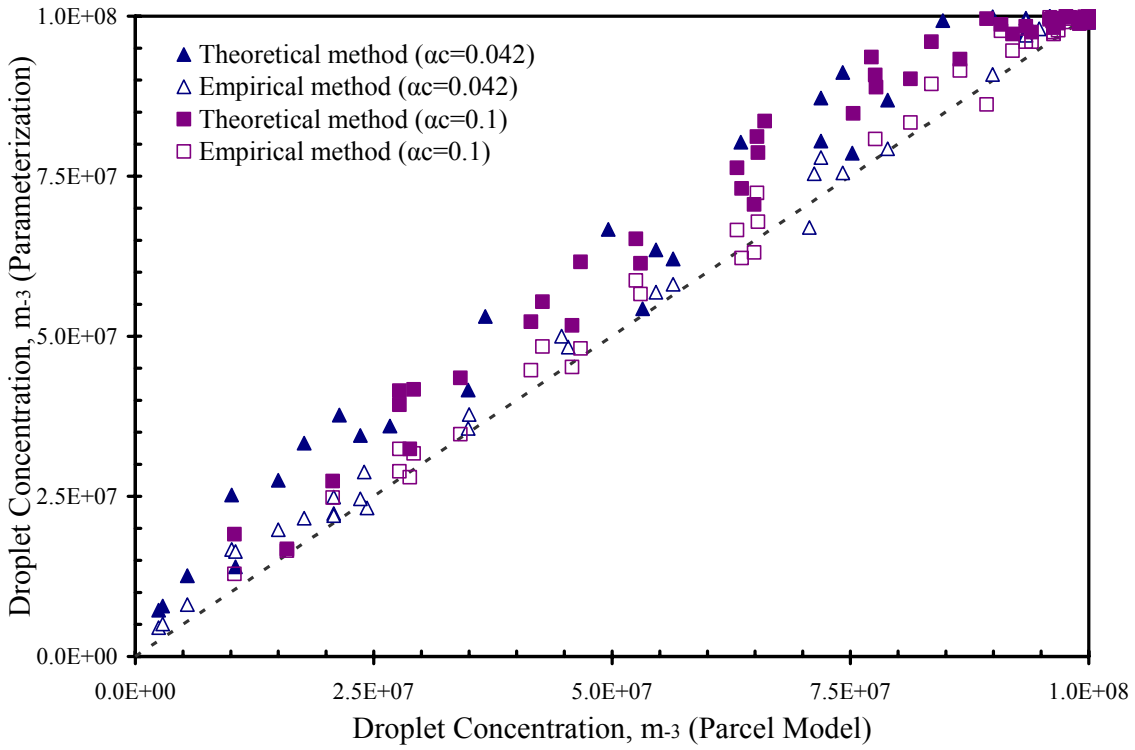

Figure 2.2: Droplet number concentration as predicted by the modified NS parameterization and by the cloud parcel model, using the sectional formulation. Results for both theoretical and empirical $D_{v,ave}$ are presented. The other simulation characteristics are given in the text.

2.6 Evaluation of Modified NS Parameterization

2.6.1 Method

The sectional formulation of the parameterization, as well as the diffusivity modification were assessed for their ability to reproduce simulations from the adiabatic cloud parcel model of Nenes *et al*., (2001) over a large range of aerosol size distributions and updraft velocities. The detailed numerical parcel model used in this study has been widely used and recently evaluated with in-situ data (Conant *et al*., 2004). Table 2.2 shows all the simulation sets used for the evaluation of the parameterization. Both single and tri-modal aerosols were considered, for number concentrations and mode diameters characteristic of tropospheric aerosol. For trimodal aerosol, we have selected four of the *Whitby* (1978) trimodal representations, namely the marine, clean continental, average background, and urban aerosol representations (Table 2.3). The updraft velocities used in our evaluation ranges between 0.1 and 3.0 m s^{-1}; together with the wide range of aerosol number concentrations considered, s_{max} varies from 0.01% to over 1%, covering the climatically important range of cloud droplet formation conditions.

Table 2.2: Aerosol and updraft velocity conditions considered in the parameterization evaluation

Simulation set[b,c]	$D_{g,i}$, µm	N_i, cm^{-3}	σ_i	W, ms^{-1}	Chemical Composition	Number of cases
SM1	0.025	100	1.1 - 1.5	0.1 - 3.0	$(NH_4)_2SO_4$:100%	15
SM2	0.025	500	1.1 - 1.5	0.1 - 3.0	$(NH_4)_2SO_4$:100%	15
SM3	0.05	500	1.1 - 2.5	0.1 - 3.0	NaCl:100%	25
SM4	0.25	100	1.1 - 2.5	0.1 - 3.0	NaCl:100%	25
SM5	0.75	1000	1.1 - 2.5	0.1 - 3.0	$(NH_4)_2SO_4$:100%	25
TM-M	Given in Table 2.3				$(NH_4)_2SO_4$:100%	4
TM-C					$(NH_4)_2SO_4$:100%	4
TM-B					$(NH_4)_2SO_4$:100%	4
TM-U					$(NH_4)_2SO_4$:100%	4

[b] SM denotes single mode

[c] TM denotes trimodal; M represents marine, C continental, B background, and U urban aerosol

Table 2.3: Aerosol characteristics for the multimodal simulations of Table 2.2. Distributions taken from Whitby (1978). $D_{g,i}$ is in µm; N_i is in cm^{-3}.

Aerosol Type	Nuclei Mode			Accumulation mode			Coarse mode		
	$D_{g,1}$	σ_1	N_1	$D_{g,2}$	σ_2	N_2	$D_{g,3}$	σ_3	N_3
Marine	0.010	1.6	340	0.070	2.0	60	0.62	2.7	3.1
Continental	0.016	1.6	1000	0.068	2.1	800	0.92	2.2	0.72
Background	0.016	1.7	6400	0.076	2.0	2300	1.02	2.16	3.2
Urban	0.014	1.8	106000	0.054	2.16	32000	0.86	2.21	5.4

2.6.2 Evaluation of the Modal Formulation

Evaluation of the modal formulation is done by comparing its predictions of N_d with those of the sectional parameterization. We consider the activation of lognormal aerosol, so both formulations should give the same droplet number (provided the discretization error of the sectional formulation is insignificant). This is shown in Figure 2.3, which depicts the parameterized N_d, using the sectional vs. the modal formulation. Cases considered were for a single mode lognormal aerosol with $D_{p,g}$ ranging between 0.05 to 0.75μm, σ_i ranging between 1.1 to 2.5, and for updraft conditions ranging between V = 0.1 to 3.0 ms^{-1}. The sectional formulation used 200 sections for discretizing the lognormal distribution. Regardless of activation conditions, the parameterization with modal formulation is as robust as the parameterization with the sectional representation (average error $\approx$ 1%, standard deviation $\approx$ 0.3%). Therefore, for lognormal aerosol, both formulations can be interchanged without any loss in accuracy. The advantage of using the lognormal distribution is that it is simpler to implement and, more than two orders of magnitude faster on a Pentium PC, than the sectional formulation (with 200 sections).

2.6.3 Evaluation of Parameterization with Modified Diffusivity

Figure 2.4 displays the droplet number concentration as predicted by NS and by the (Nenes *et al*., (2001)) parcel model for the aerosol conditions of Table 2.3. The parameterized droplet number concentrations closely follow the parcel model simulations; however, there is a tendency for underestimation, which is not significant for a_c=1.0, but worsens as a_c decreases (Figure 2.5). This problem is resolved by substituting D_v' in the G term of Eq. (2.17) with the modified diffusivity, $D_{v,ave}$. Figures 2.6 and 2.7

display the droplet number concentration from the modified parameterization against the parcel model predictions for the single mode (Figure 2.6) and trimodal (Figure 2.7) aerosol of Table 2.2.

Results are presented for a_c = 0.042 and a_c = 0.005. It is clear that the modified parameterization captures the parcel model simulations much better than the original NS, even for low values of a_c. The overestimation (average error 4.1±1.3%) observed in Figure 2.7 for marine aerosol is caused by the fact that the descriminant for these aerosol is close to zero, at the transition between the kinetically limited ($\Delta>0$) and kinetically free ($\Delta<0$) regimes. Under such conditions, the expression for calculating s_{part} is least accurate. Nevertheless, the modified diffusivity remarkably improves the performance of the parameterization, even for such challenging aerosol as those with film forming compounds. It should also be noted that the modifications pose negligible computational burden, as opposed to employing a more expensive algorithm (e.g., a section-specific D_v').

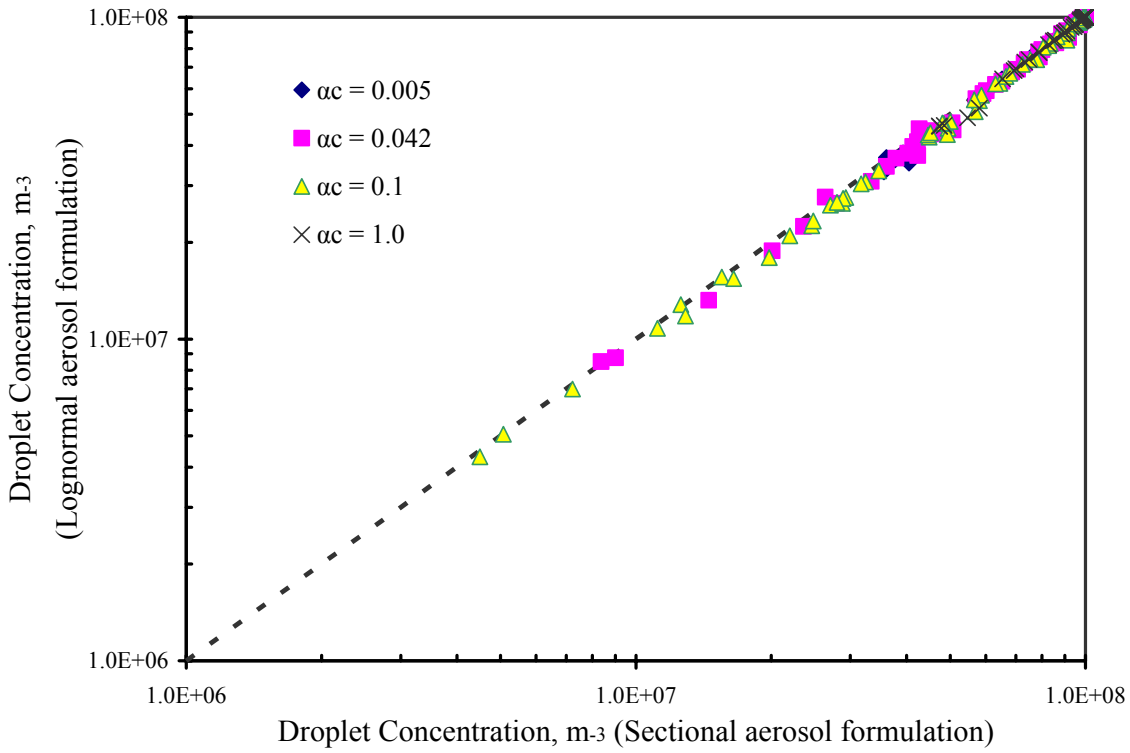

Figure 2.3: Droplet number concentration as predicted by the modified NS parameterization using the sectional and the modal formulations. Cases considered were for a single mode lognormal aerosol with $D_{p,g}$ ranging between 0.05 to 0.75μm, σ_i ranging between 1.1 to 2.5, updraft conditions ranging between V = 0.1 to 3.0 ms^{-1} and for chemical composition of pure $(NH_4)_2SO_4$, pure NaCl, and 50% $(NH_4)_2SO_4$ - 50% insoluble. Ambient P and T were set to 800 mbar and 283 K, respectively. The sectional formulation used 200 sections for discretizing the lognormal distribution. Results are for four values of a_c.

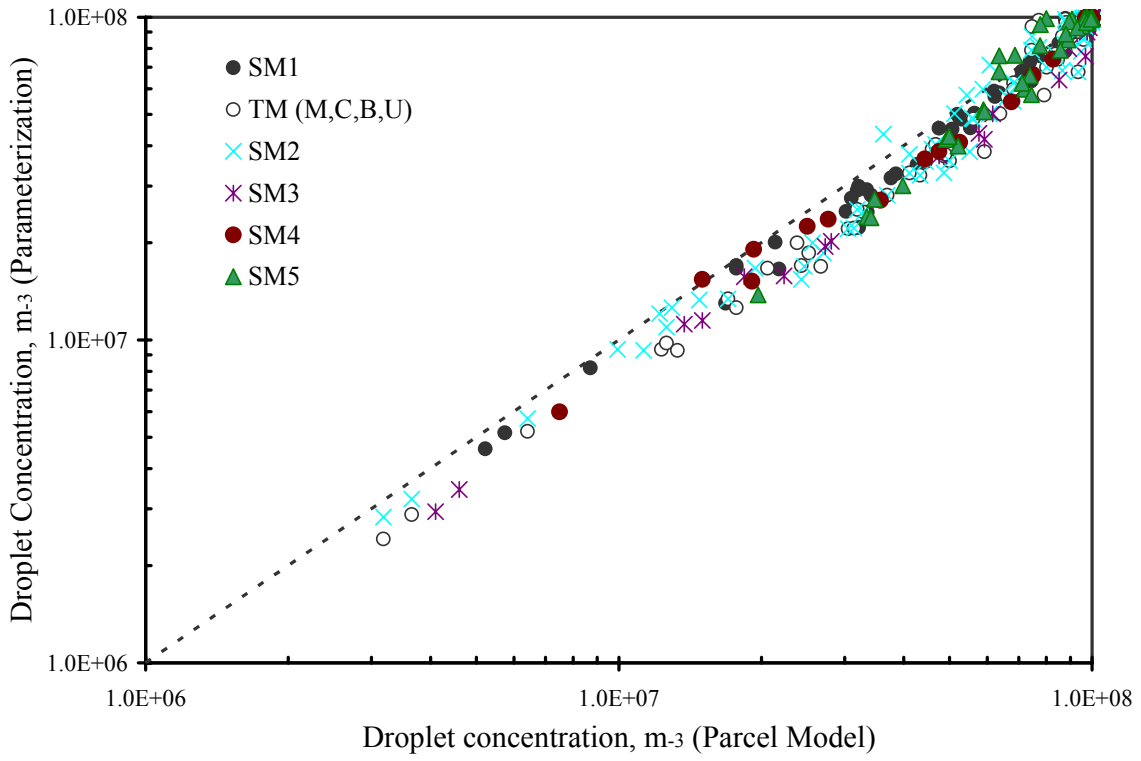

Figure 2.4: Droplet number concentration as predicted by the NS parameterization and by the cloud parcel model for all the aerosol size distributions and updraft velocities of Table 2.2. All simulations assume perfect water vapor accommodation (a_c = 1.0), P = 800mbar and T = 283K.

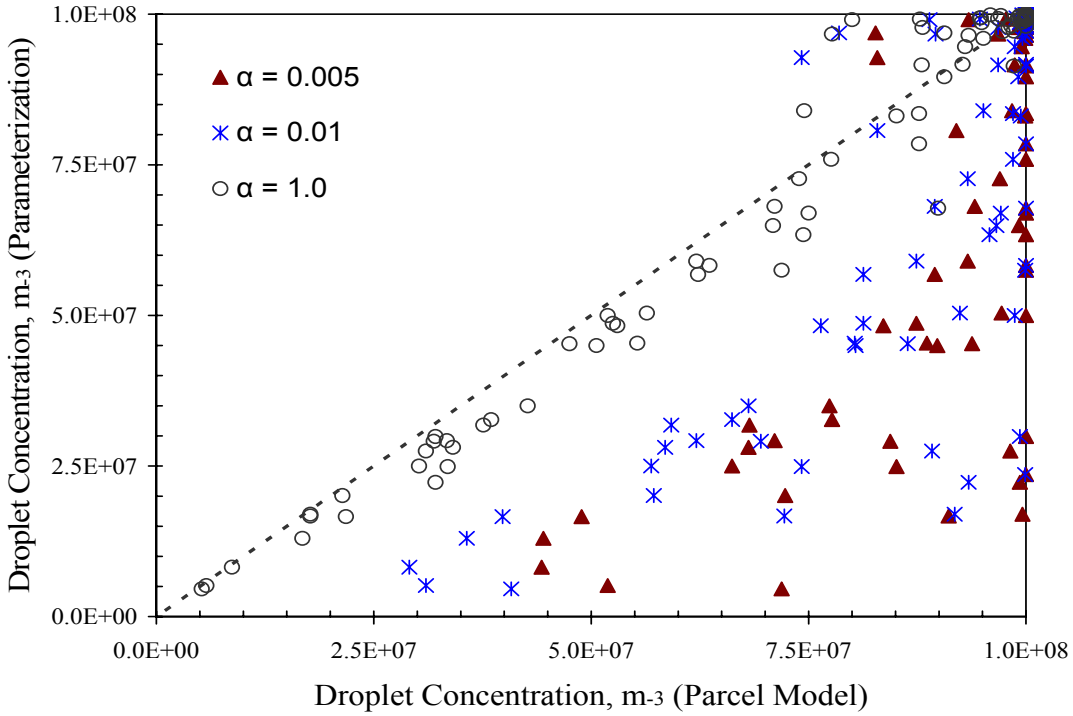

Figure 2.5: Droplet number concentration as predicted by the NS parameterization and by the cloud parcel model for cases SM1, SM2 and SM3 of Table 2.2, and for a_c = 1.0, a_c = 0.01, and a_c = 0.005. All simulations assume P = 800mbar and T = 283K.

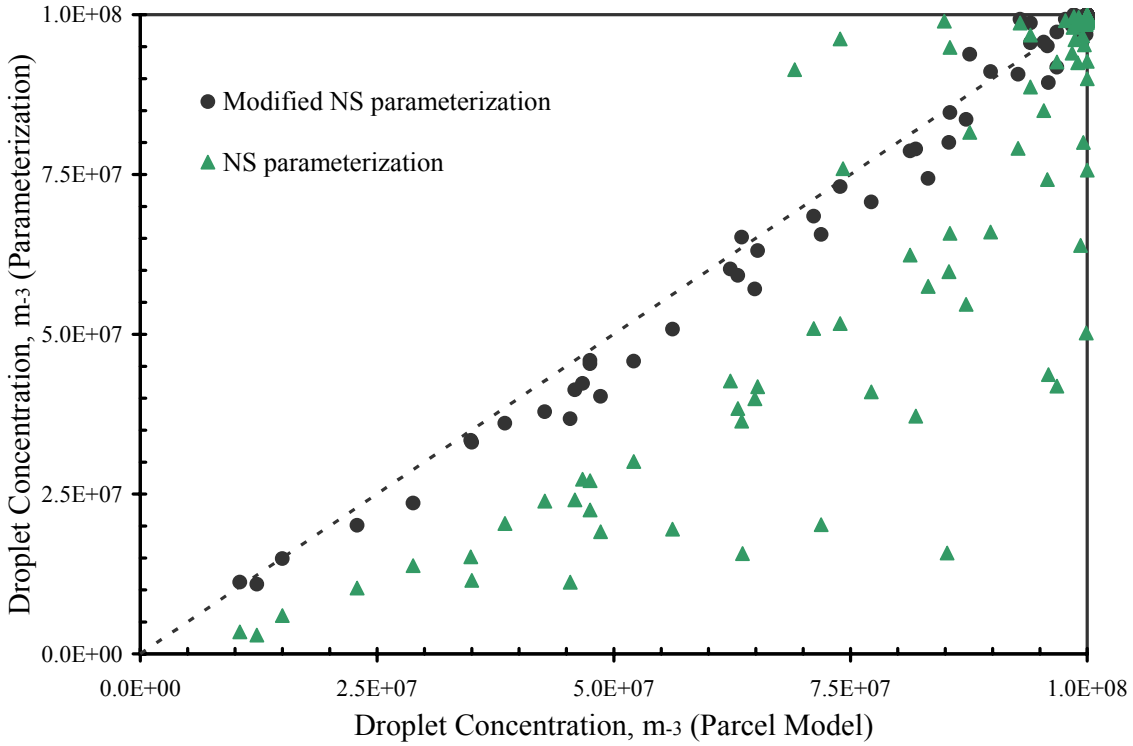

Figure 2.6: Droplet number concentration as predicted by the modified NS parameterization and by the cloud parcel model for cases SM3 and SM4 of Table 2.2, and for a_c = 0.042. All simulations assume P = 800mbar and T = 283K.

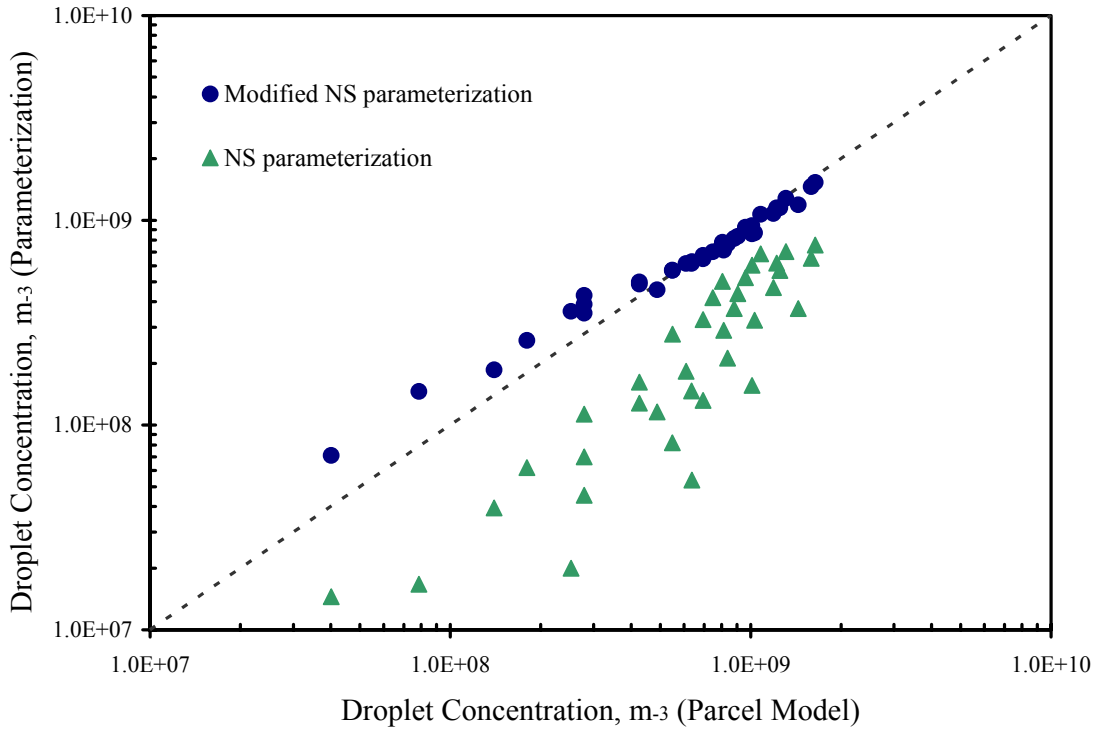

Figure 2.7: Droplet number concentration as predicted by the modified NS parameterization and by the cloud parcel model for case TM of Table 2.2, and for $a_c = 0.005$. All simulations assume P = 800mbar and T = 283K.

2.7 Conclusions

The aerosol activation parameterization developed by Nenes and Seinfeld (2003) was appropriately modified to *i)* allow for a lognormal representation of aerosol size distribution, and, *ii)* include a size-dependant mass transfer coefficient for the growth of water droplets (which explicitly includes the accommodation coefficient). To address this, an average value of the water vapor diffusivity is introduced in the parameterization. Two methods were explored for determining the upper and lower bound of the droplet diameter needed for calculating the average water vapor diffusivity. The most accurate employs an empirical correlation derived from numerical parcel simulation.

Predictions of the modified NS parameterization are compared against detailed cloud parcel model simulations for a wide variety of aerosol activation conditions. The modified NS parameterization closely tracks the parcel model simulations, even for low values of the accommodation coefficient, without any increase in computational cost. This work offers a much needed rigorous and computationally inexpensive framework for directly linking complex chemical effects on aerosol activation in global climate models.

2.8 Acknowledgements

This research was supported by a NASA EOS-IDS, a NASA New Investigator Award, and by Georgia Institute of Technology faculty startup funds.

2.9 References

Abdul-Razzak, H., and Ghan, S.J.: A parameterization of aerosol activation: 2. Multiple aerosol types, J. Geophys. Res., 105, 6837-6844, 2000.

Abdul-Razzak, H., Ghan, S.J., and Rivera-Carpio, C.: A parameterization of aerosol activation. 1. Single aerosol type, J. Geophys. Res., 103 (D6), 6123-6131, 1998.

Boucher, O., and Lohmann, U.: The sulfate-CCN-cloud albedo effect-A sensitivity study with 2 general-circulation models, Tellus, Ser. B, 47, 281-300, 1995.

Charlson, R.J., Seinfeld, J.H., Nenes, A., Kulmala, M., Laaksonen, A., and Facchini, M.C.: Reshaping the theory of cloud formation, Science, 292, 2025-2026, 2001.

Chuang, P.Y.: Measurement of the timescale of hygroscopic growth for atmospheric aerosols. J. Geophys. Res., 108 (D9), 4282, doi: 10.1029/2002JD002757, 2003.

Chuang, P., Charlson, R., and Seinfeld, J.: Kinetic limitation on droplet formation in clouds, Nature, 390, 594-596, 1997.

Conant, W.C., Vanreken, T., Rissman, T., Varutbangkul, V., Jimenez, J., Delia, A., Bahreini, R., Roberts, G., Nenes, A., Jonsson, H., Flagan, R.C., Seinfeld, J.H.,: Aerosol-cloud drop concentration closure in warm cumulus, J. Geophys. Res., 109, D13204, doi:10.1029/2003JD004324, 2004.

Facchini, M.C., Mircea, M., Fuzzi, S., and Charlson, R.: Cloud albedo enhancement by surface active organic solutes in growing droplets, Nature, 401, 257-259, 1999.

Feingold, G., and Chuang, P.: Analysis of the influence of film-forming compounds on droplet growth: Implications for cloud microphysical processes and climate, J. Atmos. Sci., 59, 2006-2018, 2002.

Fountoukis, C., and A. Nenes, Continued development of a cloud droplet formation parameterization for global climate models, J. Geophys. Res., 110, D11212, doi:10.1029/2004JD005591, 2005.

Fukuta, N., and Walter, L.A.: Kinetics of hydrometer growth from the vapor; spherical model, J. Atmos. Sci., 27, 1160-1172, 1970.

Ghan, S., Chuang, C., and Penner, J.: A parameterization of cloud droplet nucleation. part I: Single aerosol species. Atmos. Res., 30, 197-222, 1993.

Ghan, S., Leung, L., Easter, R., and Abdul-Razzak, H.: Prediction of cloud droplet number in a general circulation model, J. Geophys. Res., 102, 21, 777-21, 794, 1997.

Gultepe, I., and Isaac, G.: The relationship between cloud droplet and aerosol number concentrations for climate models, Int. J. Climatol., 16, 941-946, 1996.

Intergovernmental Panel on Climate Change: The scientific Basis, Cambridge Univ. Press, New York, 2001.

Laaksonen, A., Korhonen, P., Kulmala, M., and Charlson, R.: Modification of the Köhler Eq. to include soluble trace gases and slightly soluble substances, J. Aerosol Sci., 155, 853-862, 1998.

Lance, S., Nenes, A., and Rissman, T.: Chemical and dynamical effects on cloud droplet number: Implications for estimates of the aerosol indirect effect. J. Geoph. Res., 109, D22208, doi:10.1029/2004JD004596, 2004.

Li, Z., Williams, A.L., and Rood, M.J.: Influence of soluble surfactant properties on the activation of aerosol particles containing inorganic solute, J. Atm. Sci., 55, 1859-1866, 1998.

Li, Y.Q., Davidovits, P., Shi, Q., Jayne, J.T., and Warsnop, D.R.: Mass and thermal accommodation coefficients of $H_2O_{(g)}$ on liquid water as a function of temperature, J. Phys. Chem. A, vol. 105, 10627-10634, 2001.

Lohmann, U., Feichter, J., Chuang, C.C., and Penner, J.E.: Predicting the number of cloud droplets in the ECHAM GCM, J. Geophys. Res. 104, 9169-9198 and 24,557-24,563 (Erratum), 1999.

Medina, J., and Nenes, A.: Effects of film forming compounds on the growth of giant CCN: Implications for cloud microphysics and the aerosol indirect effect, J. Geophys. Res., 109, D20207, doi: 10.1029/2004JD004666, 2004.

Meskhidze, N., Nenes, A., Conant, W.C., and Seinfeld, J.H.: Evaluation of a new Cloud Droplet Activation Parameterization with In Situ Data from CRYSTAL-FACE and CSTRIPE, J.Geoph.Res., 110, D16202, doi:10.1029/2004JD005703, 2005.

Nenes, A., and Seinfeld, J.H.: Parameterization of cloud droplet formation in global climate models, J. Geophys. Res., 108(D14) 4415, doi: 10.1029/2002JD002911, 2003.

Nenes, A., Charlson, R.J., Facchini, M.C., Kulmala, M., Laaksonen, A., and Seinfeld, J.H.: Can chemical effects on cloud droplet number rival the first indirect effect?, Geophys. Res. Lett, 24 (17), 1848, doi: 10.1029/2002GL015295, 2002.

Nenes, A., Ghan, S.J., Abdul-Razzak, H., Chuang, P., and Seinfeld, J.H.: Kinetic limitations on cloud droplet formation and impact on cloud albedo, Tellus Ser. B, 53, 133 – 149, 2001.

Pruppacher, H.R. and Klett, J.D.: Microphysics of Clouds and Precipitation. Kluwer Academic Publishers, Dordrecht, Netherlands, 2000.

Rissman, T., Nenes, A., and Seinfeld, J.H.: Chemical amplification (or dampening) of the Twomey effect: Conditions derived from droplet activation theory, J. Atmos. Sci., 61(8), 919-930, 2004.

Seinfeld, J.H., and Pandis, S.N.: Atmospheric Chemistry and Physics: From Air Pollution to Climate Change, John Wiley & Sons, Inc., 1998.

Shantz, N.C., Leaitch, W.R., and Caffrey, P.: Effect of organics of low solubility on the growth rate of cloud droplets, J. Geophys. Res., 108, doi:10.1029/2002JD002540, 2003.

Shaw R.A., and Lamb, D.: Experimental determination of the thermal accommodation and condensation coefficients of water, J. Chem. Phys., 111 (23), 1999.

Shulman, M.L., Jacobson, M.C., Charlson, R.J., Synovec, R.E., and Young, T.E.: Dissolution behavior and surface tension effects of organic compounds in nucleating cloud droplets, Geophys. Res. Lett., 23, 277 – 280, 1996.

Twomey, S.: The nuclei of natural cloud formation. II. The supersaturation in natural clouds and the variation of cloud droplet concentration, Geofisica Pura Appl., 43, 243-249, 1959.

Whitby, K.: The physical characteristics of sulfur aerosols, Atmos. Environ., 12, 135-159, 1978.

CHAPTER 3

AEROSOL – CLOUD DROPLET CLOSURE STUDY USING *IN SITU* DATA[I]

3.1 Abstract

This study analyzes 27 cumuliform and stratiform clouds sampled aboard the CIRPAS Twin Otter during the 2004 ICARTT (International Consortium for Atmospheric Research on Transport and Transformation) experiment. The dataset was used to assess cloud droplet closure using *i*) a detailed adiabatic cloud parcel model, and, *ii*) a state-of-the-art cloud droplet activation parameterization. A unique feature of the dataset is the sampling of highly polluted clouds within the vicinity of power plant plumes. Remarkable closure was achieved (much less than the 20% measurement uncertainty) for both parcel model and parameterization. The highly variable aerosol did not complicate the cloud droplet closure, since the clouds had low maximum supersaturation and were not sensitive to aerosol variations (which took place at small particle sizes). The error in predicted cloud droplet concentration was mostly sensitive to updraft velocity. Optimal closure is obtained if the water vapor uptake coefficient is equal to 0.06, but can range between 0.03 and 1.0. The sensitivity of cloud droplet prediction error to changes in the uptake coefficient, organic solubility and surface tension depression suggest that organics

[I] Appeared in publication: Fountoukis, C., Nenes, A., Meskhidze, N., Bahreini, R., Conant, W., Jonsson, H., Murphy, S., Sorooshian, A., Varutbangkul, V., Brechtel, F., Flagan, R., and Seinfeld, J.: Aerosol–cloud drop concentration closure for clouds sampled during the International Consortium for Atmospheric Research on Transport and Transformation 2004 campaign, J. Geophys. Res., 112, D10S30, doi:10.1029/2006JD007272, 2007.

exhibit limited solubility. These findings can serve as much needed constraints in modeling of aerosol-cloud interactions in the North America; future in-situ studies will determine the robustness of our findings.

3.2 Introduction

Most of the uncertainty in anthropogenic climate change is associated with aerosol–cloud interactions (Lohmann and Feichter, 2004; Andreae *et al.*, 2005). Explicitly resolving cloud formation and microphysical evolution and aerosol-precipitation interactions in Global Climate Models (GCMs) is a challenging computational task (Khairoutdinov *et al.*, 2005; Randall *et al.*, 2003); parameterizations are used instead. In terms of predicting droplet number, empirical correlations are often used (e.g., Jones *et al.*, 1994; Gultepe and Isaac, 1996; Boucher and Lohmann, 1995; Lohmann and Feichter, 1997; Kiehl *et al*., 2000; Menon *et al*., 2002; Brasseur and Roeckner, 2005), which relate an aerosol property (usually total number or mass) to cloud droplet number concentration, N_d. The data is usually obtained from observations. Although simple and easy to implement, correlations are subject to substantial uncertainty (Kiehl *et al.*, 2000). Prognostic parameterizations of aerosol–cloud interactions have also been developed (Lohmann *et al*., 1999; Lohmann *et al*., 2000; Ghan *et al*., 2001a,b; Rotstayn and Penner, 2001; Peng *et al.*, 2002; Nenes and Seinfeld, 2003; Fountoukis and Nenes, 2005) in which N_d is calculated using cloud-scale updraft velocity, aerosol size distribution and composition. These approaches are based on the "parcel" concept of 1-D Lagrangian numerical cloud models (e.g., Jensen and Charlson, 1984; Considine and Curry, 1998; Nenes *et al.*, 2001). Although inherently better than correlations, prognostic parameterizations are still subject

to uncertainties in the sub-grid (i.e., cloud-scale) updraft velocity (e.g., Menon et al., 2002), aerosol size distribution and composition (e.g., Rissman *et al.*, 2004), aerosol "chemical" effects and changes in droplet growth kinetics (e.g., Nenes *et al.*, 2002).

The ultimate test for prognostic parameterizations and cloud models is the comparison of their predictions against comprehensive *in-situ* data. When done for cloud droplet number, this procedure is termed "cloud droplet closure study", in which a discrepancy between N_d predicted by models and measured in-situ is usually determined. Hallberg *et al.,* (1997) report ~50% disagreement between predicted and observed N_d for continental stratocumulus clouds. Chuang *et al.*, (2000) studied marine and continental stratus clouds sampled during the second Aerosol Characterization Experiment (ACE-2) and found a large discrepancy (about a factor of 3) between predictions and observations for updraft velocity range expected for stratocumulus clouds. Snider and Brenguier (2000) and Snider *et al.*, (2003) found up to 50% discrepancy between predicted and measured droplet concentrations for ACE-2 and marine stratocumulus clouds. Part of this discrepancy was attributed to the usage of ground-based observations in the closure. Conant *et al.,* (2004) achieved remarkable closure, to within 15%, for cumulus clouds of marine and continental origin sampled during the NASA Cirrus Regional Study of Tropical Anvils and Cirrus Layers – Florida Area Cirrus Experiment (CRYSTAL - FACE). Meskhidze *et al.*, (2005) also found excellent agreement between predicted and measured N_d (~30%) for the stratiform cloud data gathered during Coastal Stratocumulus Imposed Perturbation Experiment (CSTRIPE, Monterey, California, July 2003). In general, cloud droplet closure has been successful for clouds formed in clean airmasses, and to a lesser degree for polluted clouds. It is however unclear if the latter results from

limitations in the observations or in the theory used for predicting cloud droplet number. In this study we assess aerosol-cloud drop number closure using *i*) a detailed cloud parcel model (Nenes et al., 2001), and, *ii*) the parameterization of Nenes and Seinfeld (2003) with recent extensions by Fountoukis and Nenes (2005) (hereon referred to as "modified NS" parameterization). The observations used in this study were collected on board the Center for Interdisciplinary Remotely Piloted Aircraft Studies (CIRPAS) Twin Otter aircraft (http://www.cirpas.net) during the NASA International Consortium for Atmospheric Research on Transport and Transformation experiment (ICARTT). A unique feature of this dataset is the sampling of highly polluted cloudy air within the vicinity of power plant plumes. Closure with the parcel model tests our predictive understanding of cloud droplet formation under extremely polluted conditions, while using the parameterization assesses its performance and quantifies the uncertainty arising from its simplified physics.

3.3 *In-situ* Observation Platform and Analysis Tools

During ICARTT, the Twin Otter realized twelve research flights in the vicinity of Cleveland and Detroit (Figure 3.1), several of which sampled cumuliform and stratiform clouds. Seven flights are considered in this study. The cloud sampling strategy involves several under-cloud "passes" to characterize the aerosol size distribution and chemical composition, followed by in-cloud "legs" to sample the cloud microphysics, chemistry and turbulence.

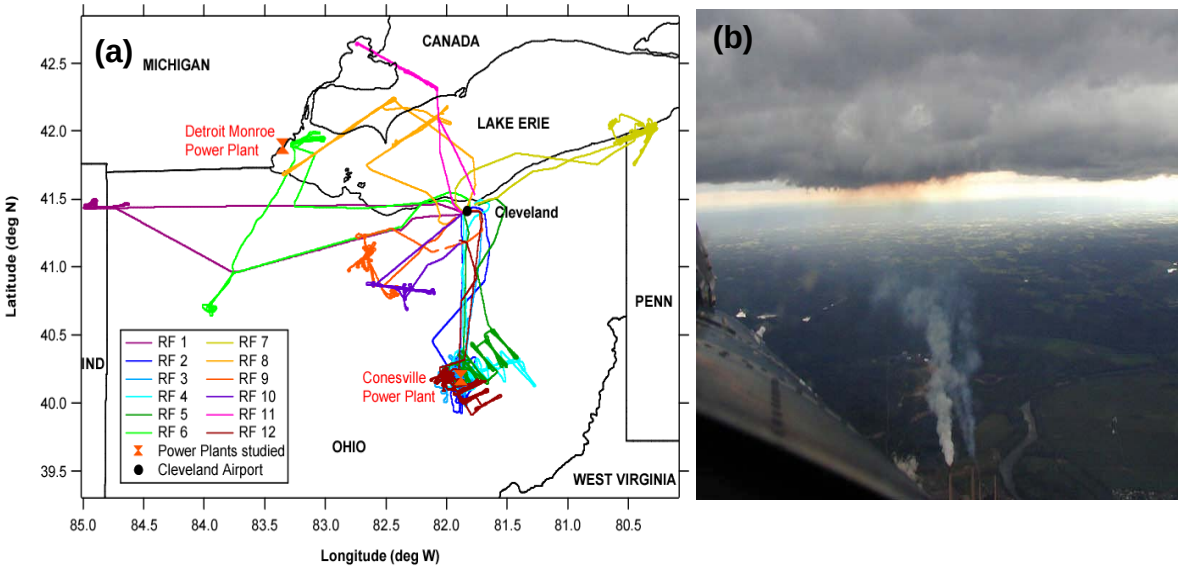

Figure 3.1: (a) Map of the 12 Twin Otter research flight tracks during ICARTT. (b) Photograph of Conesville power plant plume affecting cloud depth (flight IC3; August 6, 2004).

Table 3.1: Instrumentation and Measurement Parameters during ICARTT

Instrument	Measurement	Measured Property	Measurement Principle
Forward scattering spectrometer probe (FSSP)	Cloud droplet number distribution	Geometric diameter: 1.5 – 37 μm	Optical forward scattering
Cloud, aerosol, and precipitation spectrometer (CAS)		Geometric diameter: 0.5 – 50 μm	Optical forward scattering and 2-D imaging
Condensation Particle Counter (CPC)	Aerosol number concentration	Geometric diameter > (3 nm, 7 nm, 13 nm)	varying supersaturations of butanol
Dual Automated Classifier Aerosol Detector (DACAD)	Aerosol size distribution	Geometric diameter: 10-800 nm	Classification by electrical mobility
Passive Cavity Aerosol Spectrometer Probe (PCASP)		Geometric diameter: 100-2500 nm	Optical scattering
Aerodynamic Particle Sizer (APS)		Aerodynamic diameter: 500 – 10,000 nm	Aerodynamic classification
3-column cloud condensation nuclei counter (CCN)	CCN concentration	3 supersaturations	Activation at constant supersaturation; optical detection of droplets
Aerodyne aerosol mass spectrometer (AMS)	Aerosol chemical composition	Mass concentration: $SO_4^{2-}, NH_4^+, NO_3^-, OC$	Flash ionization; quadrapole mass spectrometer
Particle-into-liquid sampler (PILS)		Mass concentration: $SO_4^{2-}, NH_4^+, NO_3^-, oxalate$	Ion chromatography
C-Navigational System and Novatel GPS	Updraft velocity, wind speed	Wind velocity; aircraft position and altitude	Wind velocity = aircraft ground velocity(C-MIGITS INS/GPS) – aircraft air velocity (turbulence and Pitot-static probes)

3.3.1 Description of Airborne Platform

Table 3.1 summarizes the instruments and measured quantities aboard the CIRPAS Twin Otter aircraft. A Dual Automatic Classifier Aerosol Detector (DACAD; Wang *et al.*, 2003) was used to measure dry aerosol size between 10 and 800 nm. The DACAD consists of two scanning Differential Mobility Analyzers (DMAs) operating in parallel, one at a "dry" relative humidity (RH) less than 20%, and another at a "humid" RH of ~75%. From the dry-wet size distributions, the size-resolved hygroscopicity is obtained. Aerosol chemical composition (sulfate, nitrate, ammonium and organics) was measured in real-time by an Aerodyne Aerosol Mass Spectrometer (AMS; Bahreini *et al.*, 2003; Jayne *et al.*, 2000). Concurrently, aerosol inorganics (NO_3^-, SO_4^{2-}, NH_4^+) and some organics (oxalate) were measured with a Particle–into–Liquid Sampler (PILS; Sorooshian *et al.*, 2006). Updraft velocities were obtained from a five-hole turbulence probe, a Pitot-static pressure tube, a C-MIGITS GPS/INS Tactical System, GPS/inertial navigational system (INS), and the Novatel GPS system.

Droplet number concentrations were measured with a Cloud and Aerosol Spectrometer (CAS) optical probe (Baumgardner *et al.*, 2001), and the Forward Scattering Spectrometer Probe (FSSP; Brenguier *et al.*, 1998; Jaenicke and Hanusch, 1993). The FSSP measures droplets ranging from 1.5 to 37 μm diameter. As with any optical counter, the FSSP is subject to numerous uncertainties such as variations of the size calibration and of the instrument sampling section, nonuniformity in light intensity of the laser beam, probe deadtime and coincidence errors (Baumgardner and Spowart, 1990; Brenguier 1989). The FSSP is most accurate for measurements of N_d below 200 cm^{-3} (Burnet and Brenguier, 2002). At high droplet concentrations, N_d can be noticeably underestimated

when measured with the Fast-FSSP (Burnet and Brenguier, 2002). The CAS measures droplet sizes from 0.4 to 50 μm in 20 size bins using a measurement principle similar to that of the FSSP, but improved electronics relaxes the requirement for deadtime and coincidence corrections (Burnet and Brenguier, 2002). A Passive Cavity Aerosol Spectrometer Probe (PCASP) was also flown, which is an optical probe that measures particles between 100 and 2500 nm.

3.3.2 Cloud Parcel Model

The numerical cloud parcel model used in this study (Nenes *et al*., 2001; Nenes *et al*., 2002) simulates the dynamical balance between water vapor availability from cooling of an ascending air parcel and water vapor depletion from condensation onto a growing droplet population. The model has successfully been used to assess cloud droplet closure in cumulus during CRYSTAL-FACE (Conant *et al.*, 2004) and has been used in numerous model assessments of aerosol-cloud interactions (e.g., Nenes *et al.*, 2002; Rissman *et al.*, 2002; Lance *et al.*, 2004). The model predicts cloud droplet number concentration and size distribution using as input the cloud updraft velocity, aerosol size distribution and chemical composition. "Chemical effects", such as surface tension depression (Shulman *et al.*, 1996; Facchini *et al.*, 1999), partial solubility or the presence of film-forming compounds (Feingold and Chuang, 2002; Nenes *et al*., 2002; Rissman *et al.*, 2004; Lance *et al.*, 2004) can also be easily considered; their effect on droplet closure will be assessed through sensitivity analysis.

3.3.3 The Droplet Formation Parameterization

The modified NS parameterization (Fountoukis and Nenes, 2005) is one of the most comprehensive, robust and flexible formulations available for global models. The calculation of droplet number is based on the computation of maximum supersaturation, s_{max}, within an ascending air parcel framework. The parameterization provides a computationally inexpensive algorithm for computing droplet number and size distribution and can treat externally-mixed aerosol subject to complex chemical effects (e.g. surface tension effects, partial solubility, changes in water vapor uptake). The parameterization's excellent performance has been evaluated with detailed numerical cloud parcel model simulations (Nenes and Seinfeld, 2003; Fountoukis and Nenes, 2005) and *in-situ* data for cumuliform and stratiform clouds of marine and continental origin (Meskhidze et al., 2005). Formulations for sectional (Nenes and Seinfeld, 2003) or lognormal (Fountoukis and Nenes, 2005) aerosol have been developed. The latter (lognormal) formulation is used in this study.

Table 3.2: ICARTT cloud characteristics for the flights considered in this study.

Flight (Cloud) Number	Flight Date	w_+ (ms^{-1})	σ_+ (ms^{-1})	Observed N_d, cm^{-3} (± st.dev %)	Predicted N_d, cm^{-3} parcel model (*parameterization*)	Originating airmass (*Cloud type*)	Mission Description	Wind Direction
IC3 (1)	6-Aug	1.67	0.868	1086 (15.9)	1046 (*1066*)	Clean (*cumulus*)	Conesville PP†	N
IC3 (2)	6-Aug	0.39	1.732	354 (45.6)	321 (*356*)	Clean (*stratocu*)	Conesville PP†	N
IC3 (3)	6-Aug	1.89	0.750	825 (44.5)	1109 (*1116*)	Clean (*cumulus*)	Conesville PP†	N
IC3 (4)	6-Aug	1.18	0.619	828 (27.0)	980 (*943*)	Clean (*cumulus*)	Conesville PP†	N
IC5 (1)	9-Aug	0.69	0.407	1293 (9)	1607 (*1420*)	Polluted (*cumulus*)	Conesville PP†	W-SW
IC5 (2)	9-Aug	0.28	0.209	1160 (17)	1147 (*1224*)	Polluted (*stratocu*)	Conesville PP†	W-SW
IC5 (3)	9-Aug	0.59	0.528	1045 (37.8)	1223 (*1281*)	Polluted (*cumulus*)	Conesville PP†	W-SW
IC6 (1)	10-Aug	0.69	0.430	695 (14.7)	744 (*813*)	Polluted (*stratocu*)	Monroe PP†	W-SW
IC6 (2)	10-Aug	0.35	0.283	415 (50.1)	508 (*577*)	Polluted (*stratus*)	Monroe PP†	NW-SW
IC6 (3)	10-Aug	0.44	0.303	668 (28.4)	555 (*636*)	Polluted (*stratus*)	Monroe PP†	NW-SW
IC6 (4)	10-Aug	0.69	0.375	808 (25.6)	745 (*809*)	Polluted (*stratocu*)	Monroe PP†	NW-SW
IC6 (5)	10-Aug	0.57	0.477	700 (47.8)	649 (*730*)	Polluted (*stratocu*)	Monroe PP†	NW-SW
IC6 (6)	10-Aug	1.07	0.819	1075 (15.7)	1008 (*1073*)	Polluted (*stratocu*)	Monroe PP†	NW-SW
IC9 (1)	16-Aug	0.59	0.360	1012 (31.9)	1000 (*1089*)	Clean (*stratocu*)	SW of Cleveland	NW-SW
IC9 (2)	16-Aug	0.17	0.131	540 (36)	487 (*455*)	Clean (*stratus*)	SW of Cleveland	NE-N
IC9 (3)	16-Aug	0.15	0.170	524 (48.5)	413 (*392*)	Clean (*stratus*)	SW of Cleveland	NE-N
IC9 (4)	16-Aug	0.72	0.727	1229 (8.7)	1507 (*1384*)	Clean (*stratocu*)	SW of Cleveland	NE-N
IC10 (1)	17-Aug	0.69	0.401	1258 (6)	1306 (*1367*)	Polluted (*cumulus*)	SW of Cleveland	NE-N
IC10 (2)	17-Aug	0.47	0.228	1040 (19.6)	1309 (*1060*)	Polluted (*stratocu*)	SW of Cleveland	S-SW
IC10 (3)	17-Aug	0.17	0.212	811 (20.4)	718 (*495*)	Polluted (*stratocu*)	SW of Cleveland	S-SW
IC11 (1)	18-Aug	0.35	0.313	963 (14.1)	803 (*780*)	Polluted (*stratocu*)	SW of Ontario	S-SW
IC11 (2)	18-Aug	0.54	0.621	954 (32.1)	1056 (*1054*)	Polluted (*stratocu*)	SW of Ontario	S-SW
IC11 (3)	18-Aug	0.62	0.428	965 (13.1)	1145 (*1153*)	Polluted (*stratocu*)	SW of Ontario	S-SW
IC11 (4)	18-Aug	0.56	0.239	1141 (18.6)	1060 (*1080*)	Polluted (*stratocu*)	SW of Ontario	S-SW
IC12 (1)	21-Aug	0.55	0.823	1314 (24.3)	1269 (*1265*)	Polluted (*cumulus*)	Conesville PP†	S-SW
IC12 (2)	21-Aug	0.38	0.250	1016 (32.1)	783 (*766*)	Polluted (*stratocu*)	Conesville PP†	NW-SW
IC12 (3)	21-Aug	0.12	0.134	322 (11.1)	287 (*296*)	Polluted (*stratocu*)	Conesville PP†	N

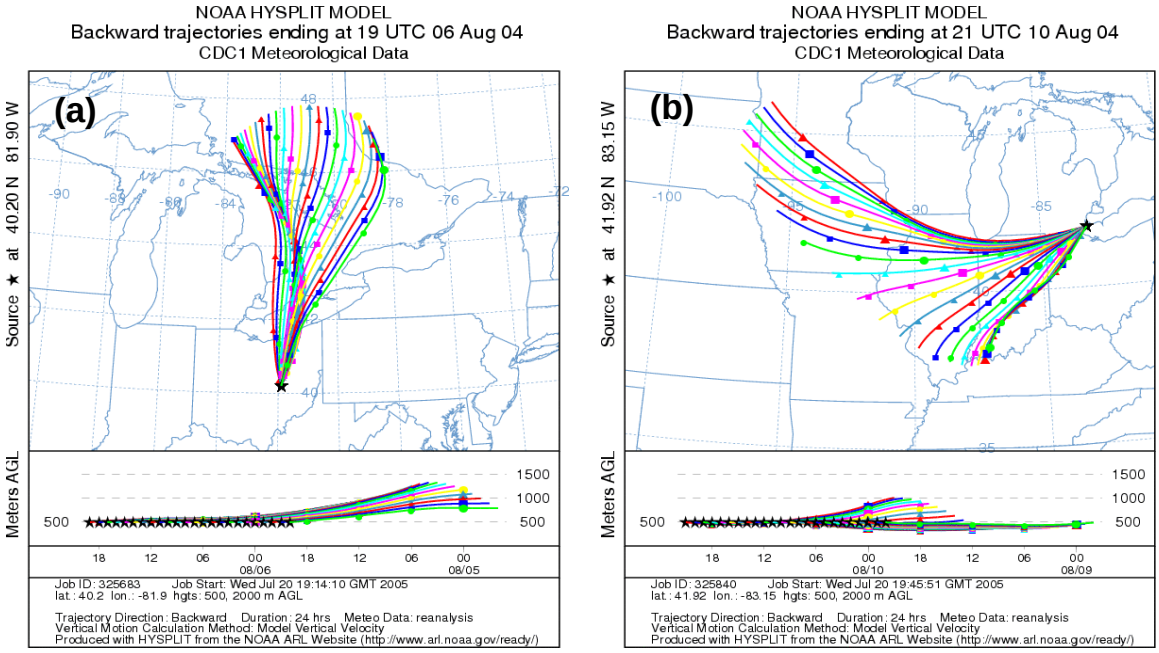

Figure 3.2: HYSPLIT backward trajectory analysis for (a) flight IC3, and, (b) flight IC6.

3.4 Observations and Analysis

3.4.1 Description of Research Flights

Seven flights are analyzed in this study, in which 27 clouds are profiled (Table 3.2). The clouds formed downwind of power plants, Cleveland and Detroit. Three research flights (IC3,5 and 12) sampled clouds downwind of the Conesville power plant (Figure 3.1a), one flight (IC6) sampled clouds downwind of the Monroe power plant (Figure 3.1a), two flights (IC 9,10) sampled clouds southwest of Cleveland (Figure 3.1a) and one flight (IC11) sampled clouds southwest of Ontario (Figure 3.1a).

Flight IC3 was the first to probe the Conesville power plant plume; its visible impact on local clouds (Figure 3.1b) motivated two more research flights (IC5 and 12) that fully characterized the plume and its influence on clouds. Backward Lagrangian trajectory analysis computed from the NOAA-HYSPLIT model (http://www.arl.noaa.gov/ready/hysplit4.html) suggests that during flights IC3 and IC9, the airmass sampled was transported by northerlies (Figure 3.2a). The air sampled in all other flights originated in the boundary layer and was transported by westerly winds (Figure 3.2b). Prevailing wind directions, cloud types and other characteristics for each cloud case are given in Table 3.2.

3.4.2 Cloud droplet number and updraft velocity measurements

The observed cloud droplet spectra are carefully screened to eliminate biases in N_d. Dilution biases are avoided by considering only measurements with effective droplet diameter greater than 2.4 μm and geometric standard deviation less than 1.5 (Conant *et al*., 2004). A lack of a drizzle mode (liquid water) present, i.e., negligible concentrations

of droplets larger than 30 μm (typically 0 - 0.2 cm^{-3}) suggest that collision-coalescence and drizzle formation were not important for the clouds sampled. Particles below 1μm are either evaporating or unactivated haze and not counted as droplets.

For flights before August 13, the CAS suffered from a saturation bias for concentrations above 1500 cm^{-3}. About 3% of the dataset was subject to this bias and was disregarded from this study. The CAS was also found to overcount droplets smaller than 6 μm but reliably counted droplet larger than 6 μm. This problem is addressed by disregarding the 1-6 μm CAS data and replacing them with FSSP data corrected for deadtime and coincidence errors (Burnet and Brenguier, 2002). Droplet concentration uncertainty was assessed by comparing FSSP and CAS concentrations in the 6-10 μm range; the former was to be about 40% lower than the latter. As all known sources of bias are accounted for in the FSSP correction, we assume that the difference between the two probes (40%) expresses an unbiased uncertainty (±20%) in observed droplet concentration for the whole dataset and droplet size range.

The observed cloud droplet concentrations for each flight are presented in Table 3.2. Average N_d varied from 320 cm^{-3} to 1300 cm^{-3} and as expected, correlated with cloud updraft velocity, w; clouds with $N_d > 1000$ cm^{-3} typically had $w > 1$ m s^{-1}, $N_d \sim 500$ - 1000 for $w \sim 0.5$ m s^{-1} and $N_d \sim 300$ - 500 for $w \sim 0.25$ m s^{-1}. High droplet concentration (even for clouds with low updraft velocity) is indicative of the high aerosol loading in almost all clouds profiled.

As expected, updraft velocity varied significantly in each cloud (even at cloud base); we chose to fit observations to a mass-flux-weighted Gaussian probability density function (pdf), as discussed by Meskhidze *et al.*, (2005) and Conant *et al.*, (2004). Aircraft turns

were eliminated from our analysis and the pdf in the measurements were shifted to have a mean of zero (consistent with the assumption of a slowly evolving boundary layer). Table 3.2 shows the values of average updraft velocity (closest to cloud base) and its standard deviation. Average cloud updraft velocity (at cloud base), w_+, varied between 0.12 (± 0.13) and 1.89 (± 0.73) m s^{-1}. w_+ and its standard deviation, σ_+, were highly correlated (Figure 3.3); typical of stratocumulus clouds, σ_+ is significant and comparable to the mean updraft velocity.

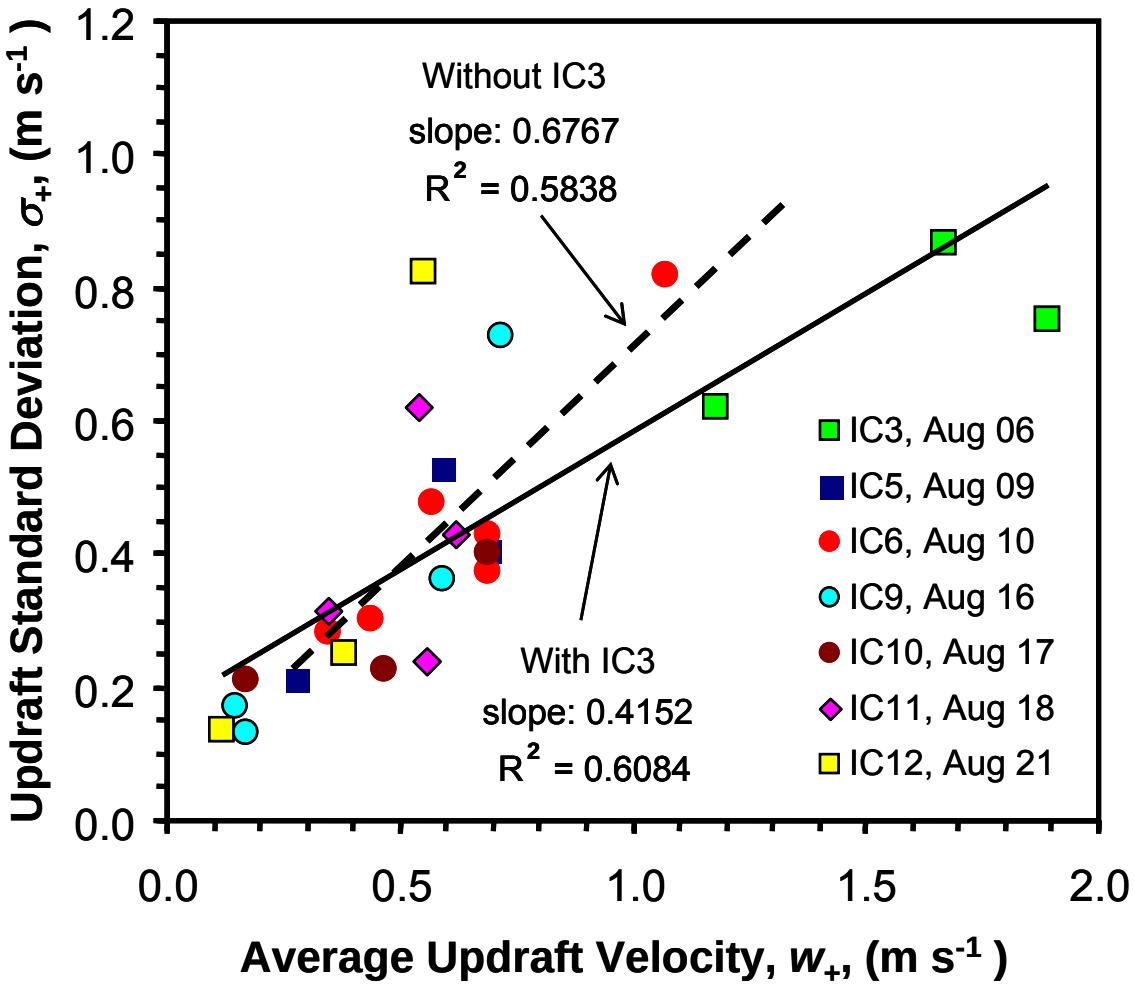

Figure 3.3: Correlation between average cloud-base updraft velocity and velocity standard deviation. All clouds listed in Table 3.2 are used.

Table 3.3: Aerosol size distribution and chemical composition for ICARTT clouds.

Flight Number (Date)	Aerosol Mode	Modal D_{pg} (µm)	Modal σ	Modal N_{ap} (cm^{-3})	$(NH_4)_2SO_4$ Mass Fraction (%)
IC3	Nucleation	0.014	1.253	6667	40
(8/6/2004)	Accumulation	0.024	1.222	2630	40
	Coarse	0.064	1.720	1541	40
IC5 - a	Nucleation	0.027	1.477	2813	61
(8/9/2004)	Accumulation	0.112	1.638	3353	61
	Coarse	0.253	1.176	530	61
IC5 - b	Nucleation	0.030	1.330	2949	61
(8/9/2004)	Accumulation	0.051	1.121	486	61
	Coarse	0.124	1.712	3170	61
IC5 - c	Nucleation	0.013	1.066	163	66
(8/9/2004)	Accumulation	0.035	1.479	2578	66
	Coarse	0.138	1.708	2995	66
IC6 - a	Nucleation	0.015	1.336	2287	65
(8/10/2004)	Accumulation	0.042	1.400	3856	65
	Coarse	0.141	1.663	652	65
IC6 - b	Nucleation	0.014	1.230	1881	65
(8/10/2004)	Accumulation	0.040	1.496	4381	65
	Accumulation	0.163	1.534	533	65
	Coarse	0.738	1.027	0.1	65
IC9 - a	Nucleation	0.032	1.720	11890	15
(8/16/2004)	Accumulation	0.128	1.380	1310	15
	Coarse	0.274	1.150	420	15
IC9 - b	Nucleation	0.051	1.438	8491	70
(8/16/2004)	Accumulation	0.135	1.339	1365	70
	Coarse	0.249	1.161	289	70
IC9 - c	Nucleation	0.056	1.384	7959	50
(8/16/2004)	Accumulation	0.141	1.354	1300	50
	Coarse	0.260	1.140	244	50
IC10 - a	Nucleation	0.016	1.161	469	38
(8/17/2004)	Accumulation	0.037	1.360	4702	38
	Accumulation	0.077	1.060	243	38
	Coarse	0.143	1.581	1953	38
IC10 - b	Nucleation	0.024	1.269	3577	38
(8/17/2004)	Accumulation	0.042	1.123	355	38
	Coarse	0.112	1.841	2393	38
IC11	Nucleation	0.017	1.521	1322	15
(8/18/2004)	Accumulation	0.098	1.676	2339	15
	Coarse	0.237	1.289	587	15
IC12	Nucleation	0.013	1.117	133	36
(8/21/2004)	Accumulation	0.096	1.296	206	36
	Coarse	0.082	1.728	4336	36

3.4.3 Aerosol size distribution and composition

Flight legs were first conducted below cloud base to characterize aerosol composition and size distribution, followed by constant-altitude transects through the cloud; a final pass was done at the cloud top (at 300-1000 m). The vertical profiles and horizontal transects are used to deduce cloud spatial extent and height. The under-cloud aerosol size distributions are averaged and fit to three (or four) lognormal modes (depending on the observations) using least-squares minimization. Average total aerosol concentration ranged from 4200 cm^{-3} to 13300 cm^{-3}; the distribution information for each cloud case is summarized in Table 3.3.

Whenever available (flights IC3, IC5, IC6), AMS measurements were used to describe the dry aerosol composition. The AMS always detected significant amounts of organics, constituting 35-85% of the total aerosol mass. Highest organic mass fractions were observed outside of power plant plumes (Table 3.3). The ammonium – sulfate molar ratio obtained both by the PILS and the AMS was larger than 2 for most flights (ranging from 2.0 to 3.7), except for IC5, where the ratio was 1.75. This suggests that the aerosol was neutralized in all flights except IC5. Lack of size-resolved composition precludes the detection of acidity changes throughout the aerosol distribution, but any gas-phase ammonia (for all flights except IC5) would quickly condense and neutralize acidic particles formed from in-cloud production of sulfate. The PILS analysis showed small amounts of nitrate and oxalate, the latter being generated by in-cloud oxidation of organic precursors (Sorooshian *et al.*, 2006).

It is unclear whether particulate nitrate is associated with aerosol-phase organics. When combined, nitrates and oxalate did not exceed 2% of the total (soluble + insoluble)

aerosol mass and were excluded from our analysis; a small change in the soluble fraction would not significantly impact droplet concentrations (Rissman *et al.*, 2004). Table 3.3 presents the aerosol size distribution and composition for each cloud case considered in this study.

Additional compositional insight (and its spatial variability) can be obtained from the DACAD; the hygroscopic growth factor (wet over dry aerosol diameter) during flight IC3 was ~1.17, (compared to 1.44 for pure ammonium sulfate at 77% relative humidity), characteristic of carbonaceous material with low sulfate content. Ageing of the plume downwind showed an increase in hygroscopicity, consistent with condensation of sulfates on the aerosol. The influence of the power plant plume could be detected for more than 20 miles downwind of the plant (Figure 3.4).

Representative examples of measured and fitted size distributions are shown in Figure 3.5; the discrepancy for CCN-relevant size range (larger than 30 nm) is generally small, less than 10%.

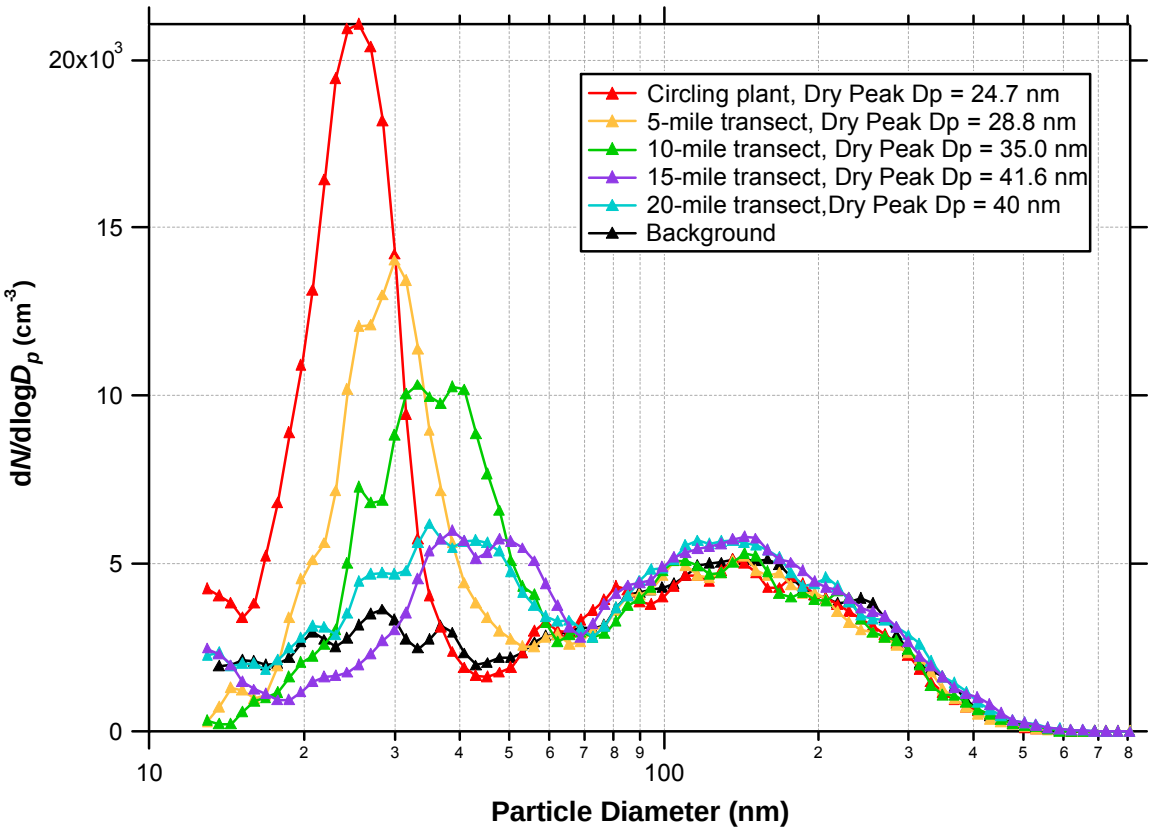

Figure 3.4: Dry aerosol size distributions for flight IC5 (Conesville power plant). Distributions are shown for plume transects downwind of the power plant.

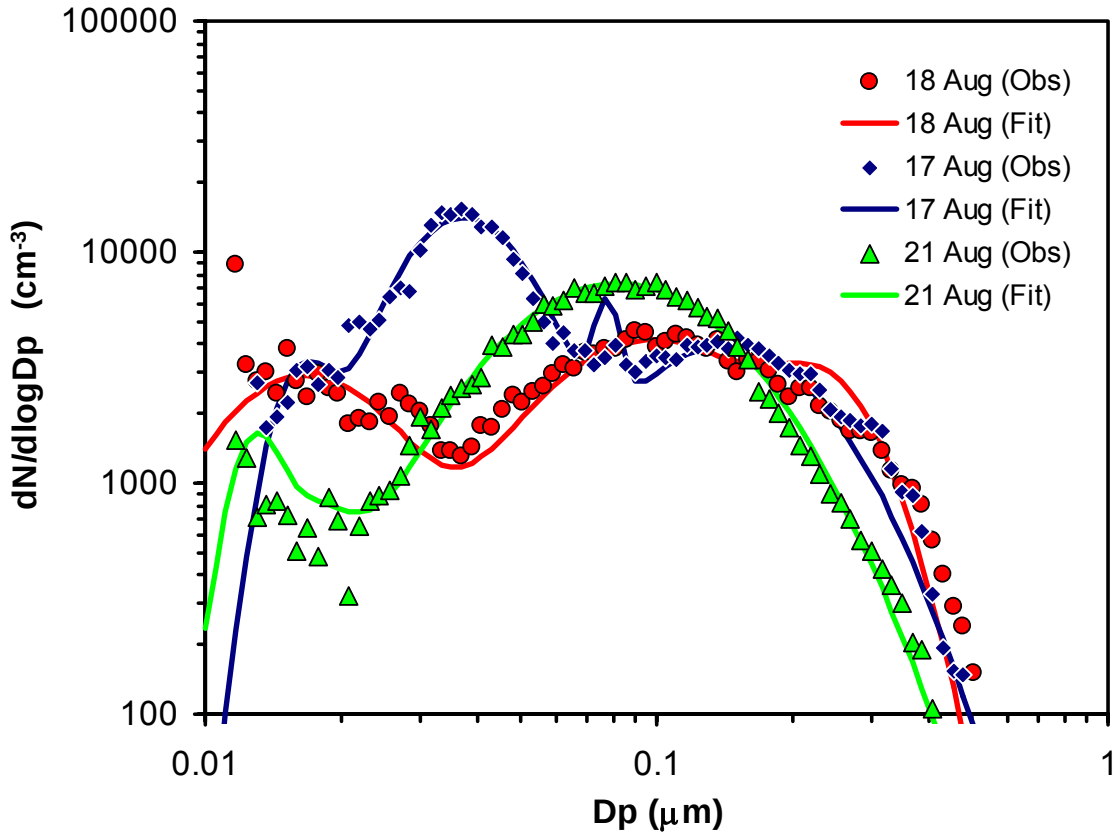

Figure 3.5: Examples of observed size distributions and corresponding lognormal fits.

3.4.4 Cloud Droplet Closure: Parcel Model

The average updraft velocity, w_+, is used to compute N_d; this was shown by Meskhidze *et al.*, (2005) to give optimal closure for cumulus and stratocumulus clouds. w_+ is defined as, $w_+ = \int_0^\infty wp(w)dw \Big/ \int_0^\infty p(w)dw$, where $p(w)$ is the vertical velocity probability density function (pdf).

For a Gaussian pdf with standard deviation ψ_w and zero average velocity, $p(w) = \frac{1}{(2\pi)^{1/2}\psi_w}\exp\left\{-\frac{w^2}{2\psi_w^2}\right\}$, and,

$$w_+ = \frac{-\frac{\psi_w}{(2\pi)^{1/2}}\int_0^\infty \exp(-x)d(-x)}{0.5} = \left(\frac{2}{\pi}\right)^{1/2}\psi_w \cong 0.8\psi_w \qquad (3.1)$$

w_+, as calculated from Eq. (3.1), is identical to the "characteristic" velocity found by Peng *et al.* (2005) used for assessing cloud droplet closure for stratocumulus clouds sampled in the North Atlantic Ocean. Eq. (3.1) is also reflected in the updraft velocity observations (Figure 3.3); σ_+, which is roughly half of ψ_w, yields after substitution into Eq. (3.1) $\sigma_+ \cong 0.65w_+$, which is consistent with the slope of Figure 3.3.

The under-cloud temperature, pressure and relative humidity describe the pre-cloud thermodynamic state of the atmosphere and are used as initial conditions for the parcel model. Aerosol observations and cloud updraft velocity are obtained from Tables 3.2 and 3.3.

It is assumed that the aerosol is internally mixed and composed of two compounds: ammonium sulfate (with density $\rho_{sul.}$ =1760 kg m^{-3}) and organic (with density $\rho_{org.}$ =1500 kg m^{-3}). The "organic" density is slightly larger than the 1200-1250 kg m^{-3} value of

Turpin and Lim, (2001) proposed for Los Angeles to account for ageing and the presence of some crustal species. For flights which AMS data were not available (i.e. IC9, IC10, IC11, IC12), the "insoluble" volume fraction, V_{ins}, was inferred by subtracting the ammonium sulfate volume, V_{sul}, (obtained from PILS measurements) from the total aerosol volume, V_{total} (obtained from size distribution measurements). The mass fraction of the insoluble material is then calculated as,

$$m_{ins.} = \frac{\rho_{org.} V_{ins.}}{\rho_{sul.} V_{sul.} + \rho_{org.} V_{ins.}} \tag{3.2}$$

The assumption that only inorganics contribute soluble mass relevant for CCN activation appears to be reasonable in CCN closure studies conducted in North America (e.g., Medina *et al.*, 2007; Broekhuizen *et al.*, 2005). Eq. (3.2) assumes uniform composition with size; this can introduce a significant amount of uncertainty in predicting CCN concentrations (e.g., Medina *et al.*, 2007; Broekhuizen *et al.*, 2005). The importance of both assumptions in cloud droplet number prediction is discussed in section 3.4.6.

The mass water vapor uptake (condensation) coefficient, a_c, needed for computing the water vapor mass transfer coefficient (Fountoukis and Nenes, 2005) is currently subject to considerable uncertainty. Li *et al*., (2001) have shown that if uptake is controlled by the accommodation of water vapor molecules onto droplets, a_c can range from 0.1 to 0.3 for pure water droplets, from 0.04 - 0.06 for aged atmospheric CCN (Shaw and Lamb, 1999; Pruppacher and Klett, 2000; Chuang, 2003; Conant *et al.*, 2004), while a recent work suggests that it should be close to unity for dilute droplets and pure water (Laaksonen *et al.*, 2004). However, ambient CCN at the point of activation are concentrated solutions composed of electrolytes and potentially organic surfactants, so other kinetic processes (e.g., solute dissolution, Asa-Awuku and Nenes, *in press*) can

slow water uptake and droplet growth, giving an uptake coefficient much less than unity (even if a_c were unity). Because of this, and following the suggestions of Shaw and Lamb (1999) and Conant *et al.*, (2004), we consider a "base case" value of a_c equal to 0.06. The dataset (Tables 3.2, 3.3) is used to determine a "best fit" value for a_c and constrain its uncertainty (section 3.4.6).

Figure 3.6 shows the cloud droplet number closure for all 27 clouds analyzed in this study. The parcel model predictions of N_d are close to the 1:1 line of perfect agreement with observations. In most cases, predictions are within 25% of the observations (average error 3.0 ± 15.4%; average absolute error 12.8 ± 8.7%), which is considerably less than the estimated N_d uncertainty of ~ 20%.

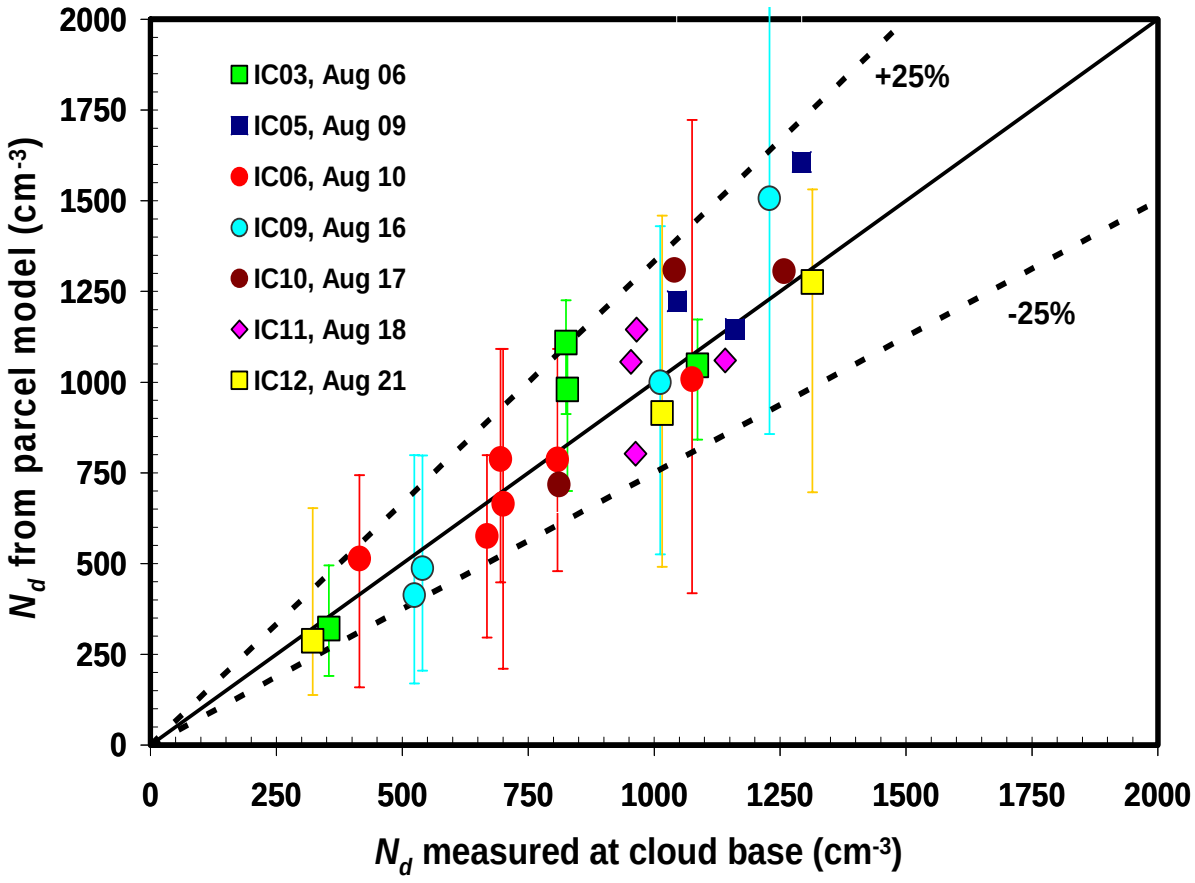

Figure 3.6: Cloud droplet number closure using the parcel model. The conditions for predicting N_d are summarized in Tables 3.2 and 3.3.

3.4.5 Cloud Droplet Closure: Modified NS Parameterization

Evaluation of the modified NS parameterization is carried out via a closure study, using the procedure outlined in section 3.4.4. The results are shown in Figure 3.7; on average, the modified NS parameterization was found to reproduce observed N_d with the same accuracy as the parcel model (average error 1.5 ± 17.9%; average absolute error 13.5 ± 11.5%). There is no systematic bias between the modeled and the observed N_d. This is remarkable, given that highly polluted clouds formed from CCN containing large amounts of organics have long been considered a challenge for any parameterization and parcel model (e.g., Conant *et al.*, 2004). This study, combined with the work of Meskhidze *et al.* (2005) clearly show that the modified NS parameterization can accurately and robustly predict the process of cloud droplet activation and reliably be used in GCM assessments of the aerosol indirect effect.

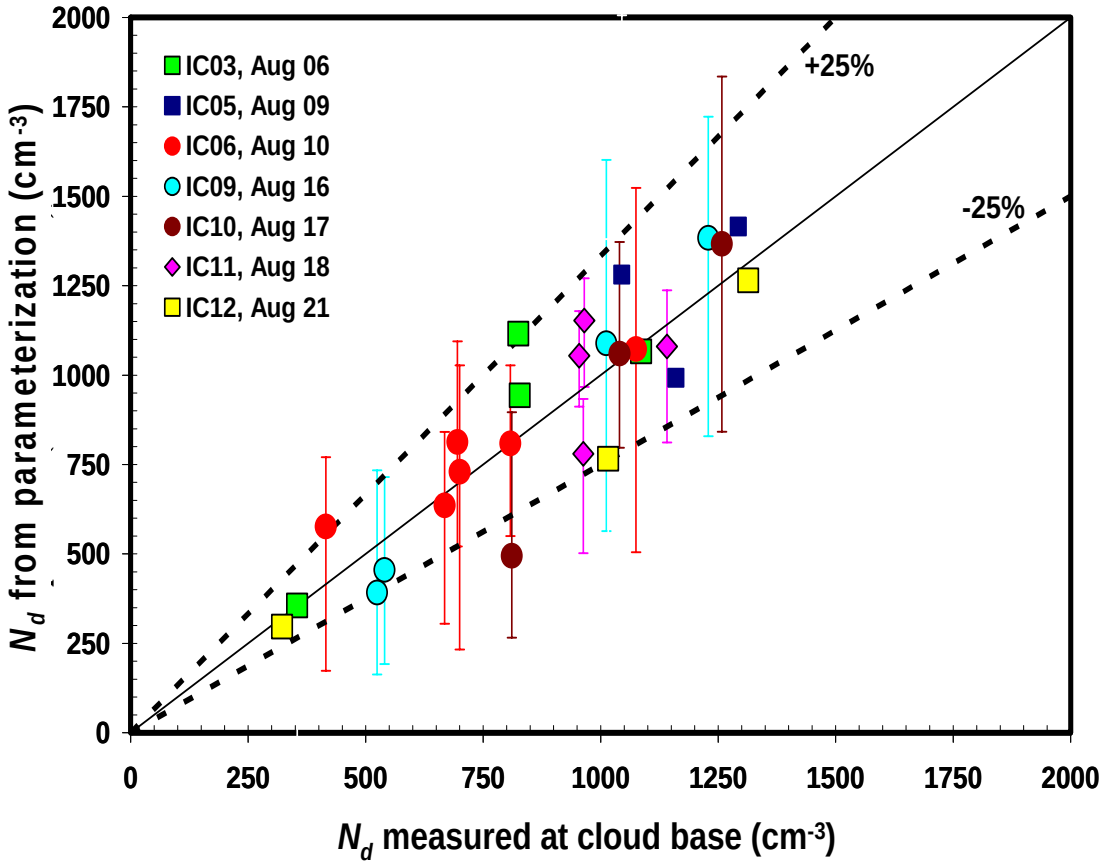

Figure 3.7: Same as Figure 3.6, but using the modified NS parameterization for predicting N_d.

Table 3.4: Correlation of droplet number error with important aerosol-cloud interaction properties. The parcel model was used for computing cloud droplet number. Strongest correlations are shown in bold.

Observed Property	Correlation Coefficient (R^2)		
	Whole dataset	**Non-power plant**	**Power plant only**
Total aerosol number	0.002	0.018	**0.111**
Accumulation mode aerosol number	0.002	0.043	**0.198**
Cloud updraft velocity	**0.358**	**0.500**	**0.209**
Updraft velocity standard deviation	**0.150**	**0.383**	0.066
Cloud droplet number	0.067	**0.343**	0.014
Aerosol sulfate mass fraction	0.025	0.036	0.014

3.4.6 Sources of uncertainty and sensitivity analyses

Despite the excellent closure, it is important to identify key contributors to N_d error (defined as the difference between predicted and measured N_d normalized to measured N_d). This is done by examining the correlation of N_d error with key parameters affecting N_d, being *i*) total aerosol number, *ii*) accumulation mode aerosol number, *iii*) average cloud-base updraft velocity, *iv*) cloud-base updraft velocity variance, *v*) observed cloud droplet number, and *vi*) aerosol sulfate mass fraction. The first two parameters are used as a proxy for pollution. The next two parameters are used as a proxy for cloud dynamics, which strongly impact cloud droplet number and its sensitivity to "chemical effects" (e.g., Nenes *et al.*, 2002; Rissman *et al.*, 2004). Sulfate mass fraction itself is a proxy for "chemical effects", as low sulfate is usually correlated with high organic content, which in turn may be water-soluble and contain surfactants. Finally, observed cloud droplet number is used to explore whether the N_d observations are subject to some concentration-dependant bias (section 3.2). Table 3.4 presents the results of the correlation analysis. When the whole dataset is considered, N_d error only correlates significantly with w_+ (R^2 in Table 3.4 is for $w_+ < 1$ m s^{-1}) and its variance. There is practically no correlation of droplet error with w_+ when it is above 1.0 m s^{-1} (roughly 50% of the dataset). The correlation of error with updraft is stronger as the w_+ decreases; this is expected as vertical velocity uncertainty becomes substantial for low updrafts. Lack of droplet error correlation with chemical composition variations is consistent with Rissman *et al.* (2004), who show droplet number is most sensitive to variations in updraft velocity under conditions of low supersaturation (i.e., strong competition for water vapor from high aerosol concentration and low updraft velocity). When considering subsets of data,

updraft velocity still correlates with droplet error (Table 3.4), more weakly ($R^2 = 0.2$) for power plant flights alone (IC3,5,6,12) and more strongly ($R^2 = 0.5$) for non-power plant plume flights (IC9,10,11). The strength of correlation is expected, as power plant clouds are more vigorous (56% have $w_+ > 1.0$, and only 6% with $w_+ < 0.25$), than non-power plant clouds (55% have $w_+ > 1.0$, and 27% with $w_+ < 0.25$).

For power plant flights alone, droplet error also correlates with aerosol number. This is likely from the temporal averaging of the aerosol size distribution; an averaged distribution cannot account for the spatial heterogeneity of the aerosol (hence droplet number) in the vicinity of power plant plumes. Therefore droplet error does not arise from the presence of very high aerosol concentrations at cloud base, but variations thereof. The observations support this hypothesis; N_d error decreases as the plume ages and dilutes to the polluted (but homogeneous) background aerosol. Despite the correlation, the droplet number variability is still small compared to the highly variable aerosol near the vicinity of a power plant plume (Figure 3.4) for two reasons: droplet number variability is inherently less than the CCN variability (Sotiropoulou *et al.*, 2006), and, clouds may not respond to aerosol variations when they take place at small particle sizes and s_{max} is not sufficiently high to activate them. The latter can be seen in Figure 3.4; most of the aerosol variability is seen in small diameters (<60nm), while droplets formed upon CCN with diameter greater than 70nm (simulations suggest that $s_{max} \sim$ 0.085%). For non-power plant plume flights (IC9,10,11), cloud droplet error correlates with cloud droplet number (but not sulfate fraction or aerosol number), which suggests the presence of minor biases in the N_d observations, which however are not significant enough to affect the closure study.

Droplet number error also arises by assuming that aerosol chemical composition is invariant with particle size. Broekhuizen *et al.*, (2005), Medina *et al.*, (2007) and Sotiropoulou et al., (2006) have shown that this assumption for polluted areas can result in up to 50% error in CCN predictions. If our dataset is subject to similar uncertainty, the resulting N_d error should range between 10 and 25% (Sotiropoulou *et al.*, 2006), well within the observational uncertainty. If organics partially dissolve and depress droplet surface tension, N_d can become less sensitive to variations in chemical composition (Rissman *et al.*, 2004).

Figure 3.8 presents the sensitivity of droplet number prediction error, averaged over the dataset, to the uptake coefficient, a_c. Figure 3.8 displays the N_d standard deviation only for the parcel model, as the parameterization exhibits roughly the same behavior. The sensitivity analysis was done using the parcel model and activation parameterization, and assuming that the organic fraction is insoluble. Assuming that the droplet number prediction error is random, our simulations indicate that the "best fit" value of a_c (i.e., the value which the average N_d error is minimal and its standard deviation lies between the measured droplet uncertainty range) is 0.06, which is in agreement with values obtained from the Conant *et al.*, (2004) and Meskhidze *et al.*, (2005) closure studies. Assuming a 20% uncertainty in observed N_d (and neglecting the N_d error standard deviation) constrains a_c between 0.03 and 1.0 (Figure 3.8). Peng et al., (2005) also obtain good closure using a much different a_c (=1) in their analysis; this does not suggest that the closure is insensitive to a_c, but rather that updraft velocity and droplet number measurements require reduction in their uncertainty (Figure 3.8) to further constrain a_c.

Finally, we assess the sensitivity of droplet closure to "chemical effects" (i.e., solubility

of the organic fraction and depression of surface tension); the focus is to assess whether different values of the uptake coefficient and organic solubility (compared with the "base case" simulations for a_c=0.06) can yield good closure.

In the sensitivity analysis, the dissolved organic was assumed to have a molar volume of 66 cm^3 mol^{-1} and a Van't Hoff factor of 1, which is consistent with properties derived from the activation of water-soluble organic carbon extracted from biomass burning samples (Personal communication, Akua Asa-Awuku, Georgia Institute of Technology, 2006). Organic solubility varied from 10^{-4} to 1 kg kg^{-1}; when surface tension is allowed to decrease, we use the correlation of Facchini *et al.*, (1999), assuming 8 mols of carbon per mol of dissolved organic (Nenes *et al.*, 2002). We also consider two values of the uptake coefficient, 0.06 and 1.0. Simulations indicate (Figure 3.9) that organic solubility less than 10^{-3} kg kg^{-1} is not enough to affect CCN (thus droplet number) concentrations. All the organic dissolves during activation when its solubility is larger than 10^{-2} kg kg^{-1}; this leads to an average increase in droplet number (error) by 10-15%, accompanied with a substantial increase in droplet error variability. If surface tension depression is included, droplet number (error) is on average increased by about 30% compared to the "base case" simulation. Surface tension depression is considered only for simulations with a_c=1.0, as a lower value would yield droplet error outside of the uncertainty range. Using a larger organic molar volume (i.e., molecular weight) would just decrease their effect on CCN activation; a lower molar volume is unlikely, given that a lower estimate was already used. The simulations suggest that combinations of organic solubility, degree of surface tension depression and uptake coefficient can give cloud droplet closure within experimental uncertainty. However, the "base case" conditions give by far the best

closure since average droplet error and its variability are within measurement uncertainty (Figure 3.9). This suggests that “chemical effects” do not considerably influence aerosol activation. The sensitivity analysis above illustrates the importance of reducing the droplet number measurement uncertainty. Based on Figure 3.9, a 10% uncertainty would further constrain the extent of “chemical effects” on cloud droplet formation.

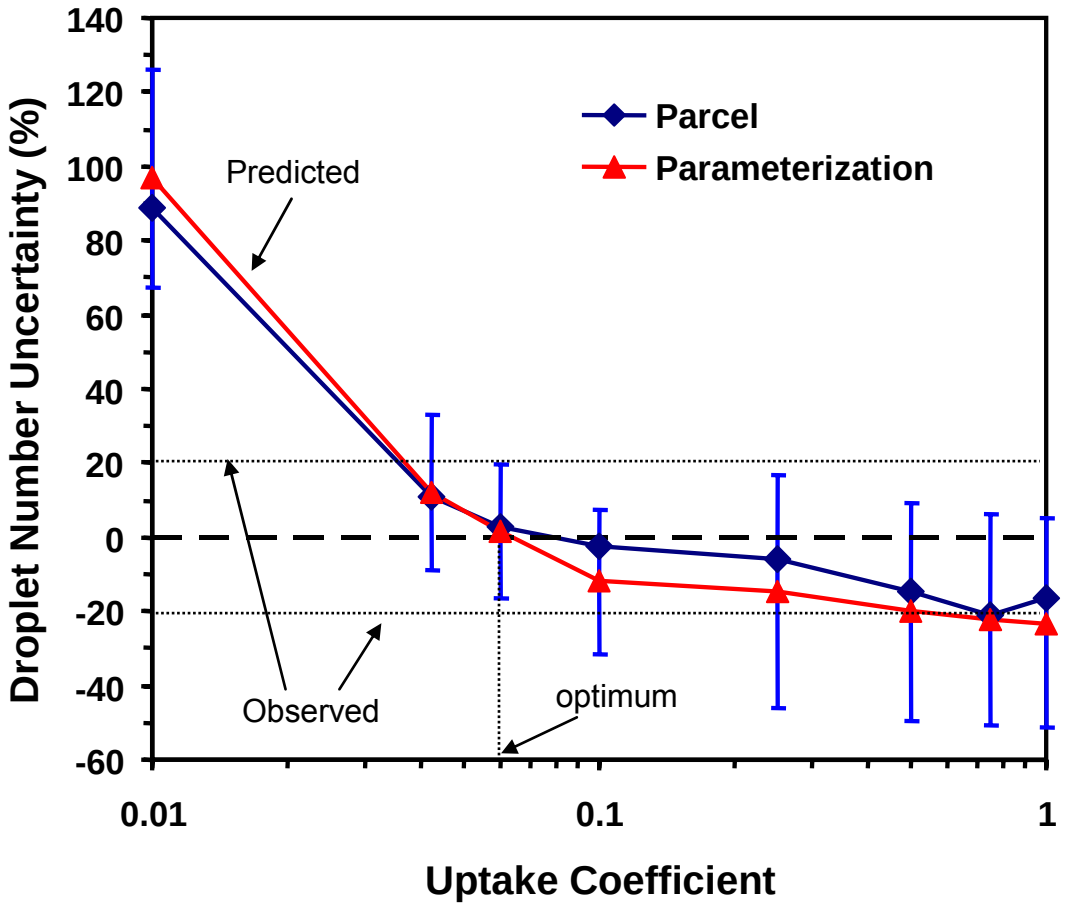

Figure 3.8: Sensitivity of droplet number error (between model and observations) to the value of the water vapor uptake coefficient.

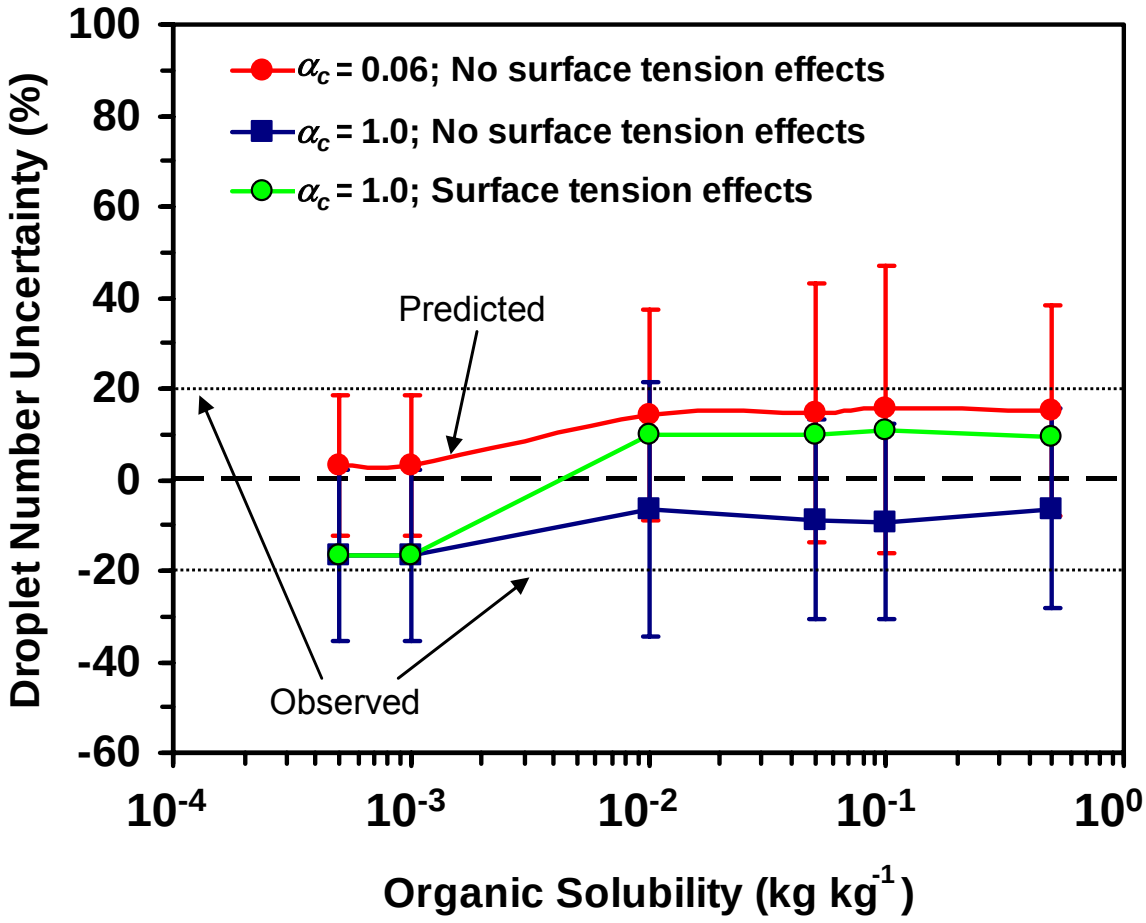

Figure 3.9: Sensitivity of droplet number error (between model and observations) to the solubility of the aerosol organic mass. The dissolved organic was assumed to have a molar volume of 66 g mol^{-1} and a Van't Hoff factor of 1.

3.5 Conclusions

This study analyzes 27 cumuliform and stratiform clouds sampled aboard the CIRPAS Twin Otter during the 2004 ICARTT (International Consortium for Atmospheric Research on Transport and Transformation). A unique feature of the dataset is the sampling of highly polluted clouds within the vicinity of power plant plumes. *In-situ* observations of aerosol size distribution, chemical composition and updraft velocity were input to *i*) a detailed adiabatic cloud parcel model (Nenes *et al.*, 2001; Nenes *et al.*, 2002), and, *ii*) the modified NS parameterization (Fountoukis and Nenes, 2005; Nenes and Seinfeld, 2003); predicted droplet number is then compared with the observations. Remarkable closure was achieved (on average to within 10%) for parcel model and parameterization. The error in predicted cloud droplet concentration was found to correlate mostly with updraft velocity. Aerosol number also correlated with droplet error for clouds affected by power plant plumes (which is thought to stem from spatial variability of the aerosol not considered in the closure). Finally, we assess the sensitivity of droplet closure to "chemical effects". A number of important conclusions arise from this study:

1. Cloud droplet number closure is excellent even for the highly polluted clouds downwind of power plant plumes. Droplet number error does not correlate with background pollution level, only with updraft velocity and aerosol mixing state.
2. A highly variable aerosol does not necessarily imply a highly variable N_d concentration. The clouds in this study often do not respond to aerosol variations because they take place primarily at small particle sizes, and cloud s_{max} is not high enough to activate them. Any droplet variability that does arise is inherently less than

the CCN variability it originated from (Sotiropoulou *et al.*, 2006).

3. Usage of average updraft velocity is appropriate for calculating cloud droplet number.
4. The water vapor uptake coefficient ranges between 0.03 and 1.0. Optimum closure (for which average N_d error is minimal and its standard deviation is within droplet measurement uncertainty) is obtained when the water vapor uptake coefficient is about 0.06. This agrees with values obtained from previous closure studies for polluted stratocumulus (Meskhidze *et al.*, 2005) and marine cumulus clouds (Conant *et al.*, 2004).
5. On average, organic species do not seem to influence activation through contribution of solute and surface tension depression. Optimal cloud droplet closure is obtained if the CCN are approximated by a combination of soluble inorganics and partially-soluble organics (less than 1 g kg^{-1} water assuming a molar volume of 66 cm^3 mol^{-1} and a Van't Hoff factor of 1).
6. The cloud droplet activation parameterization used in this study (Nenes and Seinfeld, 2003; Fountoukis and Nenes 2005) has performed as well as the detailed cloud parcel model. Excellent performance has also been reported by Meskhidze *et al.*, (2005). Together, both studies suggest that the parameterization can robustly be used in GCM assessments of the aerosol indirect effect.
7. Distinguishing the "chemical effects" on the cloud droplet spectrum requires the observational uncertainty to be of order 10%.

The above conclusions can serve as much needed constraints for the parameterization of aerosol-cloud interactions in the North America. Future *in-situ* studies will determine the robustness of our findings.

3.6 Acknowledgements

We acknowledge the support of the National Science Foundation under award ATM-0340832. C.F., A.N. and N.M. acknowledge support from an NSF CAREER award, a NASA EOS-IDS and a NASA NIP. C.F. acknowledges support from a Gerondelis Foundation Fellowship.

3.7 References

Andreae, O. M., Jones, C.D., and Cox, P.M.: Strong present - day aerosol cooling implies a hot future, Nature, 435, 1187 - 1190, 2005.

Asa-Awuku, A., and Nenes, A.: The Effect of Solute Dissolution Kinetics on Cloud Droplet Formation: 1. Extended Köhler Theory, J. Geophys. Res., in press.

Bahreini, R., Jimenez, J.L., Wang, J., Flagan, R.C., Seinfeld, J.H., Jayne, J.T., and Worsnop, D.R.: Aircraft-based aerosol size and composition measurements during ACE-Asia using an Aerodyne aerosol mass spectrometer, J. Geophys. Res., 108, D8645, 2003.

Baumgardner, D., Jonsson, H., Dawson, W., O'Connor, D., and Newton, R.: The cloud, aerosol and precipitation spectrometer: A new instrument for cloud investigations, Atmos. Res., 60, 251-264, 2001.

Baumgardner, D., and Spowart, M.: Evaluation of the Forward Scattering Spectrometer Probe. Part III: Time response and laser inhomogeneity limitations, J. Atmos. Oceanic Technol., 7, 666 - 672, 1990.

Boucher, O., and Lohmann, U.: The sulfate-CCN-cloud albedo effect-A sensitivity study with 2 general-circulation models, Tellus, Ser. B, 47, 281 - 300, 1995.

Brasseur, G.P., and Roeckener, E.: Impact of improved air quality on the future evolution of climate, Geoph. Res. Let., 32, L23704, doi:10.1029/2005GL023902, 2005.

Brenguier, J.-L.: Coincidence and deadtime corrections for particle counters. Part II: High concentration measurements with an FSSP, J. Atmos. Oceanic Technol., 6, 575-584, 1989.

Brenguier, J.-L., Bourrianne, T., Coelho, A., Isbert, J., Peytavi, R., Trevarin, D., and Weschler, P.: Improvements of droplet size distribution measurements with the Fast-FSSP (Forward Scattering Spectrometer Probe). J. Atmos. Oceanic Technol., 15, 1077-1090, 1998.

Broekhuizen, K., Chang, R.Y.-W., Leaitch, W.R., Li, S.-M., and Abbatt, J.P.D.: Closure between measured and modeled cloud condensation nuclei (CCN) using size-resolved aerosol compositions in downtown Toronto, Atmos. Chem. Phys. Discuss., 5, 6263-6293, 2005.

Burnet, F., and Brenguier, J.-L.: Comparison between standard and modified forward scattering spectrometer probes during the small cumulus microphysics study, J. Atmos. Oceanic Technol., 19, 1516 – 1531, 2002.

Chuang, P.: Measurement of the timescale of hygroscopic growth for atmospheric aerosols, J. Geophys. Res., 108 (D9), 4282, doi:10.1029/2002JD002757, 2003.

Chuang, P.Y., Collins, D.R., Pawlowska, H., Snider, J.R., Jonsson, H.H., Brenquier, J.L., Flagan, R.C., and Seinfeld, J.H.: CCN measurements during ACE-2 and their relationship to cloud microphysical properties, Tellus, 52B, 843-867, 2000.

Chuang, C.C., and Penner, J.E.: Effects of anthropogenic sulfate on cloud drop nucleation and optical properties, Tellus B, 47, 566-577, 1995.

Considine, G., and Curry, J.A.: Effects of entrainment and droplet sedimentation on the microphysical structure of stratus and stratocumulus clouds, Q. J. R. Meteorol. Soc. 124, 123-150, 1998.

Conant, W.C., VanReken, T.M., Rissman, T.A., Varutbangkul, V., Jonsson, H.H., Nenes, A., Jimenez, J.L., Delia, A.E., Bahreini, R., Roberts, G.C., Flagan, R.C. and Seinfeld, J.H.: Aerosol–cloud drop concentration closure in warm cumulus, J. Geophys. Res., 109, D13204, doi:10.1029/2003JD004324, 2004.

Facchini, M., Mircea, M., Fuzzi, S., and Charlson, R.: Cloud albedo enhancement by surface-active organic solutes in growing droplets, Nature, 401, 257-259, 1999.

Feingold, G., and Chuang, P.Y.: Analysis of the influence of film-forming compounds on droplet growth: Implications for cloud microphysical processes and climate, J. Atmos. Sci., 59, 2006–2018, 2002.

Fountoukis, C., and Nenes, A.: Continued development of a cloud droplet formation parameterization for global climate models, J. Geophys. Res., 110, D11212, doi:10.1029/2004JD005591, 2005.

Fountoukis, C., Nenes, A., Meskhidze, N., Bahreini, R., Conant, W., Jonsson, H., Murphy, S., Sorooshian, A., Varutbangkul, V., Brechtel, F., Flagan, R., and Seinfeld, J.: Aerosol–cloud drop concentration closure for clouds sampled during the International Consortium for Atmospheric Research on Transport and Transformation 2004 campaign, J. Geophys. Res., 112, D10S30, doi:10.1029/2006JD007272, 2007.

Ghan, S.J., Easter, R., Chapman, E., Abdul-Razzak, H., Zhang, Y., Leung, L., Laulainen, N., Saylor, R., and Zaveri, R.: A physically-based estimate of radiative forcing by anthropogenic sulfate aerosol, J. Geophys. Res., 106, 5279 – 5293, 2001a.

Ghan, S.J., Laulainen, N., Easter, R., Wagener, R., Nemesure, S., Chapman, E., Zhang, Y., and Leung, R.: Evaluation of aerosol indirect forcing in MIRAGE. J. Geophys. Res., 106, 5317-5334, 2001b.

Gultepe, I., and Isaac, G.: The relationship between cloud droplet and aerosol number concentrations for climate models, Int. J. Climatol., 16, 941-946, 1996.

Hallberg, A., Wobrock, W., Flossmann, A.I., Bower, K.N., Noone, K.J., Wiedensohler, A., Hansson, H.C., Wendisch, M., Berner, A., Kruisz, C., Laj, P., Facchini, M.C., Fuzzi, S., and Arends, B.G.: Microphysics of clouds: Model versus measurements, Atmos. Environ., 31, 2453-2462, 1997.

Jaenicke, R., and Hanusch, T.: Simulation of the optical-particle counter forward scattering spectrometer probe-100 (FSSP-100) - consequences for size distribution measurements, Aerosol Sci. Technol., 18 (4), 309-322, 1993.

Jayne, J.T., Leard, D.C., Zhang, X., Davidovits, P., Smith, K.A., Kolb, C.E., and Worsnop, D.: Development of an aerosol mass spectrometer for size and composition analysis of submicron particles, Aerosol Sci. Technol., 33, 49-70, 2000.

Jensen, J.B., and Charlson, R.J.: On the efficiency of nucleation scavenging, Tellus B, 36, 367-375, 1984.

Jones, A., Roberts, D.L., and Slingo, A.: A climate model study of indirect radiative forcing by anthropogenic sulphate aerosols, Nature, 370, 450-453, 1994.

Khairoutdinov, M., Randall, D., and DeMott, C.: Simulations of the Atmospheric General Circulation Using a Cloud-Resolving Model as a Superparameterization of Physical Processes, J. Atmos. Sci., 62 (7), 2136-2154, 2005.

Kiehl, J.T., Schneider, T.L., Rasch, P.J., Barth, M.C., and Wong, J.: Radiative forcing due to sulfate aerosols from simulations with the NCAR Community Climate Model, J. Geophys. Res., 105, 1441-1457, 2000.

Laaksonen, A., Vesala, T.. Kulmala, M., Winkler, P.M., and Wagner, P.E.: On cloud modeling and the mass accommodation coefficient of water, Atmos. Chem. Phys. Discuss., 4, 7281-7290, 2004.

Lance, S., Nenes, A., and Rissman, T.: Chemical and dynamical effects on cloud droplet number: Implications for estimates of the aerosol indirect effect, J. Geophys. Res., 109, D22208, doi:10.1029/2004JD004596, 2004.

Li, Y.Q., Davidovits, P., Shi, Q., Jayne, J.T., and Warsnop, D.R.: Mass and thermal accommodation coefficients of $H_2O_{(g)}$ on liquid water as a function of temperature, J. Phys. Chem. A, 105, 10,627-10,634, 2001.

Lohmann, U., and Feichter, J.: Impact of sulfate aerosols on albedo and lifetime of clouds: A sensitivity study with the ECHAM4 GCM, J. Geophys. Res., 102, 13,685-13,700, 1997.

Lohmann, U., Feichter, J., Chuang, C.C., and Penner, J.E.: Predicting the number of cloud droplets in the ECHAM GCM, J. Geophys. Res., 104, 9169-9198, 1999.

Lohmann, U., Feichter, J., Penner, J.E., and Leaitch, R.: Indirect effect of sulfate and carbonaceous aerosols: A mechanistic treatment, J. Geophys. Res., 105, 12,193-12,206, 2000.

Lohmann, U., and Feichter, J., Global indirect aerosol effects: a review, Atmos. Chem. Phys. Discuss., 4, 7561-7614, 2004.

Medina, J., Nenes, A., Cottrell, L., Beckman, P.J., Ziemba, L.D., Griffin, R.: Cloud Condensation Nuclei (CCN) closure on New England ambient aerosol during the ICARTT 2004 field campaign: a) effects of size-dependent composition, J.Geoph.Res., **112**, D10S31, doi:10.1029/2006JD007588, 2007.

Menon, S., DelGenio, A.D., Koch, D., and Tselioudis, G.: GCM Simulations of the Aerosol Indirect Effect: Sensitivity to Cloud Parameterization and Aerosol Burden, J. Atmos. Sci., 59, 692-713, 2002.

Meskhidze, N., Nenes, A., Conant, W.C., and Seinfeld, J.H.: Evaluation of a new cloud droplet activation parameterization with in situ data from CRYSTAL-FACE and CSTRIPE, J. Geophys. Res., 110, D16202, doi:10.1029/2004JD005703, 2005.

Nenes, A., and Seinfeld, J.H.: Parameterization of cloud droplet formation in global climate models, J. Geophys. Res., 108, 4415, doi:10.1029/2002JD002911, 2003.

Nenes, A., Charlson, R.J., Facchini, M.C., Kulmala, M., Laaksonen, A., and Seinfeld, J.H.: Can chemical effects on cloud droplet number rival the first indirect effect?, Geophys. Res. Lett., 29 (17), 1848, doi:10.1029/ 2002GL015295, 2002.

Nenes, A., Ghan, S., Abdul-Razzak, H., Chuang, P., and Seinfeld, J.: Kinetic limitations on cloud droplet formation and impact on cloud albedo, Tellus, Ser. B, 53, 133-149, 2001.

Peng, Y., Lohmann, U., Leaitch, R., Banic, C., and Couture, M.: The cloud albedo-cloud droplet effective radius relationship for clean and polluted clouds from RACE and FIRE.ACE, J. Geophys. Res., 107, doi:10.029/2000JD000281, 2002.

Peng, Y., Lohmann, U., and Leaitch, R.: Importance of vertical velocity variations in the cloud droplet nucleation process of marine stratus clouds, J. Geophys. Res., 110,

D21213, doi:10.1029/2004JD004922, 2005.

Pruppacher, H.R., and Klett, J.D.: Microphysics of Clouds and Precipitation, Springer, New York, 2000.

Randall, D., Khairoutdinov, M., Arakawa, A., and Grabowski, W., Breaking the Cloud Parameterization Deadlock, Bulletin of the American Meteorological Society, 84 (11), 1547-1564, 2003.

Rissman, T., Nenes, A., and Seinfeld, J.H.: Chemical amplification (or dampening) of the Twomey effect: Conditions derived from droplet activation theory, J. Atmos. Sci., 61 (8), 919-930, 2004.

Rotstayn, L.D., and Penner, J.E.: Indirect aerosol forcing, quasi-forcing, and climate response, J. Climate, 14, 2960-2975, 2001.

Shaw, R.A., and Lamb, D.: Experimental determination of the thermal accommodation and condensation coefficients of water, J. Chem. Phys., 111, 10,659-10,663, 1999.

Shulman, M.L., Jacobson, M.C., Charlson, R.J., Synovec, R.E., and Young, T.E.: Dissolution behavior and surface tension effects of organic compounds in nucleating cloud droplets, Geophys. Res. Lett., 23, 277-280, 1996.

Snider, J.R., and Brenguier, J.L.: Cloud condensation nuclei and cloud droplet measurements during ACE-2, Tellus, Ser. B, 52, 827-841, 2000.

Snider, J.R., Guibert, S., Brenguier, J.-L., and Putaud, J.-P.: Aerosol activation in marine stratocumulus clouds: 2. Köhler and parcel theory closure studies, J. Geophys. Res., 108(D15), 8629, doi:10.1029/2002JD002692, 2003.

Sorooshian, A., Brechtel, F.J., Ma, Y., Weber, R.J., Corless, A., Flagan, R.C., and Seinfeld, J.H.: Modeling and Characterization of a Particle-into-Liquid Sampler (PILS), Aerosol Sci. Tech ., 40, 396-409, 2006.

Sorooshian, A., Varutbangkul, V., Brechtel, F.J., Ervens, B., Feingold, G., Bahreini, R., Murphy, S.M., Holloway, J.S., Atlas, E.L., Buzorius, G., Jonsson, H., Flagan, R.C.,

and Seinfeld, J.H.: Oxalic Acid in Clear and Cloudy Atmospheres: Analysis of Data from International Consortium for Atmospheric Research on Transport and Transformation 2004, J. Geophys. Res., 111, D23S45, doi:10.1029/2005JD006880, 2006.

Sotiropoulou, R.E.P., Medina, J., and Nenes, A.: CCN predictions: Is theory sufficient for assessments of the indirect effect?, Geoph. Res. Let., 33**,** L05816, doi:10.1029/2005 GL025148, 2006.

Turpin, B.J., and Lim, H.: Species Contributions to PM2.5 Mass Concentrations: Revisiting Common Assumptions for Estimating Organic Mass, Aerosol Sci. Tech., 35, 602-610, 2001.

Wang, J., Flagan, R.C., and Seinfeld, J.H.: A differential mobility analyzer (DMA) system for submicron aerosol measurements at ambient relative humidity, Aerosol Sci. Tech., 37, 46-52, 2003.

CHAPTER 4

A THERMODYNAMIC EQUILIBRIUM MODEL FOR MULTIPHASE MULTICOMPONENT INORGANIC AEROSOLS[I]

4.1 Abstract

This study presents ISORROPIA II, a thermodynamic equilibrium model for the K^+ – Ca^{2+} – Mg^{2+} – NH_4^+ – Na^+ – SO_4^{2-} – NO_3^- – Cl^- – H_2O aerosol system. A comprehensive evaluation of its performance is conducted against the thermodynamic module SCAPE2 over a wide range of atmospherically relevant conditions. The two models overall agree well, to within 13% for aerosol water content and total PM mass, 16% for aerosol nitrate and 6% for aerosol chloride and ammonium. Largest discrepancies were found under conditions of low RH, primarily from differences in the treatment of water uptake and solid state composition. In terms of computational speed, ISORROPIA II was always found to be more than an order of magnitude faster than SCAPE2, with robust and rapid convergence under all conditions. The addition of crustal species does not slow down the thermodynamic calculations (compared to the older ISORROPIA code) because of optimizations in the activity coefficient calculation algorithm. Based on its computational rigor and performance, ISORROPIA II appears to be a highly attractive alternative for use in large scale air quality and atmospheric transport models.

[I] Under review: Fountoukis, C., and Nenes, A.: ISORROPIA II: A computationally efficient thermodynamic equilibrium model for K^+-Ca^{2+}-Mg^{2+}-NH_4^+-Na^+-SO_4^{2-}-NO_3^--Cl^--H_2O aerosols, Atmos. Chem. Phys. Discuss., 7, 1893-1939, 2007.

4.2 Introduction

Aerosols, or airborne particulate matter (PM), play a central role in atmospheric processes. They reflect a significant amount of radiation back to space, thus enhancing the planetary albedo. Atmospheric aerosols can cause visibility impairment in highly polluted areas (Altshüller, 1984) through their interactions with electromagnetic radiation. By acting as cloud condensation nuclei (CCN), they affect cloud droplet number concentration, cloud droplet effective radius, and cloud reflectivity. Changes in aerosol concentrations also affect droplet size distribution affecting precipitation frequency and cloud lifetime. Aerosols can also be responsible for acid rain production, which can adversely affect soil and water quality, especially in environments rich in SO_2 and NO_x. It has been established that inhaled aerosol particles are detrimental to human health; as particles can contain toxic inorganic and organic substances that are often correlated with asthma and chronic obstructive pulmonary disease (Zanobetti et al., 2000; Ramachandran and Vincent, 1999; Brauer and Brook, 1997; Schwartz, 1994). Recent studies (Kaiser, 2005) have suggested that fine particles ($PM_{2.5}$) are more effective in causing respiratory illness and premature death than larger particles due to their ability to penetrate deeper into the lung. Dockery et al., (1993), who conducted a survey on six cities over 16 years, found that people living in areas with higher aerosol concentrations had a lifespan two years less than those living in cleaner areas. The knowledge of the chemical composition and physical state of atmospheric particles may be a critical link between toxicity and particulate matter.

Atmospheric aerosols are composed of water, inorganic salts, crustal material, organics

and trace metals. A large part of the particle (dry) mass is inorganic (25-50 %) with ammonium (NH_4^+), sodium (Na^+), sulfate (SO_4^{2-}), bisulfate (HSO_4^-), nitrate (NO_3^-) and chloride (Cl^-) being the most important contributors to the dry inorganic $PM_{2.5}$ (Heitzenberg, 1989). Crustal species, such as Ca^{2+}, K^+, Mg^{2+} are a major component of dust, hence an important constituent of ambient particles. These inorganic species may be in the form of aqueous ions, or in the form of precipitated solids, in thermodynamic equilibrium with atmospheric gases and humidity.

To compute the composition and phase state of aerosols, every atmospheric gas/aerosol model requires knowledge of the thermodynamic equilibrium state because the driving force for mass transfer of species between gas and aerosol phases is the departure from equilibrium. Performing thermodynamic equilibrium calculations for aerosol systems is a demanding computational task (e.g., Nenes et al., 1999) because it involves the global optimization of a nonlinear convex problem, or, the solution of numerous nonlinear equations. At low relative humidities aqueous aerosol solutions are highly concentrated (i.e., have a high ionic strength). Under these conditions the solutions may behave non-ideally. This non-ideality can be modeled with activity coefficients (which increases computational cost). Therefore, efficient and accurate solution algorithms are highly needed.

Numerous aerosol inorganic equilibrium models have been developed over the years, differing in the chemical species that they can treat, the solution method used and the type of input they can accept. Recent examples include AIM2 (Clegg and Pitzer, 1992; Clegg et al., 1992, 1994, 1995, 1998a,b; Wexler and Clegg, 2002), SCAPE2 (Kim et al., 1993a,b; Kim and Seinfeld, 1995; Meng et al., 1995), EQUISOLV II (Jacobson et al.,

1996; Jacobson, 1999a,b), ISORROPIA (Nenes et al., 1998; Nenes et al., 1999), GFEMN (Ansari and Pandis, 1999a,b), EQSAM2 (Metzger et al., 2002a,b; Metzger et al., 2006), HETV (Makar et al., 2003), MESA (Zaveri et al., 2005a,b) and UHAERO (Amundson et al., 2006). AIM2 and GFEMN use the iterative Gibbs free energy minimization method to solve equilibrium problems for $NH_4^+/Na^+/NO_3^-/SO_4^{-2}/Cl^-$ systems. UHAERO uses the Gibbs free energy minimization method (using a primal-dual method, coupled to a Newton iteration method) and offers a choice of the Pitzer, Simonson, Clegg (PSC) mole fraction-based model (Pitzer and Simonson, 1986; Clegg and Pitzer, 1992; Clegg et al., 1992) or the ExUNIQUAC model (Thomsen and Rasmussen, 1999) for the activity coefficient calculations. These models treat either the ammonium – nitrate – sulfate system or the ammonium – sodium – nitrate – chloride – sulfate system. MESA simultaneously iterates for all solid-liquid equilibria using a pseudo-transient continuation method and solves for the $NH_4^+/Na^+/NO_3^-/SO_4^{-2}/Cl^-$ system of species with the addition of calcium cations. EQUISOLV II sequentially solves for the root of each equation in the system of equilibrium reactions and then iterates over the entire domain until convergence. This method is ideal for the incorporation of new reactions and species with minimal programming effort, but optimal computational performance is obtained only on vectorized computational platforms (Zhang et al., 2000). EQSAM2 considers activity coefficients for (semi-) volatile compounds according to Metzger et al. (2002a) to solve the $NH_4^+/Na^+/NO_3^-/SO_4^{2-}/Cl^-/Ca^{2+}/Mg^{2+}/K^+/RCOO^-$ system; earlier versions of EQSAM2 were based on a simplified parameterization of the non-ideal solution properties that employed a relationship between activity coefficients and relative humidity (Metzger et al., 1999) and excluded mineral cations and organic acids. In

comparison, EQSAM3 applies the thermodynamic principles as described in Metzger and Lelieveld (2007). SCAPE2 divides the problem into several subdomains based on major species that impact equilibrium partitioning and water uptake. By always attempting to solve for a liquid phase, SCAPE2 predicts the presence of water even at very low ambient relative humidities (<10%), and for this reason often does not predict the presence of a crystalline phase (solid precipitate).

Similar to SCAPE2, ISORROPIA determines the subsystem set of equilibrium equations and solves for the equilibrium state using the chemical potential method. The code solves analytically as many equations as possible through successive substitutions; remaining equilibrium reactions are solved numerically with bisection for stability. ISORROPIA also offers the choice of using precalculated tables of binary activity coefficients and water activities of pure salt solutions, which speeds up calculations. Another important feature of the model is the use of mutual deliquescence of multicomponent salt particle solutions, which lowers the deliquescence point of the aerosol phase. Besides the forward problem (in which total (gas + aerosol) concentrations of chemical species along with ambient temperature and relative humidity are used as input), ISORROPIA also offers the ability to solve for the "reverse problem", in which known quantities are the concentrations of sodium, ammonium, nitrate and sulfate in the aerosol phase together with the ambient temperature and relative humidity. The output of the reverse problem is (as in the forward problem) the concentration of species in solid, liquid and gas phase. Being computationally efficient, ISORROPIA has proved to be the model of choice for many three-dimensional air quality models (CMAQ, PMCAMx, etc.), chemical transport and general circulation models (Ansari and Pandis, 1999b; Yu et al., 2005). HETV is

based on the algorithms of ISORROPIA for sulfate, nitrate and ammonium aerosol systems and is optimized for running on vectorized computational architectures.

An important drawback of the above codes (with the exception of SCAPE2, EQUISOLV II and EQSAM2) is lack of treatment of crustal species (Ca, K, Mg). It has been shown (Jacobson, 1999b; Moya et al., 2001b) that the inclusion of crustal species in a thermodynamic equilibrium framework can be important in modeling size/compositional distribution of inorganic aerosols. An attempt to treat crustal species as "equivalent sodium" was met with modest success (Moya et al., 2001a) provided that Ca was a relatively small fraction of aerosol dry mass.

In the current study, we present a new model, "ISORROPIA II", in which the thermodynamics of the crustal elements of calcium, potassium and magnesium have been added to the preexisting suite of components of the computationally efficient ISORROPIA. The new model, combining the computational advances with the explicit thermodynamics of crustal species, is compared against the predictions of SCAPE2, both in terms of speciation and computational requirements.

4.3 Thermodynamic equilibrium calculations

4.3.1 Equilibrium constants

In a closed (aerosol-gas phase) system composed of *i* chemical species and *j* reactions at constant temperature *T*, and pressure *P*, the Gibbs free energy of the system, *G*, is minimum at chemical equilibrium. This condition is equivalent to stating that the system of reactants is equal to that of products, which can be written as (Nenes et al., 1998):

$$\prod_i a_i^{\nu_{ij}} = K_j(T) \tag{4.1}$$

where a_i is the activity of species i, ν_{ij} is the stoichiometric coefficient of species i participating in the reaction j, and K_j is the equilibrium constant of the j-th reaction at temperature T,

$$K_j(T) = \exp\left[-\frac{\sum_i \nu_{ij}\mu_i^o(T)}{RT}\right] \tag{4.2}$$

where R is the universal gas constant and $\mu_i^o(T)$ is the standard chemical potential of species i at 1 atm pressure and temperature T (in K).

K_j is a function of temperature according to the Van't Hoff equation:

$$\frac{d\ln K(T)}{dT} = \frac{\Delta H^o(T)}{RT^2} \tag{4.3}$$

where $\Delta H^o(T)$ is the enthalpy change of the reaction at temperature T (Denbigh, 1981). For a small temperature range, $\Delta H^o(T)$ can be approximated by:

$$\Delta H^o(T) = \Delta H^o(T_o) + \Delta c_p^o(T - T_o) \tag{4.4}$$

where $\Delta c_P^o(T)$ is the change of molar heat capacity of products minus reactants. By substituting Eq. (4.4) into Eq. (4.3) and integrating from a reference temperature T_0 (typically at 298.15 K) to T, we obtain:

$$K(T) = K_o \exp\left[-\frac{\Delta H^o(T_o)}{RT_o}\left(\frac{T_o}{T} - 1\right) - \frac{\Delta c_p^o}{R}\left(1 + \ln\left(\frac{T_o}{T}\right) - \frac{T_o}{T}\right)\right] \tag{4.5}$$

where K_o is the equilibrium constant at T_o.

4.3.2 Activity of species

The activity of species i, a_i, if an ideal gas, is equal to its partial pressure ($a_i = p_i$) (Seinfeld and Pandis, 1998). If ij is an electrolyte species dissolved in water,

$a_{ij} = (m_i\gamma_i)^{\nu_i}(m_j\gamma_j)^{\nu_j}$, where γ_{ij} is the activity coefficient of an electrolyte species *ij* in water, ν_i and ν_j are the moles of cations and anions, respectively, released per mole of electrolyte and m_i, m_j are their molalities, respectively. The activity of each solid phase species is assumed to be unity.

4.3.3 Activity coefficients

In ISORROPIA II, the multicomponent activity coefficients, γ_{12} for each ionic pair 1-2 are computed using Bromley's formula (Bromley, 1973),

$$\log\gamma_{12} = -A_\gamma \frac{z_1 z_2 I^{1/2}}{1+I^{1/2}} + \frac{z_1 z_2}{z_1+z_2}\left[\frac{F_1}{z_1}+\frac{F_2}{z_2}\right] \tag{4.6}$$

where γ_{12} is the mean activity coefficient of cation 1 and anion 2 at 298.15K, A_γ is the Debye-Hückel constant (0.511 $kg^{0.5}$ $mol^{-0.5}$ at 298.15 K) and,

$$F_1 = Y_{21}\log\gamma_{12}^o + Y_{41}\log\gamma_{14}^o + Y_{61}\log\gamma_{16}^o + \ldots + \frac{A_\gamma I^{1/2}}{1+I^{1/2}}\left[z_1 z_2 Y_{21} + z_1 z_4 Y_{41} + z_1 z_6 Y_{61} + \ldots\right] \tag{4.7}$$

$$F_2 = X_{12}\log\gamma_{12}^o + X_{32}\log\gamma_{32}^o + X_{52}\log\gamma_{52}^o + \ldots + \frac{A_\gamma I^{1/2}}{1+I^{1/2}}\left[z_1 z_2 X_{12} + z_3 z_2 X_{32} + z_5 z_2 X_{52} + \ldots\right] \tag{4.8}$$

where *odd* subscripts refer to cations and *even* subscripts refer to anions, $Y_{21} = \left(\frac{z_1+z_2}{2}\right)^2 \frac{m_2}{I}$, $X_{12} = \left(\frac{z_1+z_2}{2}\right)^2 \frac{m_1}{I}$, z_i is the absolute charge of ionic species *i*, and γ_{ij}^o is the mean ionic activity coefficient of the binary pair *i-j* ("binary" activity coefficient) computed at the ionic strength of the multicomponent solution, *I*, $I = \frac{1}{2}\sum_i m_i z_i^2$.

Following the recommendations of Kim et al., (1993), binary activity coefficients, γ_{12}^o, are calculated using the Kusik-Meissner relationship (Kusik and Meissner, 1978),

$$\log \gamma_{12}^{o} = z_1 z_2 \log \Gamma^{o} \tag{4.9}$$

where

$$\Gamma^{o} = \left[1 + B(1 + 0.1I)^{q} - B\right]\Gamma^{*} \tag{4.10}$$

$$B = 0.75 - 0.065q \tag{4.11}$$

$$\log \Gamma^{*} = \frac{-0.5107 I^{1/2}}{1 + CI^{1/2}} \tag{4.12}$$

$$C = 1 + 0.055q \exp\left(-0.023 I^{3}\right) \tag{4.13}$$

and q is a parameter specific for each binary pair (Table 4.4).

The effect of temperature on multicomponent activity coefficients is described by (Meissner and Peppas, 1973):

$$\log \gamma_{ij}(T) = \left[1.125 - 0.005(T - 273.15)\right]\log \gamma_{ij}(T_0) - \left[0.125 - 0.005(T - 273.15)\right]A \tag{4.14}$$

where $\gamma_{ij}(T)$ is the multicomponent activity coefficient of the pair of ions *i-j* at temperature *T,* and, $A = -\frac{0.41 I^{0.5}}{1 + I^{0.5}} + 0.039 I^{0.92}$.

4.3.4 Aerosol water content

During the calculation of aerosol water content, it is assumed that the ambient water vapor pressure is unaffected by the aerosol water uptake (Seinfeld and Pandis, 1998). Therefore, if ambient relative humidity is known, phase equilibrium between gas and aerosol-phase (Seinfeld and Pandis, 1998) gives that the water activity, a_w, is equal to the ambient fractional relative humidity, *RH*, (i.e., expressed on a 0.0 to 1.0 scale):

$$a_w = RH \tag{4.15}$$

Instead of determining water content that satisfies the constraint of Eq. (4.15) from

explicit calculations of water activity (which would require an iterative, hence computationally expensive procedure, (Stelson and Seinfeld, [1982]), the water uptake of aerosols is approximated through the ZSR relationship (Robinson and Stokes, 1965),

$$W = \sum_i \frac{M_i}{m_{oi}(a_w)} \tag{4.16}$$

where W is the mass concentration of aerosol water (kg m^{-3} air), M_i is the molar concentration of species i (mol m^{-3} air), and $m_{oi}(a_w)$ is the molality of an aqueous binary solution of the i-th electrolyte with the same a_w (i.e., relative humidity) as in the multicomponent solution. The water activities used and their corresponding sources are given in Table 4.6.

4.3.5 Deliquescence relative humidity (DRH)

For each salt, there is a characteristic relative humidity, known as the deliquescence relative humidity (DRH), above which a phase transition from solid to saturated aqueous solution occurs. The DRH varies with temperature and for small T changes is given by (Wexler and Seinfeld, 1991):

$$ln\frac{DRH(T)}{DRH(T_o)} = -\frac{M_w m_s L_s}{1000R}\left(\frac{1}{T} - \frac{1}{T_o}\right) \tag{4.17}$$

where M_w is the molar mass of water and m_s is the molality of the saturated solution at temperature T_o. L_s is the latent heat of fusion for the salt from a saturated solution given by $L_s = \Delta H_{cr} - \Delta H_{aq}$; $\Delta H_{cr}, \Delta H_{aq}$ are the molar enthalpies of formation of the crystalline phase and the species in aqueous solution, respectively.

4.3.6 Mutual deliquescence relative humidity (MDRH)

In every multicomponent mixture there exists a characteristic relative humidity (known as mutual deliquescence relative humidity, MDRH, [Wexler and Seinfeld, 1991]), for which all salts are simultaneously saturated with respect to all components. The MDRH is a eutectic point so it is below the DRH of all the pure solids composing the system and is the minimum RH for which a stable aqueous phase exists (Wexler and Seinfeld, 1991). When MDRH < RH < RH_{wet} (where RH_{wet} is the DRH of the salt with the lowest DRH in the mixture under consideration) the solution is said to be in the mutual deliquescence region (MDR, [Nenes et al., 1998]). Computing the aerosol composition in the MDR is a computationally demanding task (e.g., Potukuchi and Wexler, 1995a,b) which we seek to avoid. Given that the MDR corresponds usually to a narrow RH range, we use the simplified approach of Nenes et al., (1998) to calculate composition in a MDR. This approach involves computing the weighted average of a "dry" and "wet" solution:

$$W = (1-c)W_{wet} \tag{4.18}$$

$$G = cG_{dry} + (1-c)G_{wet} \tag{4.19}$$

$$S = cS_{dry} + (1-c)S_{wet} \tag{4.20}$$

$$D = (1-c)D_{wet} \tag{4.21}$$

The weighting factor, c, is given by (Nenes et al., 1998):

$$c = \frac{RH - RH_{wet}}{MDRH - RH_{wet}} \tag{4.22}$$

and G, S, D are the concentrations of gaseous, solid and dissolved species, respectively. The subscripts "wet" and "dry" in Eqs. (4.18) - (4.22) denote the two solutions which are weighted. In the above equations, we assume that gases and solids are linearly weighted according to their proximity to RH_{wet} and MDRH (as expressed by c), while dissolved

species are scaled to the amount of water. MDRH points for the new mixtures in ISORROPIA II are shown in Table 4.5. Although Eqs. (4.18) - (4.22) are an approximation of the thermodynamic solution, they qualitatively follow the RH-dependence of speciation and conserve aerosol dry mass.

4.4 ISORROPIA II: Species considered and general solution procedure

The system modeled by ISORROPIA II consists of the following potential components (species in bold are new in ISORROPIA II):

Gas phase: NH_3, HNO_3, HCl, H_2O

Liquid phase: NH_4^+, Na^+, H^+, Cl^-, NO_3^-, SO_4^{2-}, $HNO_{3(aq)}$, $NH_{3(aq)}$, $HCl_{(aq)}$, HSO_4^-, OH^-, H_2O, **Ca^{2+}, K^+, Mg^{2+}**

Solid phase: $(NH_4)_2SO_4$, NH_4HSO_4, $(NH_4)_3H(SO_4)_2$, NH_4NO_3, NH_4Cl, NaCl, $NaNO_3$, $NaHSO_4$, Na_2SO_4, **$CaSO_4$, $Ca(NO_3)_2$, $CaCl_2$, K_2SO_4, $KHSO_4$, KNO_3, KCl, $MgSO_4$, $Mg(NO_3)_2$, $MgCl_2$**

Table 4.1 shows thermodynamic properties for all species considered. Table 4.2 displays all the equilibrium reactions used in ISORROPIA II along with values for their equilibrium constants. When the concentration of crustal species (Ca, K, Mg) is zero, routines of ISORROPIA are used, which since its original release (Nenes et al., 1998) has been substantially improved for robustness, speed and expanded to solve a wider range of problems (updates can be obtained from http://nenes.eas.gatech.edu/ISORROPIA).

Table 4.1: Thermodynamic properties for all species in ISORROPIA II*

Species	$\Delta\mu_i^0$ (298K), kJ mol^{-1}	ΔH_f^o, kJ mol^{-1}	C_p^o, J mol^{-1} K^{-1}
$Ca(NO_3)_{2(s)}$ ♣	**-1713.15**	**-2132.33**	**315.65**
$CaCl_{2\,(s)}$ ♣	**-2215.6**	**-2607.9**	**322.01**
$CaSO_{4\,(s)}$	**-1798.280**	**-2022.630**	**186.020**
$KHSO_{4\,(s)}$	**-1031.300**	**-1160.600**	**87.160**
$K_2SO_{4\,(s)}$	**-1321.370**	**-1437.790**	**131.460**
$KNO_{3\,(s)}$	**-394.860**	**-494.630**	**96.400**
$KCl_{(s)}$	**-409.140**	**-434.750**	**51.300**
$MgSO_{4\,(s)}$	**-1170.600**	**-1284.900**	**96.480**
$Mg(NO_3)_{2\,(s)}$ ♣	**-2080.3**	**-2613.28**	**391.34**
$MgCl_{2\,(s)}$ ♣	**-2114.64**	**-2499.02**	**315.06**
$Ca^{2+}_{(aq)}$	**-553.580**	**-542.830**	-
$K^{+}_{(aq)}$	**-283.270**	**-252.380**	**21.800**
$Mg^{2+}_{(aq)}$	**-454.800**	**-466.850**	-
$NaCl_{(s)}$	-384.138	-411.153	50.500
$NaNO_{3\,(s)}$	-367.000	-467.850	92.880
$Na_2SO_{4\,(s)}$	-1270.160	-1387.080	128.200
$NaHSO_{4\,(s)}$	-992.800	-1125.500	85.000
$NH_4Cl_{(s)}$	-202.870	-314.430	84.100
$NH_4NO_{3\,(s)}$	-183.870	-365.560	139.300
$(NH_4)_2SO_{4\,(s)}$	-901.670	-1180.850	187.490
$NH_4HSO_{4\,(s)}$	-823.000	-1026.960	127.500
$(NH_4)_3H(SO_4)_{2\,(s)}$	-1730.000	-2207.000	315.000
$HNO_{3\,(g)}$	-74.720	-135.060	53.350
$HCl_{(g)}$	-95.299	-92.307	29.126
$NH_{3\,(g)}$	-16.450	-46.110	35.060
$NH_{3\,(aq)}$	-26.500	-80.290	79.900
$H^{+}_{(aq)}$	0.000	0.000	0.000
$Na^{+}_{(aq)}$	-261.905	-240.120	46.400
$NH_4^{+}{}_{(aq)}$	-79.310	-132.510	79.900
$HSO_4^{-}{}_{(aq)}$	-755.910	-887.340	-84.000
$SO_4^{2-}{}_{(aq)}$	-744.530	-909.270	-293.000
$NO_3^{-}{}_{(aq)}$	-111.250	-207.360	-86.600
$Cl^{-}_{(aq)}$	-131.228	-167.159	-136.400
$OH^{-}_{(aq)}$	-157.244	-229.994	-148.500

* Compiled by: Kim and Seinfeld, (1995) and Kim et al., (1993) unless otherwise indicated; Species in bold are new in ISORROPIA II.

♣ Compiled by: Kelly and Wexler, (2005)

- Data not available

Table 4.2: Equilibrium relations and temperature dependence constants used in ISORROPIA II*

Reaction	Equilibrium Constant Expression	K^0(298.15K)	$\frac{\Delta H^0(T_0)}{RT_0}$	$\frac{\Delta c_p^0}{R}$	Units
$Ca(NO_3)_{2(s)} \leftrightarrow Ca^{2+}_{(aq)} + 2NO^-_{3(aq)}$	$[Ca^{2+}][NO_3^-]^2\gamma_{Ca^{2+}}\gamma^2_{NO_3^-}$	**6.067×10^{5}**	**-11.299♣**	-	mol^3kg^{-3}
$CaCl_{2(s)} \leftrightarrow Ca^{2+}_{(aq)} + 2Cl^-_{(aq)}$	$[Ca^{2+}][Cl^-]^2\gamma_{Ca^{2+}}\gamma^2_{Cl^-}$	**7.974×10^{11}**	**-14.087♣**	-	mol^3kg^{-3}
$CaSO_4.2H_2O_{(s)} \leftrightarrow Ca^{2+}_{(aq)} + SO^{2-}_{4\ (aq)} + 2H_2O$	$[Ca^{2+}][SO_4^{2-}]\gamma_{Ca^{2+}}\gamma_{SO_4^{2-}}a_w^2$	**4.319×10^{-5}**	-	-	mol^2kg^{-2}
$K_2SO_{4(s)} \leftrightarrow 2K^+_{(aq)} + SO^{2-}_{4(aq)}$	$[K^+]^2[SO_4^{2-}]\gamma^2_{K^+}\gamma_{SO_4^{2-}}$	**1.569×10^{-2}**	**-9.589**	**45.807**	mol^3kg^{-3}
$KHSO_{4(s)} \leftrightarrow K^+_{(aq)} + HSO^-_{4(aq)}$	$[K^+][HSO_4^-]\gamma_{K^+}\gamma_{HSO_4^-}$	**24.016**	**-8.423**	**17.964**	mol^2kg^{-2}
$KNO_{3(s)} \leftrightarrow K^+_{(aq)} + NO^-_{3(aq)}$	$[K^+][NO_3^-]\gamma_{K^+}\gamma_{NO_3^-}$	**0.872**	**14.075**	**19.388**	mol^2kg^{-2}
$KCl_{(s)} \leftrightarrow K^+_{(aq)} + Cl^-_{(aq)}$	$[K^+][Cl^-]\gamma_{K^+}\gamma_{Cl^-}$	**8.680**	**-6.167**	**19.953**	mol^2kg^{-2}
$MgSO_{4(s)} \leftrightarrow Mg^{2+}_{(aq)} + SO^{2-}_{4(aq)}$	$[Mg^{2+}][SO_4^{2-}]\gamma_{Mg^{2+}}\gamma_{SO_4^{2-}}$	**1.079×10^{5}**	**36.798**	-	mol^2kg^{-2}
$Mg(NO_3)_{2(s)} \leftrightarrow Mg^{2+}_{(aq)} + 2NO^-_{3(aq)}$	$[Mg^{2+}][NO_3^-]^2\gamma_{Mg^{2+}}\gamma^2_{NO_3^-}$	**2.507×10^{15}**	**-8.754♣**	-	mol^3kg^{-3}
$MgCl_{2(s)} \leftrightarrow Mg^{2+}_{(aq)} + 2Cl^-_{(aq)}$	$[Mg^{2+}][Cl^-]^2\gamma_{Mg^{2+}}\gamma^2_{Cl^-}$	**9.557×10^{21}**	**-1.347♣**	-	mol^3kg^{-3}
$HSO^-_{4(aq)} \leftrightarrow H^+_{(aq)} + SO^{2-}_{4(aq)}$	$\frac{[H^+][SO_4^{2-}]}{[HSO_4^-]}\frac{\gamma_{H^+}\gamma_{SO_4^{2-}}}{\gamma_{HSO_4^-}}$	1.015×10^{-2}	8.85	25.14	mol kg^{-1}
$NH_{3(g)} \leftrightarrow NH_{3(aq)}$	$\frac{[NH_{3(aq)}]}{[P_{NH_3}]}\gamma_{NH_3}$	5.764×10^{1}	13.79	-5.39	mol kg^{-1} atm^{-1}
$NH_{3(aq)} + H_2O_{(aq)} \leftrightarrow NH^+_{4(aq)} + OH^-_{(aq)}$	$\frac{[NH_4^+][OH^-]}{[NH_{3(aq)}]a_w}\frac{\gamma_{NH_4^+}\gamma_{OH^-}}{\gamma_{NH_3}}$	1.805×10^{-5}	-1.50	26.92	mol kg^{-1}
$HNO_{3(g)} \leftrightarrow H^+_{(aq)} + NO^-_{3(aq)}$	$\frac{[H^+][NO_3^-]}{P_{HNO_3}}\gamma_{H^+}\gamma_{NO_3^-}$	2.511×10^{6}	29.17	16.83	mol^2 kg^{-2} atm^{-1}
$HNO_{3(g)} \leftrightarrow HNO_{3(aq)}$ ♠	$\frac{[HNO_{3(aq)}]}{[P_{HNO_3}]}\gamma_{HNO_3}$	2.1×10^{5}	29.17	16.83	mol kg^{-1} atm^{-1}
$HCl_{(g)} \leftrightarrow H^+_{(aq)} + Cl^-_{(aq)}$	$\frac{[H^+][Cl^-]}{P_{HCl}}\gamma_{H^+}\gamma_{Cl^-}$	1.971×10^{6}	30.20	19.91	mol^2 kg^{-2} atm^{-1}
$HCl_{(g)} \leftrightarrow HCl_{(aq)}$ ♦	$\frac{[HCl_{(aq)}]}{[P_{HCl}]}\gamma_{HCl}$	2.5×10^{3}	30.20	19.91	mol kg^{-1} atm^{-1}
$H_2O_{(aq)} \leftrightarrow H^+_{(aq)} + OH^-_{(aq)}$	$\frac{[H^+][OH^-]}{a_w}\gamma_{H^+}\gamma_{OH^-}$	1.010×10^{-14}	-22.52	26.92	mol^2 kg^{-2}

Table 4.2: (Continued)

Reaction	Equilibrium Constant Expression	K^0(298.15K)	$\frac{\Delta H^0(T_0)}{RT_0}$	$\frac{\Delta c_p^0}{R}$	Units
$Na_2SO_{4(s)} \leftrightarrow 2Na^+_{(aq)} + SO^{2-}_{4(aq)}$	$\left[Na^+\right]^2\left[SO_4^{2-}\right]\gamma^2_{Na^+}\gamma_{SO_4^{2-}}$	4.799×10^{-1}	0.98	39.75	$mol^3\ kg^{-3}$
$(NH_4)_2SO_{4(s)} \leftrightarrow 2NH^+_{4(aq)} + SO^{2-}_{4(aq)}$	$\left[NH_4^+\right]^2\left[SO_4^{2-}\right]\gamma^2_{NH_4^+}\gamma_{SO_4^{2-}}$	1.817×10^{0}	-2.65	38.57	$mol^3\ kg^{-3}$
$NH_4Cl_{(s)} \leftrightarrow NH_{3(g)} + HCl_{(g)}$	$P_{NH_3}P_{HCl}$	1.086×10^{-16}	-71.00	2.40	atm^2
$NaNO_{3(s)} \leftrightarrow Na^+_{(aq)} + NO^-_{3(aq)}$	$\left[Na^+\right]\left[NO_3^-\right]\gamma_{Na^+}\gamma_{NO_3^-}$	1.197×10^{1}	-8.22	16.01	$mol^2\ kg^{-2}$
$NaCl_{(s)} \leftrightarrow Na^+_{(aq)} + Cl^-_{(aq)}$	$\left[Na^+\right]\left[Cl^-\right]\gamma_{Na^+}\gamma_{Cl^-}$	3.766×10^{1}	-1.56	16.90	$mol^2\ kg^{-2}$
$NaHSO_{4(s)} \leftrightarrow Na^+_{(aq)} + HSO^-_{4(aq)}$	$\left[Na^+\right]\left[HSO_4^-\right]\gamma_{Na^+}\gamma_{HSO_4^-}$	2.413×10^{4}	0.79	14.75	$mol^2\ kg^{-2}$
$NH_4NO_{3(s)} \leftrightarrow NH_{3(g)} + HNO_{3(g)}$	$P_{NH_3}P_{HNO_3}$	4.199×10^{-17}	-74.735	6.025	atm^2
$NH_4HSO_{4(s)} \leftrightarrow NH^+_{4(aq)} + HSO^-_{4(aq)}$	$\left[NH_4^+\right]\left[HSO_4^-\right]\gamma_{NH_4^+}\gamma_{HSO_4^-}$	1.383×10^{0}	-2.87	15.83	$mol^2\ kg^{-2}$
$(NH_4)_3H(SO_4)_{2(s)} \leftrightarrow$ $3NH^+_{4(aq)} + HSO^-_{4(aq)} + SO^{2-}_{4(aq)}$	$\left[NH_4^+\right]^3\left[SO_4^{2-}\right]\left[HSO_4^-\right]\times$ $\gamma^3_{NH_4^+}\gamma_{SO_4^{2-}}\gamma_{HSO_4^-}$	2.972×10^{1}	-5.19	54.40	$mol^5\ kg^{-5}$

* Compiled by: Kim and Seinfeld, (1995) and Kim et al., (1993) unless otherwise indicated; Reactions with constants in bold are new in ISORROPIA II.

♣ Compiled by: Kelly and Wexler, (2005)

♠ The equilibrium constant K_{1b} of the reaction $HNO_{3(aq)} \xleftrightarrow{K_{1b}} H^+_{(aq)} + NO^-_{3(aq)}$ is calculated from K_1 and K_{1a} of the reactions $HNO_{3(g)} \xleftrightarrow{K_1} H^+_{(aq)} + NO^-_{3(aq)}$ and $HNO_{3(g)} \xleftrightarrow{K_{1a}} HNO_{3(aq)}$, respectively: $K_{1b} = K_1 / K_{1a}$

♦ The equilibrium constant K_{2b} of the reaction $HCl_{(aq)} \xleftrightarrow{K_{2b}} H^+_{(aq)} + Cl^-_{(aq)}$ is calculated from K_2 and K_{2a} of the reactions $HCl_{(g)} \xleftrightarrow{K_2} H^+_{(aq)} + Cl^-_{(aq)}$ and $HCl_{(g)} \xleftrightarrow{K_{2a}} HCl_{(aq)}$, respectively: $K_{2b} = K_2 / K_{2a}$

- Data not available

4.4.1 Solution procedure

The number of species and equilibrium reactions is determined by the relative abundance of each aerosol precursor (NH_3, Na, Ca, K, Mg, HNO_3, HCl, H_2SO_4) and the ambient relative humidity and temperature. The major species potentially present are determined from the value of the following ratios:

$$R_1 = \frac{\left[NH_4^+\right]+\left[Ca^{2+}\right]+\left[K^+\right]+\left[Mg^{2+}\right]+\left[Na^+\right]}{\left[SO_4^{-2}\right]}$$

$$R_2 = \frac{\left[Ca^{2+}\right]+\left[K^+\right]+\left[Mg^{2+}\right]+\left[Na^+\right]}{\left[SO_4^{-2}\right]}$$

$$R_3 = \frac{\left[Ca^{2+}\right]+\left[K^+\right]+\left[Mg^{2+}\right]}{\left[SO_4^{-2}\right]}$$

where $\left[X\right]$ denotes the concentration of an aerosol precursor X (mol m^{-3} of air). R_1, R_2 and R_3 are termed "total sulfate ratio", "crustal species and sodium ratio" and "crustal species ratio" respectively; based on their values, 5 aerosol composition regimes are defined, the possible species for which are listed in Table 4.3.

The DRH at T_o = 298.15K, the thermodynamic data for the L_s (Eq. 4.17) as well as the Kussik-Meissner activity coefficient parameters (Eq. 4.13) are shown in Table 4.4. Table 4.6 displays the polynomial fit parameters for computing the molalities of binary solutions as a function of water activity (obtained from Kim and Seinfeld, [1995], Ha and Chan [1999] and Kelly and Wexler, [2005, 2006]) for $CaSO_{4(s)}$, $Ca(NO_3)_{2(s)}$, $CaCl_{2(s)}$, $K_2SO_{4(s)}$, $KHSO_{4(s)}$, $KNO_{3(s)}$, $KCl_{(s)}$, $MgSO_{4(s)}$, $Mg(NO_3)_{2(s)}$ and $MgCl_{2(s)}$. For $(NH_4)_2SO_{4(s)}$, $NH_4HSO_{4(s)}$, $(NH_4)_3H(SO_4)_{2(s)}$, $NH_4NO_{3(s)}$, $NH_4Cl_{(s)}$, $NaCl_{(s)}$, $NaNO_{3(s)}$, $NaHSO_{4(s)}$ and $Na_2SO_{4(s)}$, the water activity database was updated since the original release of ISORROPIA, using the output from the AIM model

(http://www.hpc1.uea.ac.uk/~e770/aim.html).

As in ISORROPIA, ISORROPIA II solves two classes of problems:

a) Forward (or "closed") problems, in which known quantities are *T*, *RH* and the total (gas + aerosol) concentrations of NH_3, H_2SO_4, Na, HCl, HNO_3, Ca, K, and Mg.

b) Reverse (or "open") problems, in which known quantities are *T*, *RH* and the precursor concentrations of NH_3, H_2SO_4, Na, HCl, HNO_3, Ca, K, and Mg in the aerosol phase.

Below the MDRH of an aerosol mixture, the particle is a solid if the aerosol is following its deliquescence branch. However, when the RH over a wet particle is decreasing, the wet aerosol may not crystallize below the MDRH but instead remain in a metastable state, where it is composed of an aqueous supersaturated solution (Seinfeld and Pandis, 1998). ISORROPIA II can address both states (termed “stable” where salts precipitate once the aqueous phase becomes saturated with respect to them, and, “metastable”, if the aerosol is composed only of an aqueous phase which can be supersaturated with respect to dissolve salts).

Depending on the three sulfate ratios and the relative humidity, ISORROPIA II solves the appropriate set of equilibrium equations and together with mass conservation, electroneutrality, water activity equations and activity coefficient calculations, the final concentrations at thermodynamic equilibrium are obtained. Figure 4.1 illustrates a general description of the solution procedure.

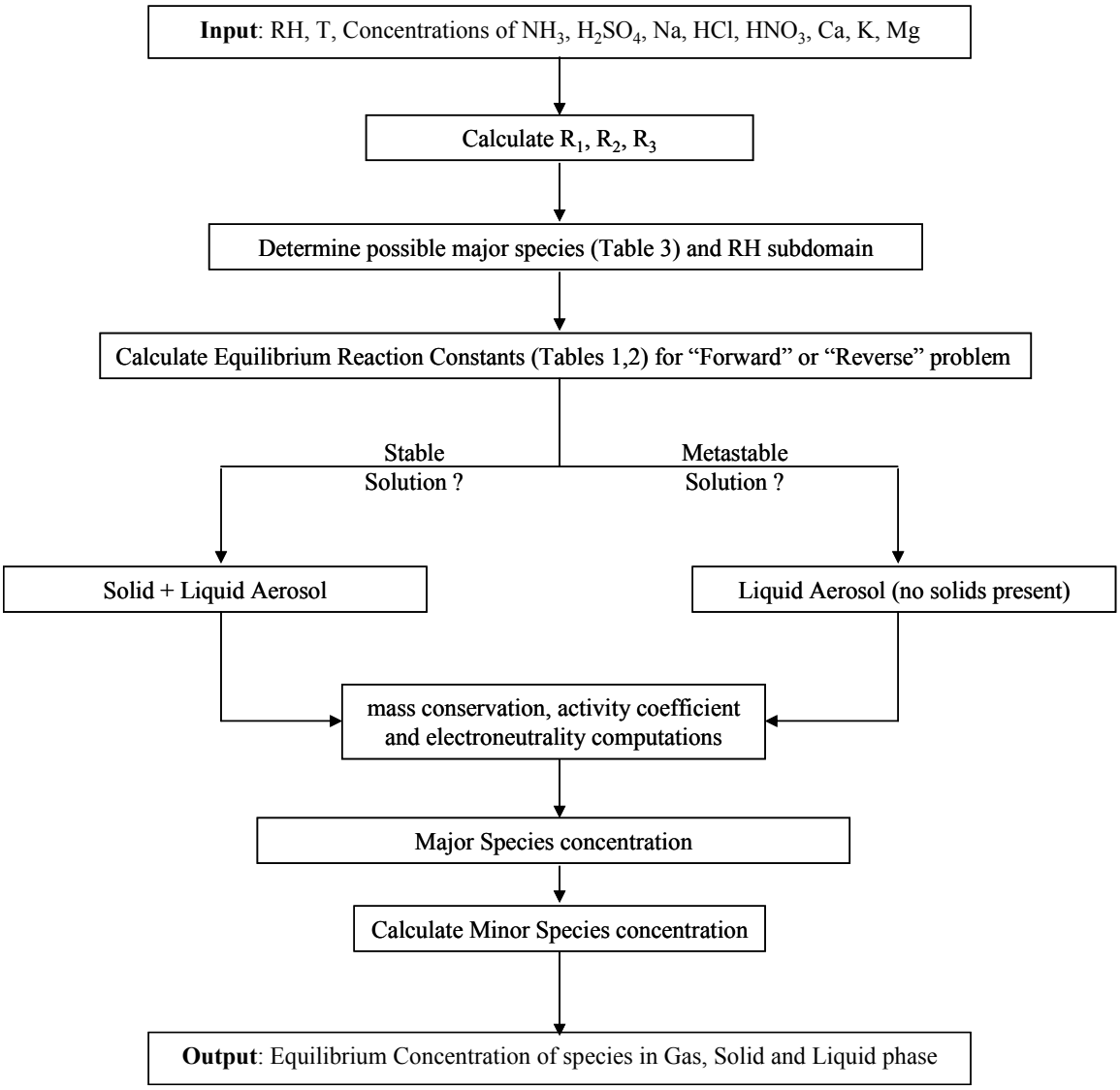

Figure 4.1: Generic solution procedure of ISORROPIA-II.

Table 4.3: Potential species for the five aerosol types

R_1	R_2	R_3	Aerosol Type	Major Species			Minor Species
				Solid Phase	Aqueous Phase	Gas Phase	
$R_1 < 1$	any value	any value	Sulfate Rich (free acid)	$NaHSO_4$, NH_4HSO_4, **$KHSO_4$, $CaSO_4$**	Na^+, NH_4^+, H^+, HSO_4^-, SO_4^{2-}, NO_3^-, Cl^-, **Ca^{2+}, K^+,** H_2O	H_2O	$NH_{3(g)}$, $NO_{3(aq)}$, $Cl_{(aq)}$, $NH_{3(aq)}$, $HNO_{3(aq)}$, $HCl_{(aq)}$
$1 \le R_1 < 2$	any value	any value	Sulfate Rich	$NaHSO_4$, NH_4HSO_4, Na_2SO_4, $(NH_4)_2SO_4$, $(NH_4)_3H(SO_4)_2$, **$CaSO_4$, $KHSO_4$, K_2SO_4, $MgSO_4$**	Na^+, NH_4^+, H^+, HSO_4^-, SO_4^{2-}, NO_3^-, Cl^-, **Ca^{2+}, K^+, Mg^{2+},** H_2O	H_2O	$NH_{3(g)}$, $NO_{3(aq)}$, $Cl_{(aq)}$, $NH_{3(aq)}$, $HNO_{3(aq)}$, $HCl_{(aq)}$
$R_1 \ge 2$	$R_2 < 2$	any value	Sulfate Poor, Crustal & Sodium Poor	Na_2SO_4, $(NH_4)_2SO_4$, NH_4NO_3, NH_4Cl, **$CaSO_4$, K_2SO_4, $MgSO_4$**	Na^+, NH_4^+, H^+, SO_4^{2-}, NO_3^-, Cl^-, **Ca^{2+}, K^+, Mg^{2+},** H_2O, $NH_{3(aq)}$, $HNO_{3(aq)}$, $HCl_{(aq)}$	HNO_3, HCl, NH_3, H_2O	$HSO_{4(aq)}$
$R_1 \ge 2$	$R_2 \ge 2$	$R_3 < 2$	Sulfate Poor, Crustal & Sodium Rich, Crustal Poor	Na_2SO_4, $NaNO_3$, $NaCl$, NH_4NO_3, NH_4Cl, **$CaSO_4$, K_2SO_4, $MgSO_4$**	Na^+, NH_4^+, H^+, SO_4^{2-}, NO_3^-, Cl^-, **Ca^{2+}, K^+, Mg^{2+},** H_2O, $NH_{3(aq)}$, $HNO_{3(aq)}$, $HCl_{(aq)}$	HNO_3, HCl, NH_3, H_2O	$HSO_{4(aq)}$
$R_1 \ge 2$	$R_2 \ge 2$	$R_3 > 2$	Sulfate Poor, Crustal & Sodium Rich, Crustal Rich	$NaNO_3$, $NaCl$, NH_4NO_3, NH_4Cl, **$CaSO_4$, K_2SO_4, $MgSO_4$, $Ca(NO_3)_2$, $CaCl_2$, $Mg(NO_3)_2$, $MgCl_2$, KNO_3, KCl**	Na^+, NH_4^+, H^+, SO_4^{2-}, NO_3^-, Cl^-, **Ca^{2+}, K^+, Mg^{2+},** H_2O, $NH_{3(aq)}$, $HNO_{3(aq)}$, $HCl_{(aq)}$	HNO_3, HCl, NH_3, H_2O	$HSO_{4(aq)}$

* Species in bold are new in ISORROPIA-II.

Table 4.4: Deliquescence relative humidities, temperature dependence and parameter q values for all the salts modeled in ISORROPIA II[I]

Salt	DRH (298.15 K)	$-\frac{18}{1000R}L_s m_s$	q
$Ca(NO_3)_2$	**0.4906**[*]	**509.4**[#]	**0.93**[*]
$CaCl_2$	**0.2830**[*]	**551.1**[#]	**2.40**[*]
$CaSO_4$	**0.9700**[*]	**-**	**-,**[a]
$KHSO_4$	**0.8600**[♣]	**-**	**-,**[b]
K_2SO_4[*]	**0.9751**	**35.6**	**-0.25**
KNO_3[*]	**0.9248**	**-**	**-2.33**
KCl[*]	**0.8426**	**158.9**	**0.92**
$MgSO_4$	**0.8613**[♦]	**-714.5**[*]	**0.15**[*]
$Mg(NO_3)_2$	**0.5400**[♦]	**230.2**[#]	**2.32**[*]
$MgCl_2$	**0.3284**[*]	**42.23**[#]	**2.90**[*]
NaCl[♠]	0.7528	25.0	2.23
Na_2SO_4[♠]	0.9300	80.0	-0.19
$NaNO_3$[♠]	0.7379	304.0	-0.39
$(NH_4)_2SO_4$[♠]	0.7997	80.0	-0.25
NH_4NO_3[♠]	0.6183	852.0	-1.15
NH_4Cl[♠]	0.7710	239.0	0.82
NH_4HSO_4	0.4000[♠]	384.0[♠]	(+),[c]
$NaHSO_4$	0.5200[♠]	-45.0[♠]	(+),[d]
$(NH_4)_3H(SO_4)_2$	0.6900[♠]	186.0[♠]	(+),[e]
H_2SO_4[♠]	0.000	-	0.70
$H\text{-}HSO_4$[♠]	0.000	-	8.00
HNO_3[♠]	N/A	-	2.60
HCl[♠]	N/A	-	6.00

[*] Kim and Seinfeld, 1995
[#] Kelly and Wexler, 2005
[♣] Pilinis and Seinfeld, 1989
[♦] Ha and Chan, 1999
[♠] Kim et al., 1993
[-] Data not available

[a] $\gamma_{CaSO_4} = 0$

[b] $\gamma_{KHSO_4} = \frac{\gamma_{H-HSO_4} \cdot \gamma_{KCl}}{\gamma_{HCl}}$

[c] $\gamma_{NH_4HSO_4} = \frac{\gamma_{H-HSO_4} \cdot \gamma_{NH_4Cl}}{\gamma_{HCl}}$

[d] $\gamma_{NaHSO_4} = \frac{\gamma_{H-HSO_4} \cdot \gamma_{NaCl}}{\gamma_{HCl}}$

[e] $\gamma_{(NH_4)_3H(SO_4)_2} = \left(\gamma^3_{(NH_4)_2SO_4} \cdot \gamma_{NH_4HSO_4}\right)^{0.2}$

[I] Species in bold are new in ISORROPIA II.

Table 4.5: Mutual deliquescence relative humidities, for the new salts modeled in ISORROPIA II[I]

Salt Mixture	MDRH[*]
$Ca(NO_3)_2$, $CaCl_2$, K_2SO_4, KNO_3, KCl, $MgSO_4$, $Mg(NO_3)_2$, $MgCl_2$, *$NaNO_3$, NaCl, NH_4NO_3, NH_4Cl*	0.200
$(NH_4)_2SO_4$, NH_4NO_3, NH_4Cl, Na_2SO_4, K_2SO_4, $MgSO_4$	0.460
$Ca(NO_3)_2$, K_2SO_4, KNO_3, KCl, $MgSO_4$, $Mg(NO_3)_2$, $MgCl_2$, *$NaNO_3$, NaCl, NH_4NO_3, NH_4Cl*	0.240
$(NH_4)_2SO_4$, NH_4Cl, Na_2SO_4, K_2SO_4, $MgSO_4$	0.691
$Ca(NO_3)_2$, K_2SO_4, KNO_3, KCl, $MgSO_4$, $Mg(NO_3)_2$, *$NaNO_3$, NaCl, NH_4NO_3, NH_4Cl*	0.240
$(NH_4)_2SO_4$, Na_2SO_4, K_2SO_4, $MgSO_4$	0.697
K_2SO_4, $MgSO_4$, *$KHSO_4$, NH_4HSO_4, $NaHSO_4$, $(NH_4)_2SO_4$, Na_2SO_4, $(NH_4)_3H(SO_4)_2$*	0.240
$(NH_4)_2SO_4$, NH_4NO_3, Na_2SO_4, K_2SO_4, $MgSO_4$	0.494
K_2SO_4, KNO_3, KCl, $MgSO_4$, $Mg(NO_3)_2$, *$NaNO_3$, NaCl, NH_4NO_3, NH_4Cl*	0.240
K_2SO_4, $MgSO_4$, $KHSO_4$, $NaHSO_4$, *$(NH_4)_2SO_4$, Na_2SO_4, $(NH_4)_3H(SO_4)_2$*	0.363
K_2SO_4, KNO_3, KCl, $MgSO_4$, *$NaNO_3$, NaCl, NH_4NO_3, NH_4Cl*	0.596
K_2SO_4, $MgSO_4$, $KHSO_4$, *$(NH_4)_2SO_4$, Na_2SO_4, $(NH_4)_3H(SO_4)_2$*	0.610
$Ca(NO_3)_2$, K_2SO_4, KNO_3, KCl, $MgSO_4$, $Mg(NO_3)_2$, *$NaNO_3$, NaCl, NH_4NO_3, NH_4Cl*	0.240
K_2SO_4, KNO_3, KCl, $MgSO_4$, $Mg(NO_3)_2$, *$NaNO_3$, NaCl, NH_4NO_3, NH_4Cl*	0.240

[*] Obtained from Potukuchi and Wexler, (1995a, 1995b) for mixtures with closest composition (T=298.15K).

[I] Species in *italics* determine the mixture from which the MDRH value has been taken for each case.

Table 4.6: Coefficients of $m(a_w)$ from the polynomial fit $m(a_w)=k_0 + k_1 a_w + k_2 a_w^2 + ...$

Species	k_0	k_1	k_2	k_3	k_4	k_5
$Ca(NO_3)_2$♠	36.356	-165.66	447.46	-673.55	510.91	-155.56
$CaCl_2$*	20.847	-97.599	273.220	-422.120	331.160	-105.450
$CaSO_4$	N/A	N/A	N/A	N/A	N/A	N/A
$KHSO_4$§	1.061	-0.101	$1.579\text{x}10^{-2}$	$-1.950\text{x}10^{-3}$	$9.515\text{x}10^{-5}$	$-1.547\text{x}10^{-6}$
K_2SO_4♣	1061.51	-4748.97	8096.16	-6166.16	1757.47	0
KNO_3♣	$1.2141\text{x}10^4$	$-5.1173\text{x}10^4$	$8.1252\text{x}10^4$	$-5.7527\text{x}10^4$	$1.5305\text{x}10^4$	0
KCl♣	179.721	-721.266	1161.03	-841.479	221.943	0
$MgSO_4$♦	-0.778	177.740	-719.790	1174.600	-863.440	232.310
$Mg(NO_3)_2$♦	12.166	-16.154	0	10.886	0	-6.815
$MgCl_2$♦	11.505	-26.518	34.937	-19.829	0	0

♠ source: Kelly and Wexler (2005)
* source: Kim and Seinfeld (1995)
♣ source: Kelly and Wexler (2006)
§ Same as $NaHSO_4$
♦ source: Ha and Chan (1999)

4.4.2 Important issues

- When calculating species concentration, the stable state solution algorithm of ISORROPIA II starts with assuming a completely dry aerosol. As the ambient relative humidity increases (or decreases) ISORROPIA II dissolves each of the salts present (depending on their DRH) and calculates solid and ion concentrations and water uptake. The exact opposite methodology is adopted by SCAPE2. SCAPE2 initially assumes that all salts present are completely dissolved and based on the ambient relative humidity and DRH of each salt calculates solid concentration if a precipitate is assumed to form. Differences in the "solution dynamics" may lead to differences in water content and speciation, especially at low RH, and are further analyzed in Sect. 4.4.
- ISORROPIA II uses the principle of "compositional invariance with RH cycling" to determine the aerosol composition at low RH (i.e., when the aerosol is solid). This is done because aerosol cycles RH many times in nature throughout its lifetime and the invariant solution will in general represent its composition more accurately in the atmosphere. Compositional invariance is applied when the aerosol contains volatile anions, sulfate and non-volatile univalent cations (Na^+, K^+). In such cases, $Na_{(aq)}$ and $K_{(aq)}$ preferentially associate with $SO_{4(aq)}$ to form $Na_2SO_{4(s)}$ and $K_2SO_{4(s)}$ before they are bound with $NO_{3(aq)}$ and $Cl_{(aq)}$ to form $NaNO_{3(s)}$, $KNO_{3(s)}$, $NaCl_{(s)}$, and $KCl_{(s)}$. Other models may not adopt this approach and may lead to differences in predicted water uptake, especially at low RH. For example, ISORROPIA II predicts that potassium will preferentially associate with sulfate to form $K_2SO_{4(s)}$. Then excess potassium associates with available $NO_{3(aq)}$

and $Cl_{(aq)}$ to form $KNO_{3(s)}$ and $KCl_{(s)}$. Therefore, in the above example ISORROPIA II assumes that potassium mainly binds with sulfate since sulfate (as H_2SO_4) is less volatile than nitrate (as $HNO_{3(g)}$) or chloride (as $HCl_{(g)}$) when exposed to RH cycling, thus more likely to stay in the aerosol phase and form $K_2SO_{4(s)}$.

4.4.3 Simplifications and assumptions

Numerous simplifying assumptions are taken to increase computational speed and numerical stability without compromising rigor substantially. These are:

- Sulfuric acid, sodium and crustal species have a very low vapor pressure and can safely be assumed that they exclusively reside in the aerosol phase.
- The first dissociation of sulfuric acid $\left(H_2SO_{4(aq)} \rightarrow H^+ + HSO_4^-\right)$ is assumed to be complete and not considered in the equilibrium calculations.
- For a wide range of ionic strengths (0 – 30M), typical of ambient aerosols, the solubility product of magnesium sulfate ($MgSO_{4(s)}$) was found to be always less than its equilibrium constant. Therefore, ISORROPIA II assumes $MgSO_{4(s)}$ is always deliquesced when an aqueous phase is present, avoiding any computations for precipitating $MgSO_{4(s)}$ out of solution.
- Calcium sulfate ($CaSO_4$) is assumed completely insoluble.
- For sulfate rich cases ($R_1 < 2$) $NH_{3(g)}$, $NO_{3(aq)}^-$ and $Cl_{(aq)}^-$ are assumed minor species that do not significantly perturb the equilibrium through the $NH_{3(g)} + H_2O_{(aq)} \leftrightarrow NH_{4(aq)}^+ + OH_{(aq)}^-$, $HNO_{3(g)} \leftrightarrow H_{(aq)}^+ + NO_{3(aq)}^-$ and $HCl_{(g)} \leftrightarrow H_{(aq)}^+ + Cl_{(aq)}^-$ reactions, respectively. The code solves the appropriate set

of equilibrium reactions (for the major species) and then the three gases $\left(NH_{3(g)}, HNO_{3(g)}, HCl_{(g)}\right)$ are subsequently dissolved through the equilibria described above. The same is assumed for the dissolved undissociated ammonia, nitric and hydrochloric acid in the aqueous phase ($NH_{3(aq)}$, $HNO_{3(aq)}$, $HCl_{(aq)}$).

- For sulfate poor cases ($R_1 > 2$) bisulfate ion (HSO_4^-) is considered a minor species from the reaction $HSO_{4(aq)}^- \leftrightarrow H_{(aq)}^+ + SO_{4(aq)}^{2-}$ (see Table 4.3).
- MDRH points for multicomponent mixtures containing crustal species are not known; They are approximated instead with data for known mixtures with as similar as possible composition (Table 4.5). For example, the MDRH point for a $(NH_4)_2SO_{4(s)}$-$NH_4NO_{3(s)}$-$NH_4Cl_{(s)}$-$Na_2SO_{4(s)}$-$K_2SO_{4(s)}$-$MgSO_{4(s)}$ mixture is (not known and) assumed to be the same as for the $(NH_4)_2SO_{4(s)}$-$NH_4NO_{3(s)}$-$NH_4Cl_{(s)}$-$Na_2SO_{4(s)}$ mixture. The absence of crustal species in the consideration of the MDRH points of those mixtures is expected to introduce small underprediction of water, since *i)* both potassium and magnesium have similar deliquescence properties with sodium (Moya et al., 2001a), and, *ii)* highly insoluble salts (i.e., $CaSO_{4(s)}$) do not significantly impact water activity, hence do not significantly contribute to DRH depression.
- OH^- is assumed a minor species.
- When crustal species are in excess compared to all the anions, ISORROPIA II assumes that the solution is close to neutral (pH ≈7). This is consistent with a presence of excess carbonate in the aerosol phase, which has a pK_a ($pK_a = -\log(K_a)$, where K_a is the equilibrium constant of the reaction: $CO_{2(g)} + H_2O \leftrightarrow HCO_3^- + H^+$, given by the equation: $Ka = [HCO_3^-][H^+]\gamma_{HCO3-}\,\gamma_{H+} / p_{CO2}\,a_w$) of ~6.4

(Meng et al., 1995).

- The DRH of $NH_4NO_{3(s)}$ is strongly dependent on temperature. Under low temperature conditions (T<270K), this changes the order (starting from low to high RH) with which salts deliquesce (Figure 4.2). For these cases the DRH of $NH_4NO_{3(s)}$ in ISORROPIA II is assumed to not "cross over" the DRH of the other salts present in the solution, especially since thermodynamic data for supercooled $NH_4NO_{3(s)}$ solutions are not known. The same is assumed for $NH_4Cl_{(s)}$ and $NaNO_{3(s)}$ which exhibit similar behavior with $NH_4NO_{3(s)}$ (Figure 4.2).
- γ_{OH^-} and γ_{H^+} are assumed equal to unity, as the activity coefficient routines cannot explicitly calculate them.
- The temperature dependence of DRH for $Ca(NO_3)_{2(s)}$, $CaCl_{2(s)}$, $Mg(NO_3)_{2(s)}$ and $MgCl_{2(s)}$ has been calculated using thermodynamic data for the most hydrated forms of these salts (i.e. $Ca(NO_3)_2.4H_2O$, $CaCl_2.6H_2O$, $Mg(NO_3)_2.6H_2O$ and $MgCl_2.6H_2O$, respectively) as suggested by Kelly and Wexler (2005). DRH values of these salts also correspond to their hydrated forms.

4.4.4 ISORROPIA II: New features

The main improvements to the original ISORROPIA release (Nenes et al., 1998) which are included in ISORROPIA II (and in the latest release of ISORROPIA version 1.7, http://nenes.eas.gatech.edu/ISORROPIA) are:

- Gas/liquid/solid partitioning has been extended to include crustal elements which resulted in 10 more salts in the solid phase and 3 more ions in the aqueous phase (Table 3).

- In addition to a thermodynamically stable state the aerosol can also be in a metastable state where no precipitate is formed (always an aqueous solution).
- The water activity database has been updated, using the output from the AIM model (http://www.hpc1.uea.ac.uk/~e770/aim.html).
- Temperature dependency of the activity coefficients is included. This has been done for both pre-calculated tables and online calculations of activity coefficients.
- The MDRH points for all the systems considered have been calculated using the GFEMN model of Ansari and Pandis (1999b).
- The activity coefficient calculation algorithm has been optimized to increase computational speed and avoid numerical errors.
- The tabulated Kusik-Meissner binary activity coefficient data have been recomputed through the online calculations for the midpoint of each ionic strength interval.
- A new subroutine has been added to provide the user with the option to "force" ISORROPIA II to conserve mass up to machine precision.

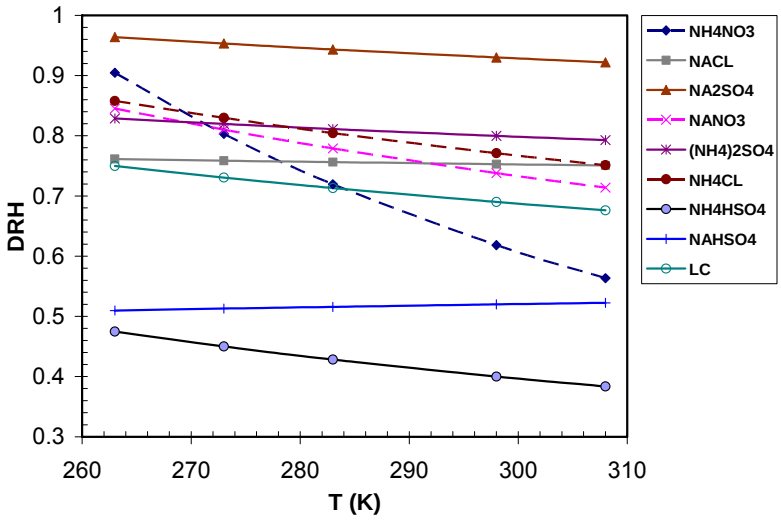

Figure 4.2: DRH as a function of temperature for all ISORROPIA salts.

4.5 Evaluation of ISORROPIA II

ISORROPIA II is evaluated against the predictions of SCAPE2 for a wide range of conditions characteristic of urban, remote continental, non-urban continental and marine aerosol (Heitzenberg, 1989; Fitzgerald, 1991; Ansari and Pandis, 1999a). For urban and non-urban continental aerosol, sulfates, nitrates and ammonium are usually dominant inorganic species. Sodium and chloride often compose the majority of the marine particulate matter (usually with some crustal species and sulfates present). This classification is mainly qualitative, as mixing between aerosol types often occurs in the atmosphere.

Table 4.7 lists the 16 different sets of precursor concentrations that were used in the intercomparison study. Sulfuric acid concentrations range between 1.0 - 5.7 $\mu g\ m^{-3}$ for marine and non-urban continental and 10.0 - 15.0 $\mu g\ m^{-3}$ for urban and remote continental aerosol. For the 16 cases considered, conditions 3, 4, 15 and 16 are sulfate-rich ($R_1 < 1$ or $1 < R_1 < 2$), conditions 1, 2, 13 and 14 represent sulfate near-neutral ($R_1 \approx 2$) aerosol and cases 5 - 12 are sulfate-poor ($R_1 > 2$), (Table 4.7). For each set of precursor concentrations, composition at thermodynamic equilibrium was calculated for 11 different RHs ranging from 10 - 98%; temperature was kept fixed at 298.15K. In the evaluation study both the thermodynamically stable and metastable state solutions of ISORROPIA II are computed.

For the intercomparison study we calculate the normalized mean error (NME) defined as

$NME = \frac{\sum_{i}^{n} |I_i - S_i|}{\sum_{i}^{n} S_i}$, where I_i represents predictions of ISORROPIA II for case i, S_i predictions of SCAPE2 and n is the total number of cases considered.

Finally we compare the CPU time requirements between SCAPE2 and ISORROPIA II, stable and metastable solution of ISORROPIA II, as well as between ISORROPIA II and ISORROPIA for all the simulation conditions of Table 4.7.

Table 4.7: List of input conditions for model simulations[a]

Case	Aerosol Type	Na	H_2SO_4	NH_3	HNO_3	HCl	Ca^{2+}	K^+	Mg^{2+}	R_1, R_2, R_3
1	Urban (1)	0.000	10.000	3.400	2.000	0.000	0.400	0.330	0.000	2.14, 0.18, 0.18
2	Urban (2)	0.023	10.000	3.400	2.000	0.037	0.900	1.000	0.000	2.44, 0.48, 0.47
3	Urban (3)	0.000	15.000	2.000	10.000	0.000	0.900	1.000	0.000	1.27, 0.31, 0.32
4	Urban (4)	0.000	15.000	2.000	10.000	0.000	0.400	0.330	0.000	0.89, 0.12, 0.12
5	N-u Cont.[b] (1)	0.200	2.000	8.000	12.000	0.200	0.120	0.180	0.000	23.9, 0.80, 0.37
6	N-u Cont. (2)	0.100	4.000	10.000	7.000	0.100	0.120	0.180	0.050	14.8, 0.34, 0.24
7	N-u Cont. (3)	0.023	5.664	12.000	2.000	0.037	0.120	0.180	0.050	12.4, 0.18, 0.17
8	N-u Cont. (4)	0.023	5.664	20.400	0.611	0.037	0.120	0.180	0.000	20.9, 0.15, 0.13
9	Marine (1)	2.000	1.000	0.010	0.300	3.121	0.100	0.100	0.070	9.36, 9.30, 0.80
10	Marine (2)	1.500	1.000	0.010	1.500	2.500	0.360	0.450	0.050	8.66, 8.60, 2.21
11	Marine (3)	2.500	3.000	0.001	3.000	2.500	0.500	1.000	0.050	4.86, 4.86, 1.31
12	Marine (4)	3.000	3.000	0.020	2.000	3.121	0.360	0.450	0.130	5.14, 5.10, 0.84
13	Rem. Cont.[b] (1)	0.000	10.000	4.250	0.145	0.000	0.080	0.090	0.000	2.49, 0.04, 0.04
14	Rem. Cont. (2)	0.023	10.000	3.000	1.000	0.037	0.080	0.090	0.000	1.78, 0.05, 0.04
15	Rem. Cont. (3)	0.100	15.000	3.000	4.000	0.100	0.080	0.090	0.000	1.21, 0.06, 0.03
16	Rem. Cont. (4)	0.200	15.000	3.000	8.000	0.200	0.080	0.090	0.040	1.25, 0.10, 0.04

[a] Simulations for each case were conducted for 10, 25, 40, 55, 65, 70, 75, 80, 85, 90 and 98% relative humidity. Temperature was set to 298.15K. Concentration given in μg m^{-3}.

[b] N-u Cont., non-urban continental; Rem. Cont., remote continental.

Table 4.8: Normalized mean errors between ISORROPIA II and SCAPE2 for the simulations in Table 4.7

NME (%)	**$H_2O_{(p)}$**	**$NO_{3(p)}$**	**$Cl_{(p)}$**	**$NH_{4(p)}$**	**Total PM**	**$H^+_{(aq)}$**
ISOROPIA-II (Stable)	13.5	16.5	6.5	2.1	13.0	64.9
ISOROPIA-II (Metastable)	14.7	23.7	6.6	6.7	14.3	68.0

Table 4.9: CPU time required for the simulations in Table 4.7

Aerosol Case	**Convergence criterion**	**ISORROPIA II (stable) CPU time (msec)**	**SCAPE2 CPU time (msec)**	$\frac{CPU_{SCAPE2}}{CPU_{ISORROPIA-II}}$	$\frac{CPU_{ISORROPIA-II(stable)}}{CPU_{ISORROPIA-II(metastable)}}$	$\frac{CPU_{ISORROPIA-II}}{CPU_{ISORROPIA}}$
Marine	10^{-3}	30	50	16.7	1.16	1.0
Urban		20	210	10.5	1.09	1.0
Remote continental		20	440	22.0	1.05	1.0
Non-urban continental		20	110	5.5	1.00	1.0
Marine	10^{-4}	30	>1000	>1000	1.16	1.0
Urban		20	280	14.0	1.09	1.0
Remote continental		20	>1000	>1000	1.05	1.0
Non-urban continental		20	420	21.0	1.00	1.0
Marine	10^{-5}	30	>1000	>1000	1.16	1.0
Urban		20	>1000	>1000	1.09	1.0
Remote continental		20	>1000	>1000	1.05	1.0
Non-urban continental		20	1250	62.50	1.00	1.0

4.5.1 Overall assessment of ISORROPIA II vs. SCAPE2

For all the simulations performed in this work, the water activity database of SCAPE2 was replaced with the one used in ISORROPIA II (reflecting the most updated water activity database). Activities of aqueous species in SCAPE2 were computed using Bromley's formula for multicomponent activity coefficients and the Kussik-Meissner method for binary coefficients.

In Figure 4.3 we compare predictions of aerosol water, nitrate, chloride, ammonium, total PM and hydrogen concentrations between ISORROPIA II (stable solution, forward problem solved), and SCAPE2 for the conditions specified in Table 4.7. Both models predict similar amount of aerosol water content (Figure 4.3a) with a normalized mean error of 13.5%. Most of this discrepancy is found in the low RH regimes (RH < 60%) where SCAPE2 predicts higher water concentration compared to ISORROPIA II. This discrepancy is attributed to a) non-convergence of SCAPE2, which is corroborated by the large CPU time required for obtaining a solution (see Table 4.9), and, b) errors in the calculations of activity coefficients (both binary and multicomponent). At low RH (i.e., low liquid water content), the aqueous solution is highly non-ideal (hence the solution highly non-linear), consequently small changes in activity coefficients may result in large changes in the dissolved species concentrations and the predictions of liquid water content. A few cases exist (for RH > 65%) for which ISORROPIA II predicts less aerosol water than SCAPE2 (Figure 4.3a); this originates from differences in aerosol nitrate which then affects water uptake. For a few marine cases, SCAPE2 predicts negligible water due to non-convergence (Figure 4.3a).

In Figure 4.3b, total aerosol nitrate concentrations are compared for all the input

conditions of Table 4.7. Overall, the agreement is very good with a mean error of 16.5%. ISORROPIA II predicts non-negligible amount of nitrate for some urban cases while SCAPE2 does not. For a few non-urban continental cases ISORROPIA II underpredicts aerosol nitrate compared to SCAPE2. The sources of these discrepancies are further investigated through specific examples in Sect. 4.5.2.

Aerosol chloride concentration predictions are shown in Figure 4.3c where both models show similar results (NME=6.5%) with small discrepancies for a few marine cases (due to non-convergence of SCAPE2 solution) in which chloride exists in significant amount due to significant presence of sea salt particles.

For aerosol ammonium predictions (Figure 4.3d), no substantial differences between the two models were found (NME = 2.1%). Discrepancies were primarily found in some non-urban continental cases which represent a sulfate-poor, ammonium-rich environment and are further analyzed in Sect. 4.5.2. Even though a few differences exist in the predicted concentrations of semi-volatile species, the total PM composition (Figure 4.3e) shows very good agreement (NME=13.0%). The worst agreement between the two models was seen for H^+ predictions (Figure 4.3f) with the normalized mean error significantly higher than for any other component (NME=64%). The discrepancy occurs at low RH (as it scales with water content).

SCAPE2 predictions are also compared against the metastable state solution of ISORROPIA II (Figure 4.4). Table 4.8 shows normalized mean errors between ISORROPIA II (both stable and metastable solutions) and SCAPE2 for the simulations of Table 4.7. As can be seen in Figures 4.3, 4.4 and Table 4.8, the stable state predictions of ISORROPIA II are closer to SCAPE2 predictions. This is expected since only for low

RHs (<40%) SCAPE2 solution, by always attempting to solve for a liquid phase, deviates from the stable state behavior, moving towards the metastable state (see Sect. 4.4.2).

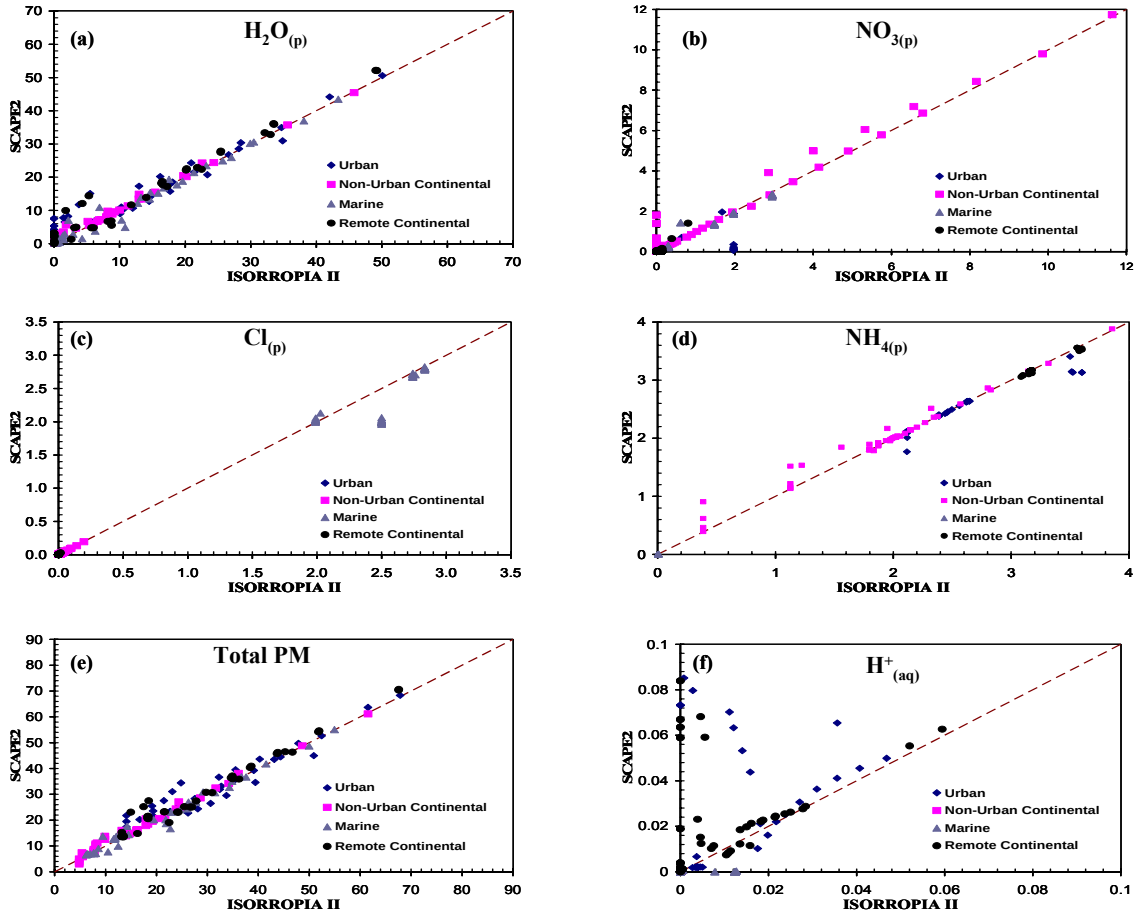

Figure 4.3: Concentration of aerosol water (a), nitrate (b), chloride (c), ammonium (d), total PM (e), and hydrogen (f), as predicted by ISORROPIA-II (thermodynamically stable solution) and SCAPE2 for all the conditions described in Table 4.7. Temperature is set to 298.15K. All units are in μg m^{-3}.

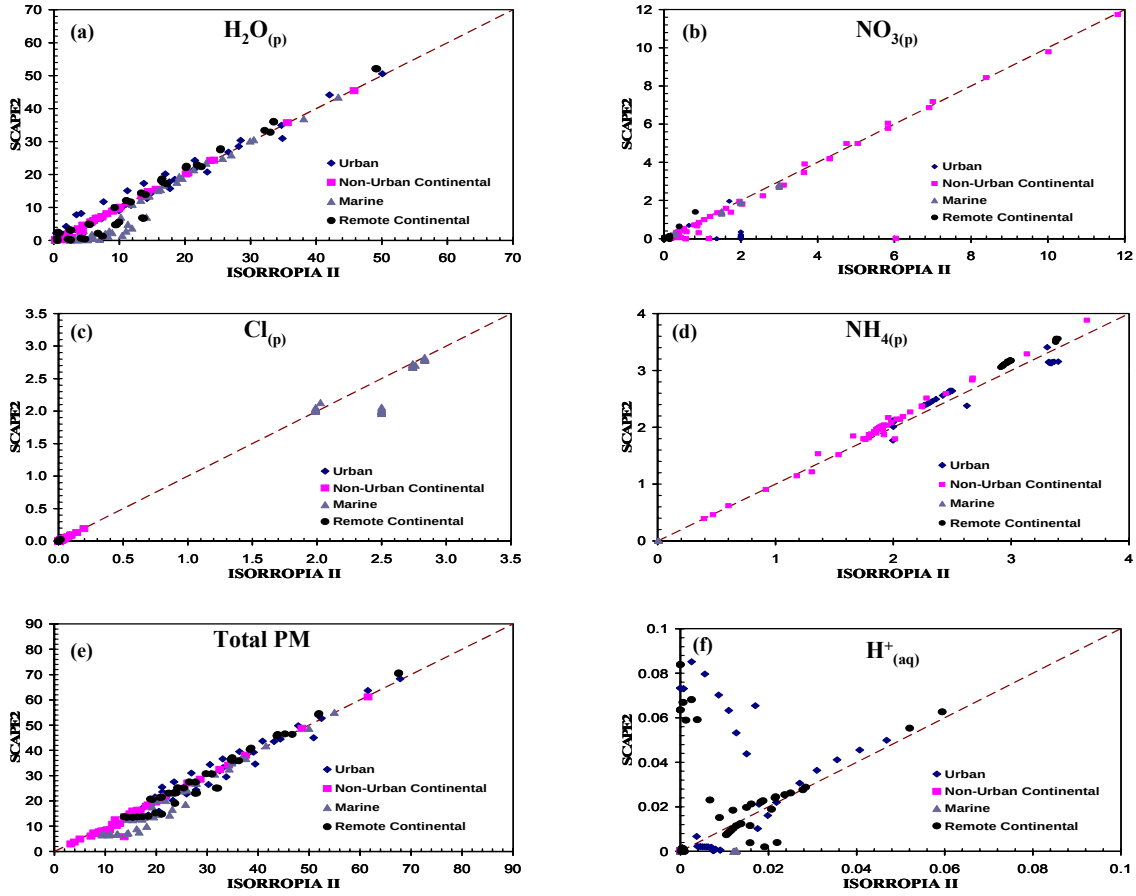

Figure 4.4: Same as Figure 4.3 but using the metastable solution of ISORROPIA-II. All units are in μg m^{-3}.

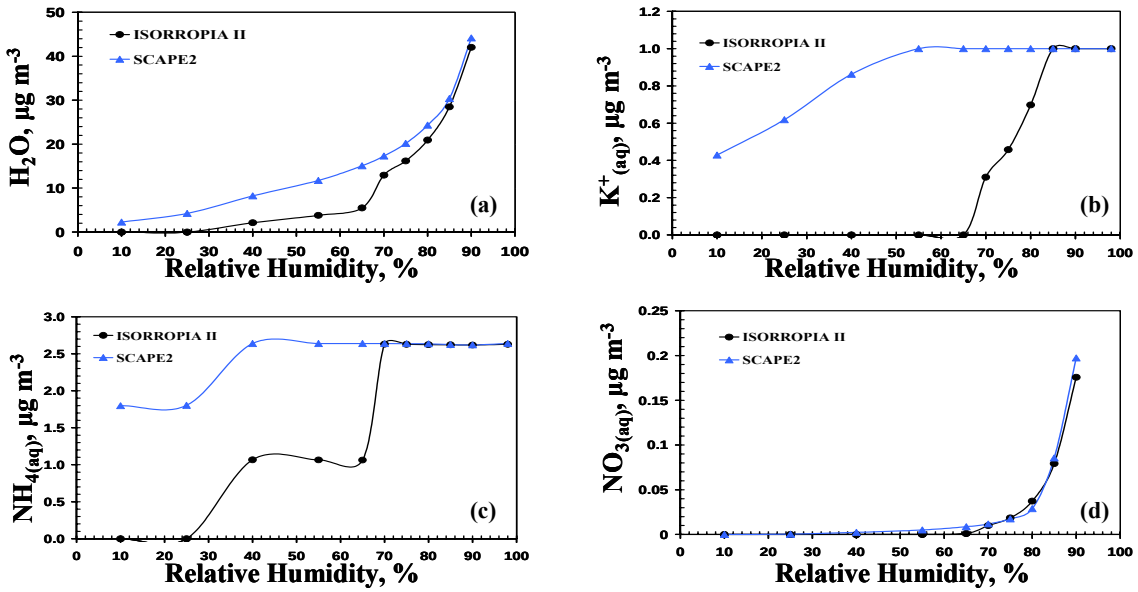

Figure 4.5: Concentration of aerosol water (a), aqueous potassium (b), aqueous ammonium (c), and aqueous nitrate (d) as predicted by ISORROPIA II (thermodynamically stable solution) and SCAPE2 for the urban (3) case (Table 4.7) corresponding to a sulfate rich aerosol behavior ($1<R_1<2$). Temperature is set to 298.15K.

4.5.2 Understanding the discrepancies between ISORROPIA II and SCAPE2

The previous discussion provides an overall intercomparison of the two models for a broad RH and composition domain; some cases are further examined to gain more insight as to the cause of discrepancies. In Figure 4.5 we compare aerosol water content, aqueous phase potassium, aqueous phase ammonium and aqueous phase nitrate concentration predictions for case 3 (see Table 4.7) which produced the largest discrepancy in aerosol water and total PM concentrations. This case represents an urban type aerosol with the solution being highly acidic (R_1=1.27). Under such conditions, the water content discrepancy between the models is largest for low RHs for the reasons outlined in Sect. 4.4.2. This is clearly shown in Figure 4.5a where only for RH>70% SCAPE2 and ISORROPIA II closely follow each other. SCAPE2 predicts significant amount of aqueous phase potassium (Figure 4.5b) and ammonium (Figure 4.5c) at low relative humidities, while ISORROPIA II predicts gradual deliquescence of K_2SO_4 from 65% to 85% RH. However, SCAPE2 predicts complete deliquescence of K_2SO_4 at RH=55% which may be due to non-convergence of its numerical solution. Particulate phase ammonium is mainly present as ammonium bisulfate ($NH_4HSO_{4(s)}$) and letovicite ($(NH_4)_3H(SO_4)_{2(s)}$) in ISORROPIA II. However, SCAPE2 predicts the formation of $(NH_4)_3H(SO_4)_2$ only, throughout the whole RH regime. This can also be seen in Figure 4.5c where ISORROPIA II predicts a two-step dissolution of ammonium; one at RH=40% from the deliquescence of $(NH_4)_3H(SO_4)_{2(s)}$ and one at RH=70% from the deliquescence of $NH_4HSO_{4(s)}$. Water uptake with SCAPE2 exhibits deliquescence only of $(NH_4)_3H(SO_4)_{2(s)}$ at RH=40%. Both models predict similar amounts of aqueous phase nitrate for all RHs (Figure 4.5d) which shows that the assumption of ISORROPIA II for

$NO_{3(aq)}^{-}$ being a minor species for sulfate - rich cases is a good assumption.

Figure 4.6 shows comparison of aerosol water, $NaCl_{(s)}$ and $K_{(aq)}$ and $Mg_{(aq)}$ predictions for case 12 (see Table 4.7), which is a sulfate poor, sodium and crustal species rich aerosol (R_1=5.1). The two models agree well (mean error of 5.1%) in aerosol water content predictions (Figure 4.6a). SCAPE2, however, predicts significantly higher aqueous potassium for RH<40% (Figure 4.6b). This is mainly due to different approaches used to associate $K_{(aq)}$ with $NO_{3(aq)}$ and $SO_{4(aq)}$ at low RH. ISORROPIA II uses the principle of "compositional invariance" (Sect. 4.4.2), hence it preferentially associates K with $SO_{4(aq)}$ to form K_2SO_4, and then $KNO_{3(s)}$ and $KCl_{(s)}$. SCAPE2 tends to partition first as $KNO_{3(s)}$ and $KCl_{(s)}$ and then as $K_2SO_{4(s)}$. Since the DRH of $KCl_{(s)}$ is lower than $K_2SO_{4(s)}$, SCAPE2 deliquesces aerosol potassium at a lower RH than ISORROPIA II. Unlike potassium, both models predict the association of sodium between nitrate ($NaNO_{3(s)}$) and chloride ($NaCl_{(s)}$) in a similar way. This is shown in Figure 4.6c where the dissociation of $NaCl_{(s)}$ as a function of RH is similar between both models (NME=12.1%). Aqueous magnesium is the same in both models (Figure 4.6d), supporting the postulation (Sect. 4.4.3) that $MgSO_{4(s)}$ never precipitates out of solution.

In Figure 4.7 we compare aerosol water, $NO_{3(aq)}$ and $NH_{4(aq)}$ as a function of RH for case 5, a sulfate poor, ammonium rich aerosol (R_1=23.9, R_2=0.80, R_3=0.37). Compared to SCAPE2, ISORROPIA II slightly underpredicts aerosol water, aqueous nitrate and ammonium. This difference is seen for RHs between 25 - 65 %. That is because SCAPE2 predicts total deliquescence of sulfates at RH=40% while ISORROPIA II does at RH=70%. The increase of water content shifts the equilibrium of $HNO_{3(g)} \longleftrightarrow H_{(aq)}^{+} + NO_{3(aq)}^{-}$ and $NH_{3(g)} + H_2O_{(aq)} \leftrightarrow NH_{4(aq)}^{+} + OH_{(aq)}^{-}$ to the right predicting

more aqueous nitrate (Figure 4.7b) and ammonium (Figure 4.6c) for the same RH regime.

4.5.3 Metastable vs. stable solutions

The differences between metastable and stable thermodynamic solutions of ISORROPIA II are illustrated in Figure 4.8; SCAPE2 is also included for comparison. Figure 4.8 shows aerosol water and aqueous potassium concentration as a function of relative humidity for a sulfate near-neutral aerosol (case 13 of Table 4.7). The thermodynamically stable solution of ISORROPIA II predicts deliquescence of the aerosol mixture at 60% RH (DRH of ammonium nitrate). The MDRH for this specific aerosol mixture is 0.46, which explains the aqueous phase potassium (and aerosol water) concentration predicted by the deliquescence solution of ISORROPIA II between 40 and 60% RH. As expected, the metastable solution predicts significant amounts of water below the MDRH (and by definition particulate potassium is deliquesced at all RHs). SCAPE2 yields a solution that is between the stable and metastable ISORROPIA II. Below 40% RH, the predicted concentration of aerosol water by SCAPE2 is slightly larger than the stable solution of ISORROPIA II (Figure 4.8a). This results in partial dissolution of aerosol potassium (RH<40%) predicted by SCAPE2 as opposed to the stable solution of ISORROPIA II which does not predict deliquescence of aerosol potassium for this RH regime (Figure 4.8b).

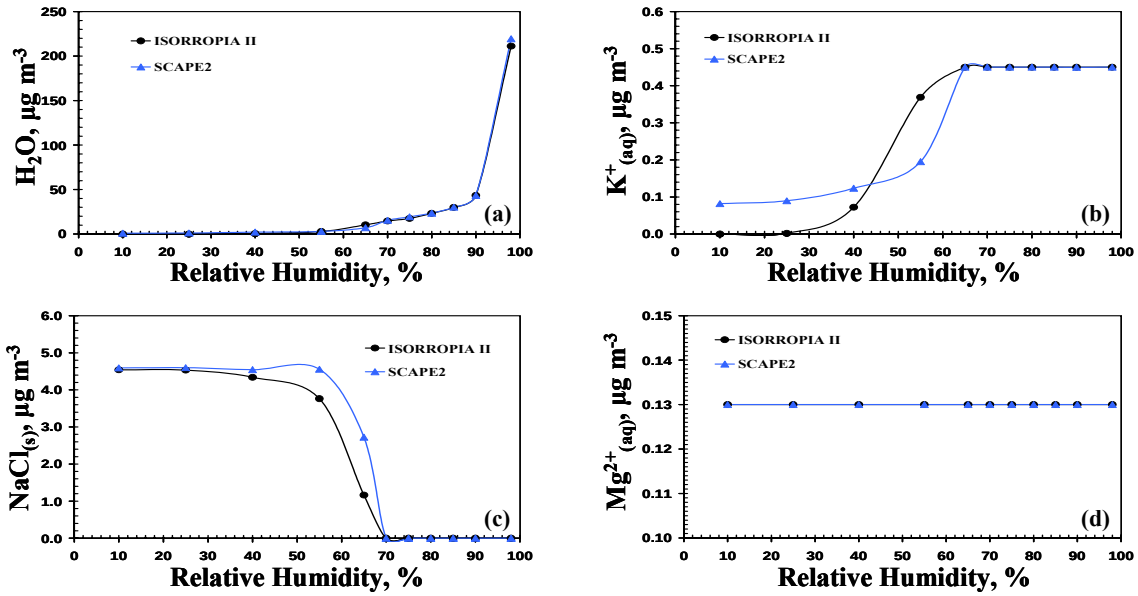

Figure 4.6: Concentration of aerosol water (a), aqueous potassium (b), solid sodium chloride (c), and aqueous magnesium (d) as predicted by ISORROPIA II (thermodynamically stable solution) and SCAPE2 for the marine (4) case (Table 4.7) corresponding to a sulfate poor, crustal and sodium rich aerosol behavior ($R_1>2$, $R_2>2$). Temperature is set to 298.15K.

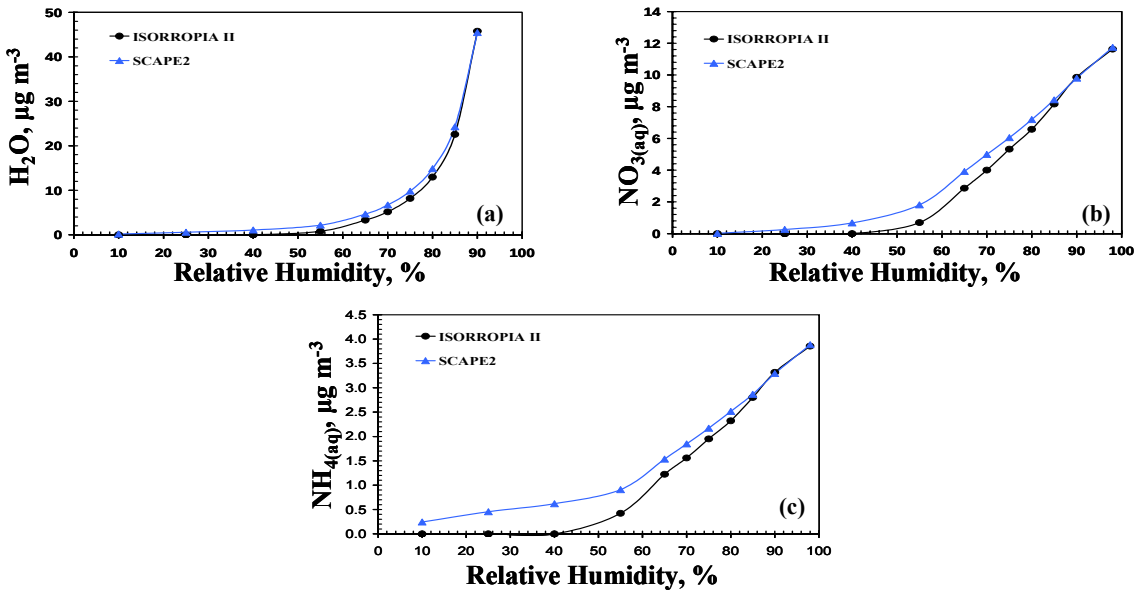

Figure 4.7. Concentration of aerosol water (a), aqueous nitrate (b), and aqueous ammonium (c) as a function of relative humidity as predicted by ISORROPIA II (thermodynamically stable solution) and SCAPE2 for the non-urban continental (1) case (Table 4.7) corresponding to a sulfate poor, ammonium rich aerosol behavior ($R_1>2$, $R_2<2$). Temperature is set to 298.15K.

4.5.4 "Forward" vs. "Reverse" problem solution

ISORROPIA II is designed to solve both forward and reverse problems. It is useful to assess whether the two solution modes predict identical outputs for the same input. For this assessment, the output from the forward problem (particulate phase concentrations of NH_4, SO_4, Na, Cl, NO_3, Ca, K, and Mg) has been used as input to the reverse problem. The two solution modes are assessed by comparing predictions of aqueous nitrate and sulfate. Since sulfate is only found in the aerosol phase, aqueous phase sulfate calculations are used to evaluate the solid/liquid partitioning behavior between the two solution algorithms, while aqueous nitrate is used as a proxy for gas-aerosol partitioning (for all the conditions specified in Table 4.7). The agreement between the two solutions was found to be excellent with the NME being 3.4 ± 1.1% for aqueous sulfate and 2.5 ± 1.3% for aqueous nitrate concentration.

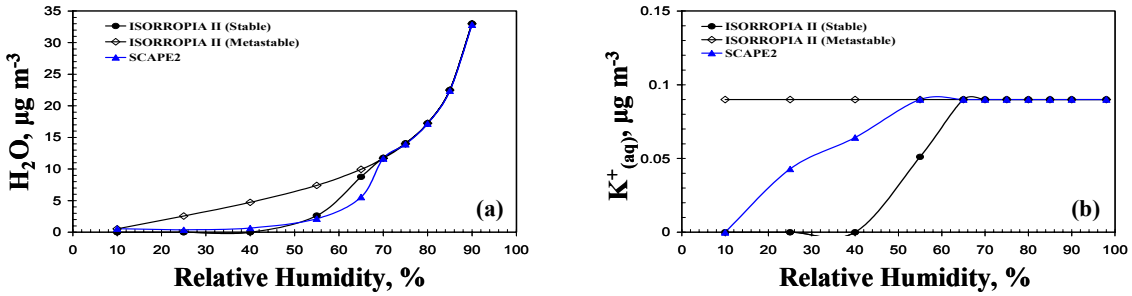

Figure 4.8: Concentration of aerosol water (a), and aqueous phase potassium (b) as a function of relative humidity as predicted by ISORROPIA II (using the thermodynamically stable and metastable solutions) and SCAPE2 for the remote continental (1) case (Table 4.7) corresponding to a sulfate near-neutral aerosol behavior. Temperature is set to 298.15K.

4.5.5 Computational speed

The timing tests were performed on a Dell 8300 Intel Pentium 4 CPU 3.20 GHz, 512 MB of RAM workstation running Windows XP operating system. Both codes were compiled with Watcom FORTRAN compiler version 2.0 with full optimization options on. Table 4.9 shows the CPU time needed by the two models for the aerosol types described in Table 4.7. ISORROPIA II consumes much less CPU time compared to SCAPE2 with the difference being at least an order of magnitude for all aerosol cases.

The amount of time required by ISORROPIA II for each aerosol case was found to be approximately the same even if the convergence criterion for solids and water was decreased down to 10^{-6} or 10^{-7} which is a proof of the rapid and robust convergence of the code. However, larger convergence criterion was used for the intercomparison study (see Table 4.9), to assure a quick and convergent solution from SCAPE2. For completeness we also compare the CPU time required by ISORROPIA (version 1.7, 03/15/2006) for all the simulation conditions of Table 4.7, but with crustal species set to zero). Although ISORROPIA II solves for more species than ISORROPIA, it is not slower because of optimizations in the activity coefficient calculation algorithm in ISORROPIA II. Finally, in Table 4.9 we compare the CPU time required by the stable and metastable solutions of ISORROPIA II. As expected, the metastable solution is slightly faster than the stable solution since the absence of solid species requires the solution of fewer equations.

4.6 Conclusions

A new model, ISORROPIA II, is developed which treats the thermodynamics of K^+-

Ca^{2+}-Mg^{2+}-NH_4^+-Na^+-SO_4^{2-}-NO_3^--Cl^--H_2O aerosol systems. A comprehensive evaluation was conducted against the thermodynamic model SCAPE2 in terms of composition predicted and computational speed for a wide variety of aerosol conditions that cover typical urban, remote continental, marine and non-urban continental environments. The overall predictions of aerosol water, total PM and concentration of semi-volatile species were generally comparable between the two models under most conditions. For aerosol water content and total PM mass the two models agreed within approximately 13%. The normalized mean error for total aerosol nitrate predictions was 16% while for aerosol chloride and ammonium concentration the agreement was within 2 – 6%. Small discrepancies were found to exist between the two models under certain conditions, primarily for relative humidities between 40 and 70%. These discrepancies are mainly attributed to the solution dynamics treatment of water uptake in mutual deliquescence regions and the association of non-volatile cations with sulfate, nitrate and chloride. For all cases examined, ISORROPIA II is more than an order of magnitude faster than SCAPE2, showing robust and rapid convergence for all conditions examined, making it one of the most computationally efficient and comprehensive inorganic thermodynamic equilibrium modules available.

4.7 Acknowledgements

This work was supported by the National Oceanic and Atmospheric Administration under contract NMRAC000-5-04017. We would like to acknowledge the contributions and support of the whole community that lead to significant improvements of the original ISORROPIA code. In particular we would like to acknowledge the contributions of (in

alphabetical order): Asif Ansari, Veronique Bouchet, Prakash Bhave, Simon Clegg, Bill Hutzel, Kevin Capaldo, Bonyoung Koo, Sonia Kreidenweis, Paul Makar, Federico San Martini, Denise Mauzerall, Chris Nolte, Betty Pun, Armistead Russell, Uma Shankar, Daniel Tong, Jason West, Douglas Waldron, Ashraf Zakey, and Yang Zhang. We also would like to thank C. Pilinis for his comments on the manuscript.

4.8 References

Altshüller, A.P.: Atmospheric particle sulfur and sulfur dioxide relationships at urban and nonurban locations, Atmos. Environ., 18, 1421 - 1431, 1984.

Amundson N.R., Caboussat, A., He, J.W., Martynenko, A.V., Savarin, V.B., Seinfeld, J.H., and Yoo, K.Y.: A new inorganic atmospheric aerosol phase equilibrium model (UHAERO), Atmos. Chem. Phys., 6, 975 - 992, 2006.

Ansari A.S., and Pandis, S.N.: Prediction of multicomponent inorganic atmospheric aerosol behavior, Atmos. Environ., 33, 745 - 757, 1999a.

Ansari A.S., and Pandis, S.N.: An analysis of four models predicting the partitioning of semivolatile inorganic aerosol components, Aerosol Sci. Technol., 31, 129 - 153, 1999b.

Brauer, M., and Brook, J.R.: Ozone personal exposures and health effects for selected groups residing in the Fraser Valley, Atmos. Environ., 31, 2113 - 2122, 1997.

Bromley, L.A.: Thermodynamic properties of strong electrolytes in aqueous solutions, AIChE J., 19, 313 - 320, 1973.

Chan, M.N., and Chan, C.K.: Mass transfer effects in hygroscopic measurements of aerosol particles, Atmos. Chem. Phys., 5, 2703 - 2712, 2005.

Clegg, S.L., and Pitzer, K.S.: Thermodynamics of multicomponent, miscible, ionic solutions: generalized equations for symmetrical electrolytes, J. Phys. Chem., 96,

3513 - 3520, 1992.

Clegg, S.L., Pitzer, K.S., and Brimblecombe, P.: Thermodynamics of multicomponent, miscible, ionic solutions. II. Mixture including unsymmetrical electrolytes, J. Phys. Chem., 96, 9470 - 9479, 1992.

Clegg, S.L., Pitzer, K.S., and Brimblecombe, P.: (additions and corrections for their published papers), J. Phys. Chem., 98, 1368, 1994.

Clegg, S.L., Pitzer, K.S., and Brimblecombe, P.: (additions and corrections for their published papers), J. Phys. Chem., 99, 6755, 1995.

Clegg, S.L., Brimblecombe, P., and Wexler, A.S.: Thermodynamic model of the system $H^+ - NH_4^+ - SO_4^{2-} - NO_3^- - H_2O$ at tropospheric temperatures, J. Phys. Chem., A, 102, 2137 - 2154, 1998a.

Clegg, S.L., Brimblecombe, P., and Wexler, A.S.: Thermodynamic model of the system $H^+ - NH_4^+ - Na^+ - SO_4^{2-} - NO_3^- - Cl^- - H_2O$ at 298.15 K, J. Phys. Chem., A, 102, 2155 - 2171, 1998b.

Denbigh, K., The principles of chemical equilibrium, Fourth Ed., Cambridge University Press, Cambridge, 1981.

Dockery, D.W., Pope, C.A., Xu, X., Spengler, J.D., Ware, J.H., Fay, M.E., Ferris, B.G., and Speizer, F.E.: An Association between Air Pollution and Mortality in Six U.S. Cities, The New England Journal of Medicine, 329, 1753 - 1759, 1993.

Fitzgerald, J.W.: Marine aerosols: A review, Atmos. Environ., 25A, 533 - 545, 1991.

Fountoukis, C., and Nenes, A.: ISORROPIA II: A computationally efficient thermodynamic equilibrium model for K^+-Ca^{2+}-Mg^{2+}-NH_4^+-Na^+-SO_4^{2-}-NO_3^--Cl^--H_2O aerosols, Atmos. Chem. Phys. Discuss., 7, 1893-1939, 2007.

Ha, Z., and Chan, C.K.: The water activities of $MgCl_2$, $Mg(NO_3)_2$, $MgSO_4$, and their mixtures, Aerosol Sci. Technol., 31, 154 - 169, 1999.

Heitzenberg, J.: Fine particles in the global troposphere: a review, Tellus 41B, 149 - 160, 1989.

Intergovernmental Panel on Climate Change: The scientific Basis, Cambridge Univ. Press, New York, 2001.

Jacobson, M.Z., Tabazadeh, A., and Turco, R.P.: Simulating equilibrium within aerosols and nonequlibrium between gases and aerosols, J. Geophys. Res., 101, 9079 - 9091, 1996.

Jacobson, M.Z.: Chemical Equilibrium and dissolution processes, Fundamentals of Atmospheric Modeling, Cambridge University Press, New York, 1999a.

Jacobson, M.Z.: Studying the effect of calcium and magnesium on size-distributed nitrate and ammonium with EQUISOLV II, Atmos. Environ., 33, 3635 - 3649, 1999b.

Ramachandran, G., and Vincent, J.H.: A Bayesian approach to retrospective exposure assessment, Applied Occupational and Environmental Hygiene, 14, 547 - 558, 1999.

Kaiser, J., Mounting evidence indicts fine-particle pollution, Science, 307, 1858 - 1861, 2005.

Kelly, J.T., and Wexler, A.S.: Thermodynamics of carbonates and hydrates related to heterogeneous reactions involving mineral aerosol, J. Geophys. Res.,, 110, D11201, doi:10.1029/2004JD005583, 2005.

Kelly, J.T., and Wexler, A.S.: Water uptake by aerosol: Water activity in supersaturated potassium solutions and deliquescence as a function of temperature, Atmos. Environ, 40, 4450 - 4468, 2006.

Kim, Y.P., Seinfeld, J.H., and Saxena, P.: Atmospheric gas - aerosol equilibrium I. Thermodynamic model, Aerosol Sci. Technol., 19, 157 - 181, 1993a.

Kim, Y.P., Seinfeld, J.H., and Saxena, P.: Atmospheric gas - aerosol equilibrium II. Analysis of common approximations and activity coefficient calculation methods, Aerosol Sci. Technol., 19, 182 - 198, 1993b.

Kim, Y.P., and Seinfeld, J.H.: Atmospheric gas - aerosol equilibrium III. Thermodynamics of crustal elements Ca^{2+}, K^{+}, and Mg^{2+}, Aerosol Sci. Technol., 22, 93 - 110, 1995.

Kusik, C.L., and Meissner, H.P.: Electrolyte activity coefficients in inorganic processing, AIChE Symp. Series, 173, 14 - 20, 1978.

Makar, P.A., Bouchet, V.S., and Nenes, A.: Inorganic chemistry calculations using HETV – a vectorized solver for the SO_4^{2-} - NO_3^{-} - NH_4^{+} system based on the ISORROPIA algorithms, Atmos. Environ., 37, 2279 - 2294, 2003.

Meng, Z.Y., Seinfeld, J.H., Saxena, P., and Kim, Y.P.: Atmospheric gas - aerosol equilibrium IV. Thermodynamics of carbonates, Aerosol Sci. Technol., 23, 131 - 154, 1995.

Meissner, H.P., Kusik, C.L., and Tester, J.W.: Activity coefficients of strong electrolytes in aqueous solution - effect of temperature, AIChE Journal, Vol. 18, No. 3, 661-662, 1972.

Meissner, H.P., and Peppas, N.A.: Activity coefficients - aqueous solutions of polybasic acids and their salts, AIChE Journal, Vol. 19, No. 4, 806-809, 1973.

Metzger, S.M., Dentener, F.J., and Lelieveld, J.: Aerosol multiphase chemistry - A parameterization for global modeling, Int. Rep. 99 - 12, for Mar. and Atmos. Res., Utrecht, Netherlands, 1999.

Metzger, S.M., Dentener, F.J., Lelieveld, J., and Pandis, S.N.: Gas/aerosol partitioning I: a computationally efficient model, J. Geophys. Res., 107, D16, 4312, doi:10.1029/2001JD001102, 2002a.

Metzger, S.M., Dentener, F.J., Jeuken, A., Krol, M., and Lelieveld, J.: Gas/aerosol partitioning II: global modeling results, J. Geophys. Res., 107, D16, 4313, doi:10.1029/2001JD001103, 2002b.

Metzger, S., Mihalopoulos, N., and Lelieveld, J.: Importance of mineral cations and

organics in gas-aerosol partitioning of reactive nitrogen compounds: case study based on MINOS results, Atmos. Chem. Phys., 6, 2549 - 2567, 2006.

Moya, M., Ansari, A.S., and Pandis, S.N.: Partitioning of nitrate and ammonium between the gas and particulate phases during the 1997 IMADA-AVER study in Mexico City, Atmos. Environ., 35, 1791 - 1804, 2001a.

Moya, M., Pandis, S.N., and Jacobson, M.Z.: Is the size distribution of urban aerosols determined by thermodynamic equilibrium? An application to Southern California, Atmos. Environ., 36, 2349 - 2365, 2001b.

Nenes, A., Pandis, S.N., and Pilinis, C.: ISORROPIA: A new thermodynamic equilibrium model for multiphase multicomponent inorganic aerosols, Aquatic Geochemistry, 4, 123 - 152, 1998.

Nenes, A., Pilinis, C., and Pandis, S.N.: Continued development and testing of a new thermodynamic aerosol module for urban and regional air quality models, Atmos. Environ., 33, 1553 - 1560, 1999.

Pilinis, C., and Seinfeld, J.H.: Continued development of a general equilibrium model for inorganic multicomponent atmospheric aerosols, Atmos. Environ, 21, 2453 - 2466, 1987.

Pilinis, C., and Seinfeld, J.H.: Water content of atmospheric aerosols, Atmos. Environ., 23, 1601 - 1606, 1989.

Pitzer, K. S., and Simonson, J.M.: Thermodynamics of multicomponent, miscible, ionic systems: Theory and equations, J. Phys. Chem., 90, 3005 - 3009, 1986.

Potukuchi, S., and Wexler, A.S.: Identifying solid-aqueous phase transitions in atmospheric aerosols - I. Neutral-acidity solutions, Atmos. Environ., 29, 1663 - 1676, (1995a).

Potukuchi, S., and Wexler, A.S.: Identifying solid-aqueous phase transitions in atmospheric aerosols - II. Acidic solutions, Atmos. Environ., 29, 3357 - 3364, 1995b).

Seinfeld, J.H., and Pandis, S.N.: Atmospheric Chemistry and Physics: From Air Pollution to Climate Change, John Wiley & Sons, Inc., 1998.

Stelson, A.W., and Seinfeld, J.H.: Relative humidity and temperature dependence of the ammonium nitrate dissociation constant, Atmos. Environ., Vol. 16, No 5, 983 - 992, 1982.

Thomsen, K., and Rasmussen, P.: Modeling of vapor-liquid-solid equilibrium in gas-aqueous electrolyte systems, Chem. Eng. Sci., 54, 1787 - 1802, 1999.

Wexler, A.S., and Clegg, S.L.: Atmospheric aerosol models for systems including the ions H^+, NH_4^+, Na^+, SO_4^{2-}, NO_3^-, Cl^-, Br^-, and H_2O, J. Geophys. Res., 107, 4207, doi:10.1029/2001JD000451, 2002.

Wexler, A.S., and Seinfeld, J.H.: The distribution of ammonium salts among a size and composition dispersed aerosol, Atmos. Environ., 24A, 1231 - 1246, 1990.

Wexler, A.S., and Seinfeld, J.H.: Second - generation inorganic aerosol model, Atmos. Environ., 25A, 2731 - 2748, 1991.

Wexler, A.S., and Clegg, S.L.: Atmospheric aerosol models for systems including the ions H^+, NH_4^+, Na^+, SO_4^{2-}, NO_3^-, Cl^-, Br^-, and H_2O, J. Geophys. Res., 107, 4207, doi:10.1029/2001JD000451, 2002.

Yu, S., Dennis, R., Roselle, S., Nenes, A., Walker, J., Eder, B., Schere, K., Swall, J., and Robarge, W.: An assessment of the ability of three-dimensional air quality models with current thermodynamic equilibrium models to predict aerosol NO_3^-, J. Geophys. Res., 110, D07S13, doi:10.1029/2004JD004718, 2005.

Zanobetti, A., Schwartz, J., and Dockery, D.W.: Airborne particles are a risk factor for hospital admissions for heart and lung disease, Environmental Health Perspective, 108, 1071 - 1082, 2000.

Zaveri, R.A., Easter, R.C., and Peters, L.K.: A computationally efficient multicomponent equilibrium solver for aerosols (MESA), J. Geophys. Res., 110, D24203, doi:10.1029/2004JD005618, 2005a.

Zaveri, R.A., Easter, R.C., and Wexler, A.S.: A new method for multicomponent activity coefficients of electrolytes in aqueous atmospheric aerosols, J. Geophys. Res., 110, D02201, doi:10.1029/2004JD004681, 2005b.

Zhang, Y., Seigneur, C., Seinfeld, J.H., Jacobson, M., Clegg, S.L., and Binkowski, F.S.: A comparative review of inorganic aerosol thermodynamic equilibrium models: similarities, differences, and their likely causes, Atmos. Environ., 34, 117 - 137, 2000.

CHAPTER 5

THERMODYNAMIC CHARACTERIZATION OF AEROSOL FROM A MEGACITY[I]

5.1 Abstract

Fast measurements of aerosol and gas-phase constituents coupled with the ISORROPIA-II thermodynamic equilibrium model are used to study the partitioning of semivolatile inorganic species and phase state of Mexico City aerosol sampled at the T1 site during the MILAGRO 2006 campaign. Overall, predictions agree very well with measurements of ammonium, nitrate, chloride and gas phase ammonia. In the ammonia-rich environment of Mexico City, nitrate and chloride primarily partition in the aerosol phase with a 20-min equilibrium timescale; $PM_{2.5}$ is insensitive to changes in ammonia but is to acidic semivolatile species. When RH is below 50%, predictions improve substantially if the aerosol is assumed to follow the deliquescent phase diagram. Treating crustal species as "equivalent sodium" (rather than explicitly) in the thermodynamic equilibrium calculations introduces substantial biases in predicted aerosol water uptake, nitrate and ammonium. This suggests that comprehensive thermodynamic calculations are required to predict the partitioning and phase state of aerosols containing crustal material.

[I] Under review: Fountoukis, C., Sullivan, A., Weber, R., Vanreken, T., Fischer, M., Matías, E., Moya, M., Farmer, D., Cohen, R., and Nenes, A.: Thermodynamic characterization of Mexico City Aerosol during MILAGRO 2006, Atmos. Chem. Phys., in review, 2007.

5.2 Introduction

Atmospheric particulate matter plays a central role in atmospheric phenomena like visibility reduction, public health, formation of acid rain and climate change. Fine particles, otherwise called $PM_{2.5}$ (particles with diameter less than 2.5μm) are prime contributors to the above processes, a quantitative understanding of which requires knowledge of their phase and composition. Much of the dry particle mass is inorganic (25-75 %) (Heitzenberg, 1989) with the main components often being ammonium (NH_4^+), sulfate (SO_4^{2-}), and nitrate (NO_3^-). Depending on the location, sodium (Na^+) and chloride (Cl^-) may also be found in atmospheric particle composition as well as crustal species (Ca^{2+}, K^+, Mg^{2+}) which are a major component of dust (Heitzenberg, 1989; Malm et al., 1994). These species may be in the form of aqueous ions, or in the form of precipitated solids, or they may partially volatilize (e.g. NH_4^+, NO_3^-, Cl^-). The partitioning of these species between gas, liquid and solid phase is driven by thermodynamic equilibrium and can be simulated by thermodynamic equilibrium models, such as AIM2 (Wexler and Clegg, 2002), SCAPE2 (Meng et al., 1995), GFEMN (Ansari and Pandis, 1999a,b), UHAERO (Amundson et al., 2006) and ISORROPIA-II (Fountoukis and Nenes, 2007). These models differ in the chemical species that they can treat, the method used to solve for equilibrium composition, the type of input they can accept, and their computational efficiency. Similarities and differences between these models are discussed elsewhere (e.g., Ansari and Pandis, 1999a,b; Zhang et al., 2000; Amundson et al., 2006; Fountoukis and Nenes, 2007).

An important question regarding the partitioning of semivolatile inorganic aerosol phase is whether the assumption of thermodynamic equilibrium is adequate to predict chemical

composition. A key factor is aerosol size (Wexler and Seinfeld 1991, 1992; Meng and Seinfeld, 1996; Dassios and Pandis, 1999; Cruz et al., 2000); for submicron particles, equilibrium is achieved typically within a few minutes, often faster than ambient conditions change (Meng and Seinfeld, 1996; Dassios and Pandis, 1999; Cruz et al., 2000) so that the assumption of instantaneous equilibrium can be used to model composition. Coarse mode particles however require substantial time, on the order of an hour or more (Meng and Seinfeld, 1996; Dassios and Pandis, 1999; Cruz et al., 2000). In this case, a condensation/evaporation dynamics driven by departure from equilibrium is required (e.g., Pilinis et al., 2002; Capaldo et al., 2000).

Several studies have been conducted to test the validity of the equilibrium assumption by comparing thermodynamic model performance against observational data. Moya et al., (2001) used ISORROPIA, SCAPE2 and GFEMN to study the partitioning of nitrate and ammonium in Mexico City during the 1997 IMADA-AVER field campaign. Using daily and 6-hour average $PM_{2.5}$ data, Moya et al., (2001) found the equilibrium approach reproducing most of the data, however a few discrepancies were found and were attributed to the implicit treatment of crustal species (treated as "equivalent" sodium). Zhang et al. (2003) assessed the nitrate – ammonium equilibrium assumption using the ISORROPIA model and high resolution (5-minute average) data obtained during the 1999 Atlanta Supersite Experiment. They found good agreement for nitrate and ammonium when a 15% correction in $PM_{2.5}$ SO_4^{2-} was applied. Takahama et al., (2004) used GFEMN to model the partitioning of nitrate during the 2001-2002 Pittsburg Air Quality Study (PAQS). Using 1 and 2-hour average measurements of $PM_{2.5}$ they found most of the predictions of nitrate to agree with observations to within experimental

uncertainty. Yu et al., (2005) used the 1999 Atlanta Supersite Experiment data, the PAQS dataset, and 12-hour measurement data from North Carolina in 1999 to assess the ability of the three-dimensional (3-D) Community Multiscale Air Quality (CMAQ) model (which includes ISORROPIA) to predict aerosol nitrate. They found that errors associated with sulfate and total ammonium predictions of the 3-D model can lead to large errors in predicted aerosol nitrate. Using CMAQ and ISORROPIA, Nowak et al., (2006) analyzed gas phase ammonia measurements (using a PILS for the aerosol and a CIMS instrument for the gas phase data) from the 2002 Atlanta Aerosol Nucleation and Real–Time Characterization Experiment (ANARChE) and found excellent agreement for NH_3 and NH_4^+ concentrations.

The phase state of aerosols is another important issue in aerosol modeling, as they can follow the deliquescence branch (in which solids precipitate out of the aqueous aerosol phase upon saturation) or the efflorescence branch (in which the aerosol is always an aqueous phase and solids are not allowed to form). Depending on their RH history particles can follow different paths. As RH increases the particles deliquesce as water is absorbed, while when RH decreases the particle may not crystallize at its initial deliquescence point, but retain water until a much lower relative humidity (hysteresis phenomenon). Ansari and Pandis (2000) studied the impact of assuming a deliquescent vs. effluorescent path on the partitioning of nitrate in Southern California; when nitrate concentrations were low (< 8 μg m^{-3}), the considerations of both branches of aerosol behavior is essential, while no significant difference between stable and metastable predictions was found for high (> 8 μg m^{-3}) aerosol nitrate concentrations. Moya et al., (2002) showed that the assumption of metastable state for sub-micrometer particles may

introduce large errors when RH < 60% highlighting the importance of deliquescence predictions at low RH.

Most studies to date either use measurements averaged over long times or use models that do not explicitly treat crustals. If measurements are slow, significant variations in *T*, RH and aerosol precursor concentrations may occur during sampling which cannot be accounted for in equilibrium calculations. Additionally, the consideration of crustal material in predicting the partitioning of nitrate and ammonium, especially in areas where dust comprises a significant portion of total PM, can considerably affect the aerosol thermodynamics and improve model predictions (Ansari and Pandis, 1999; Moya et al., 2002).

In the present work, we use ISORROPIA-II, which treats the thermodynamics of the K^+-Ca^{2+}-Mg^{2+}-NH_4^+-Na^+-SO_4^{2-}-HSO_4^--NO_3^--Cl^--H_2O aerosol system, to a) test the thermodynamic equilibrium assumption for the Mexico City environment during the MILAGRO 2006 campaign, b) gain insight on the preferred phase behavior of the aerosol (i.e. deliquescent or metastable), and, c) assess the importance of a full thermodynamic treatment versus neglecting the presence of crustals (or treating them as equivalent sodium). The MILAGRO 2006 dataset analyzed here is ideal for the purpose of this study due to the presence of significant concentrations of all the inorganic species mentioned above.

5.3 Observational data

The Megacity Initiative: Local and Global Research Observations (MILAGRO) Campaign took place in March 1 - 30, 2006 (http://www.eol.ucar.edu/projects/milagro/).

The three main ground locations were: one site at the Instituto Mexicano del Petróleo (T0 site, latitude: 19.25 N, longitude: 99.10 W), another at the Universidad Tecnológica de Tecámac in the State of Mexico (T1 site, latitude: 19.703 N, longitude: 98.982 W) and a third in Rancho La Bisnaga in the State of Hidalgo (T2 site, latitude: 20.01 N, longitude: 98.909 W). The data analyzed in this study were collected at the T1 site from 21 to 30 March 2006 and include fine particulate matter concentrations ($PM_{2.5}$) of NH_4^+, SO_4^{2-}, NO_3^-, Na^+, Cl^-, Ca^{2+}, K^+, Mg^{2+}, gas phase concentrations of NH_3, HNO_3, HCl and ambient temperature, and relative humidity.

The $PM_{2.5}$ ion concentrations were measured by a Particle Into Liquid Sampler (PILS) with a 5-min sampling period and a 10-min duty cycle (Orsini et al., 2003). The advantage of this instrument is the simultaneous measurements of important inorganic anions and cations at high time-resolution. $NH_{3(g)}$ concentrations were obtained every minute with quantum-cascade laser (QCL) spectrometer (Fischer et al., 2007), while volatile nitrate (i.e. $HNO_{3(g)} + NH_4NO_3$) concentrations were measured every 5 minutes by a thermal dissociation-laser induced fluorescence of nitrogen oxides (TD-LIF, Farmer et al., 2006; Day et al., 2002). Ambient temperature (*T*), pressure and relative humidity (RH) data are based on the measurements of the Vaisala Y50 Sensor which was operated with a 1-min time resolution. Aerosol particles (PM_1 and $PM_{2.5}$) were also collected with a cascade micro-orifice uniform deposit impactor (MOUDI), MSP Model 100 (Marple et al., 1991) at the same site and sampling period.

5-minute averages of $NH_{3(g)}$ concentrations, *T* and RH were obtained to correspond to the 5-min averages of $HNO_{3(g)}$ and $PM_{2.5}$ ion concentrations. In ~26% of the cases, the 5-min averages of $HNO_{3(g)}$ data were not coincident with the 5-min PILS concentrations,

therefore a 20-min average were considered instead (average of two 5-min measurements with a 10-min interval between the two data points). The TD-LIF measurement is the sum of gas-phase and semivolatile nitrate (i.e. $HNO_{3(g)}$ + NH_4NO_3), from which $HNO_{3(g)}$ is obtained by subtracting $PM_{2.5}$ ammonium nitrate concentrations from the PILS; this can be done because preliminary ISORROPIA-II calculations suggest that the PILS nitrate is entirely semivolatile (i.e. NH_4NO_3 only). Aerosol K^+ is not directly measured by PILS; instead, it was estimated based on a nearly constant ratio (~0.4) of K^+ to the sum of crustal species (Ca^{2+}, K^+, Mg^{2+}) obtained from the MOUDI impactor data for the same site and sampling period. Gas-phase hydrochloric acid ($HCl_{(g)}$) concentrations were assumed to be zero (hence total Cl^- was equal to aerosol Cl^-). The validity of this assumption is assessed in section 5.5. The measurement uncertainty was estimated to be approximately ±20% for the PILS instrument (Orsini et al., 2003), ±10% for the $NH_{3(g)}$ measurement (Fischer et al., 2007), ±30% for the TD-LIF instrument (Farmer et al., 2006; Day et al., 2002) and ±5% for *T* and RH. The $HNO_{3(g)}$ uncertainty, $\sigma_{HNO_{3(g)}}$, was estimated from the uncertainties of volatile $\sigma_{(TD-LIF\ nitrate)}$, and PILS nitrate $\sigma_{(PILS\ nitrate)}$, respectively, as:

$$\sigma^2_{HNO_{3(g)}} = \sigma^2_{(TD-LIF\ nitrate)} + \sigma^2_{(PILS\ nitrate)} \quad (5.1)$$

The reported detection limit for the PILS concentrations is 0.02 μg m^{-3} for Na^+, NH_4^+, NO_3^- and SO_4^{2-}, 0.002 μg m^{-3} for Ca^{2+}, Mg^{2+} and Cl^- and 0.35 μg m^{-3} for the QCL $NH_{3(g)}$ measurement.

Overall, 102 5-minute data points were obtained for which measurements of all particulate and gaseous species are available. Ammonia was predominantly in the gas phase while nitrate was dominant in the aerosol phase. The total (gas + particulate)

ammonia (TA) to sulfate molar ratio was much larger than 2 (average value = 26.5) indicating sulfate poor aerosols. Relatively low concentrations of Na^+ (0.063 ± 0.113 μg m^{-3}), Ca^{2+} (0.116 ± 0.206 μg m^{-3}), K^+ (0.097 ± 0.140 μg m^{-3}) and Mg^{2+} (0.033 ± 0.051 μg m^{-3}) were detected while the total $PM_{2.5}$ mass was, on average, 28.47 ± 13.03 μg m^{-3}. Temperature did not vary significantly over the measurement period of study (mean value of 289.5 ± 5.1 K) while RH varied significantly (mean value of 58.1 ± 22.6 %), exhibiting a typical diurnal cycle which peaks in the evening and early morning and is minimum at around noon. A detailed overview of the dataset and meteorological conditions is given elsewhere (e.g. Doran et al., 2007; Fast et al., 2007).

5.4 Aerosol equilibrium modeling

ISORROPIA-II (Fountoukis and Nenes, 2007) is a computationally efficient code that treats the thermodynamics of K^+-Ca^{2+}-Mg^{2+}-NH_4^+-Na^+-SO_4^{2-}-NO_3^--Cl^--H_2O aerosol systems and is used in this study. ISORROPIA-II is designed to solve two classes of problems: (a) forward (or "closed") problems, in which known quantities are *T*, RH and the total (gas + aerosol) concentrations of NH_3, H_2SO_4, Na, HCl, HNO_3, Ca, K, and Mg, and, (b) reverse (or "open") problems, in which known quantities are *T*, RH and the concentrations of aerosol NH_4, SO_4, Na, Cl, NO_3, Ca, K, and Mg. ISORROPIA-II can predict composition for the “stable” (or deliquescent path) solution where salts precipitate once the aqueous phase becomes saturated with respect to a salt, and, a “metastable” (efflorescent path) solution, in which the aerosol is composed only of an aqueous phase regardless of its saturation state. For the dataset of this study, the forward mode of ISORROPIA-II is used.

5.5 Results and discussion

5.5.1 Model vs. observations

In this section we evaluate the ability of ISORROPIA-II to reproduce the observed partitioning of ammonia, nitrate and chloride, which will test the expectation that thermodynamic equilibrium is adequate to predict the partitioning of semivolatile aerosol species for timescales between 5 and 30 minutes. Figure 5.1a-e shows predicted vs. observed concentrations of gas-phase ammonia ($NH_{3(g)}$), nitric acid ($HNO_{3(g)}$), aerosol phase ammonium ($NH_{4(p)}$), nitrate ($NO_{3(p)}$) and chloride ($Cl_{(p)}$), respectively; Table 5.1 summarizes the corresponding error metrics. For the simulations of Figure 5.1, ISORROPIA-II was run in forward mode and stable state conditions. Most of the total ammonia (88.7% on average) resides in the gas phase. The data have been separated into 4 classes based on a "completeness factor" (CF). For half of the data analyzed (51%), 5-min average measurements of all (gas + particulate phase) species were available; these data are represented as "CF=0". For ~26% of the data, only 20-min average measurement of ion concentrations from the PILS instrument were available and are "CF=1" data. Subtracting the PILS ammonium nitrate measurement from the TD-LIF (i.e. $HNO_{3(g)}$ + NH_4NO_3) occasionally resulted in a negative $HNO_{3(g)}$. Under such conditions, $HNO_{3(g)}$ is assumed zero, and the data is indicated as "CF=2" if they correspond to 5-minute averages (13% of the data), and "CF=3" for 20 min averages (10% of the data). The error metrics used in Table 5.1 are the normalized mean error (NME), $NME = \frac{\sum_i^n |I_i - O_i|}{\sum_i^n O_i}$, and

normalized mean bias (NMB), $NMB = \frac{\sum_{i}^{n}(I_i - O_i)}{\sum_{i}^{n} O_i}$, where I_i represents predictions of ISORROPIA-II for data point i, O_i represents observations and n is the total number of data points. NME gives an estimation of the overall discrepancy (scatter) between predictions and observations, while NMB systematic errors (biases).

An excellent agreement between model predictions and observations was found for $NH_{3(g)}$ (Figure 1a) with a NME of 5.3%, a slope of 0.991, an intercept of -0.676 μg m^{-3} (much smaller than concentrations of $NH_{3(g)}$) and an R^2 of 0.992. Particulate ammonium (Figure 1b) was systematically overpredicted, as shown by the 37.1% NMB (Table 1). This overprediction could arise from the phase state assumption, departure from equilibrium or measurement uncertainty; all of these possibilities are explored in section 5.5.3.

Predictions of $HNO_{3(g)}$ were subject to much uncertainty (Figure 5.1c), with a NME of 80.8% (Table 5.1). This discrepancy is attributed to a) zero concentrations of $HNO_{3(g)}$ for a portion of the data (CF=2 and 3), and, b) low, on average, concentrations of gas phase nitrate which results in predictions of $HNO_{3(g)}$ being very sensitive to errors in particulate nitrate ($NO_{3(p)}$). When partitioning is predominantly in one phase, small errors in predicted concentration of species in the dominant phase, leads to large errors in predictions for the other phase. Additionally, the estimated uncertainty for $HNO_{3(g)}$ (using Eq. 5.1) was found to be very large (~100% on average) which makes the agreement between predicted and observed $HNO_{3(g)}$ to, in fact, be within the calculated uncertainty. For particulate nitrate (Figure 5.1d), ISORROPIA-II predictions agree well with

observations with a NME of 27.2% and a small bias (NMB = 8.0%).

Observed concentrations of $Cl^-_{(p)}$ agree well (NME=15.5%) with predicted values (Figure 5.1e); this is because ISORROPIA-II predicts very small amounts of chloride in the gas phase because the large excess of $NH_{3(g)}$ tends to drive Cl^- almost completely into the aerosol phase. This justifies (to first order) the assumption of zero $HCl_{(g)}$ in the thermodynamic calculations. However, the NME and NMB are almost identical in magnitude; this suggests that the prediction error is likely only from the "missing" (small) amount of $HCl_{(g)}$ that are not considered in the calculations of Figure 5.1e (mean predicted value for $HCl_{(g)}$=0.03 μg m^{-3}) and is consistent with the analysis of San Martini et al., (2006) for Mexico City aerosol during MCMA-2003.

Agreement between predictions and measurements depends on many factors, such as equilibrium timescale and measurement uncertainty; we assess the importance of each by examining the prediction skill between CF classes, since a) the averaging timescale changes, and, b) the calculated zero concentration of $HNO_{3(g)}$ for some of the data may lead to a biased prediction. Figure 5.1 (and Table 5.1) shows that the closure for CF=0 data is slightly worse than for CF=1 to 3 (the equilibration timescale could be a possible reason for that). This suggests that the TD-LIF provides an excellent measure of volatile nitrate (as the NMB and NME for particulate nitrate are consistent between CF classifications). Based on work to date (e.g., Meng and Seinfeld, 1996; Dassios and Pandis, 1999; Cruz et al., 2000) we expect the equilibration timescale to be on the order of 10 minutes; indeed the Table 5.1 results support this, as NMB is consistently minimum for the 20 min data (Table 5.1). To further explore that the decrease in NMB is a result of equilibration timescale (and not any other experimental uncertainty), we use

the CF=0 data, compute 35 min averages and compare against the thermodynamic predictions. Table 5.2 shows results of calculations using ~20 min (CF=1) and ~35 min; the latter was computed by averaging consecutive 5-min (i.e., CF=0) measurements. As can be seen, NME and NMB decreases between the 5 and 20 min averages, but increases notably for the 35 min averages suggesting that the timescale of equilibrium indeed ranges between 5 and 20 minutes.

Table 5.1: Comparison between predicted and observed concentrations of semivolatile species during the MILAGRO 2006 (21-30 March) campaign. Simulations are done assuming the aerosol can form solids ("stable" solution).

Data Type		$NH_{3(g)}$	$NH_{4(p)}$	$HNO_{3(g)}$	$NO_{3(p)}$	$HCl_{(g)}$	$Cl_{(p)}$
All data	mean observed (μg m^{-3})	17.73 ± 11.02	2.24 ± 1.22	1.81 ± 1.88	5.37 ± 3.57	-	0.25 ± 0.56
	mean predicted (μg m^{-3})	16.89 ± 10.97	3.08 ± 1.56	1.38 ± 1.92	5.80 ± 3.86	0.03 ± 0.11	0.22 ± 0.55
	NME (%)	5.31	41.96	80.86	27.20	-	15.57
	NMB (%)	-4.70	37.14	-23.80	8.01	-	-15.57
CF=0	mean observed (μg m^{-3})	17.33 ± 9.83	2.37 ± 1.18	2.63 ± 1.87	5.57 ± 3.50	-	0.28 ± 0.56
	mean predicted (μg m^{-3})	16.16 ± 9.88	3.54 ± 1.57	1.43 ± 1.98	6.76 ± 3.77	0.04 ± 0.12	0.25 ± 0.55
	NME (%)	7.16	52.30	71.72	33.87	-	17.56
	NMB (%)	-6.73	49.16	-45.49	21.49	-	-17.56
CF=1	mean observed (μg m^{-3})	17.05 ± 12.38	1.83 ± 0.84	1.86 ± 1.64	3.88 ± 1.99	-	0.10 ± 0.30
	mean predicted (μg m^{-3})	16.49 ± 12.23	2.39 ± 1.07	1.73 ± 2.32	4.00 ± 2.36	0.01 ± 0.05	0.09 ± 0.29
	NME (%)	4.42	41.14	63.06	30.25	-	13.02
	NMB (%)	-3.26	30.38	-6.83	3.27	-	-13.02
CF=2	mean observed (μg m^{-3})	16.63 ± 8.27	2.54 ± 1.71	0.00	7.31 ± 4.89	-	0.28 ± 0.33
	mean predicted (μg m^{-3})	16.25 ± 8.09	2.92 ± 1.83	0.98 ± 1.14	6.32 ± 5.30	0.06 ± 0.17	0.24 ± 0.30
	NME (%)	2.96	19.39	-	13.46	-	23.91
	NMB (%)	-2.29	14.97	-	-13.46	-	-23.91
CF=3	mean observed (μg m^{-3})	22.47 ± 15.43	2.27 ± 1.41	0.00	5.70 ± 4.05	-	0.48 ± 1.06
	mean predicted (μg m^{-3})	21.99 ± 15.16	2.74 ± 1.64	0.73 ± 1.05	4.96 ± 4.03	0.02 ± 0.06	0.46 ± 1.05
	NME (%)	2.34	23.21	-	12.90	-	5.82
	NMB (%)	-2.12	21.02	-	-12.90	-	-5.82

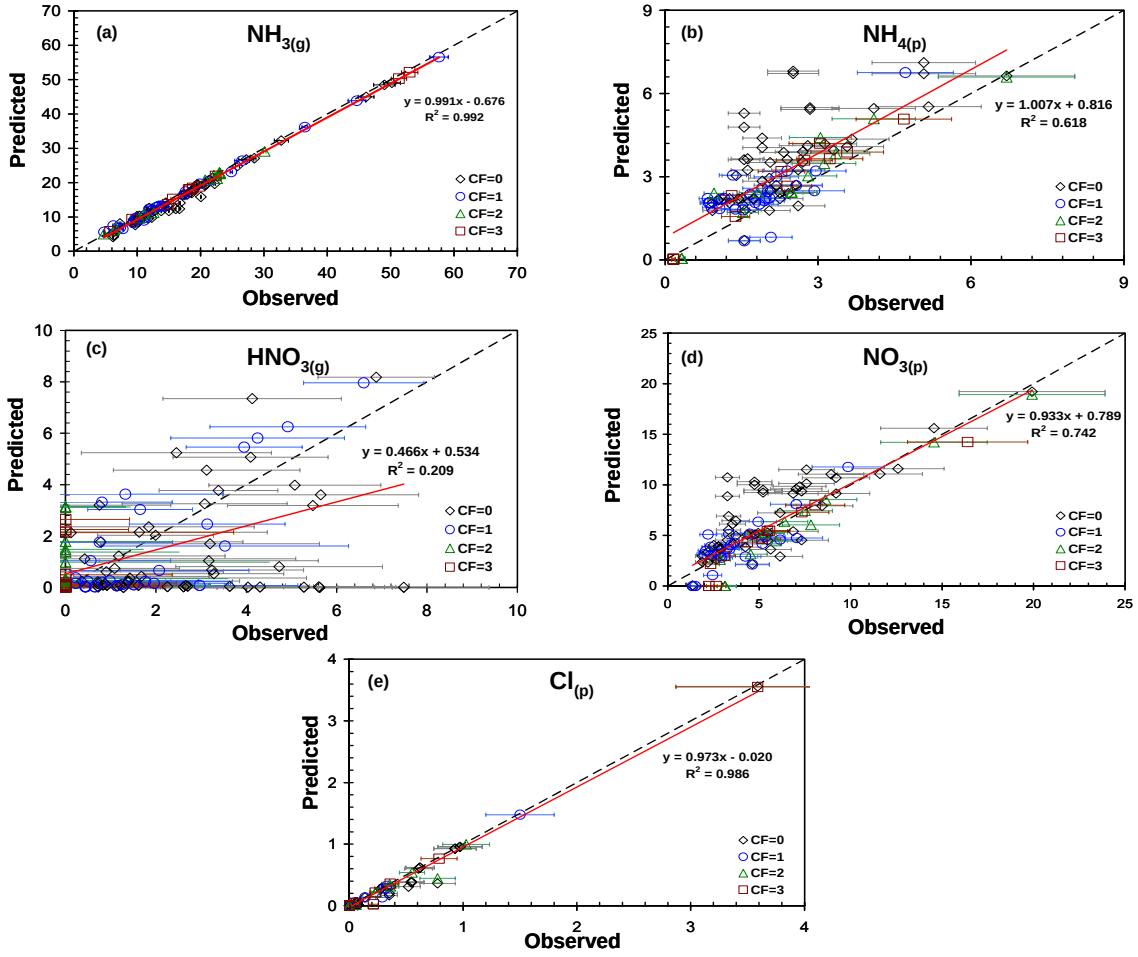

Figure 5.1: Predicted versus observed concentrations (μg m^{-3}) of $NH_{3(g)}$ (a), $NH_{4(p)}$ (b), $HNO_{3(g)}$ (c), $NO_{3(p)}$ (d), and $Cl_{(p)}$ (e) during the MILAGRO 2006 (21-30 March) campaign. Description of legend is given in text. ISORROPIA-II was run assuming stable state solution.

Table 5.2: Effect of averaging timescale on ammonia, nitrate and chloride prediction error.

Averaging time	Error metric	$NH_{3(g)}$	$NH_{4(p)}$	$HNO_{3(g)}$	$NO_{3(p)}$	$Cl_{(p)}$
5min (CF=0)	NME (%)	7.16	52.30	71.72	33.87	17.56
	NMB (%)	-6.73	49.16	-45.49	21.49	-17.56
20min (CF=1)	NME (%)	4.42	41.14	63.06	30.25	13.02
	NMB (%)	-3.26	30.38	-6.83	3.27	-13.02
35min (CF=0)	NME (%)	6.68	49.48	64.15	30.54	19.58
	NMB (%)	-6.60	48.89	-51.17	24.36	-19.58

Table 5.3: Prediction skill metrics of ISORROPIA-II, for stable and metastable solutions. Data is shown for RH < 50%.

Aerosol state		$NH_{3(g)}$	$NH_{4(p)}$	$HNO_{3(g)}$	$NO_{3(p)}$
Stable	NME (%)	3.56	24.32	67.67	25.83
	NMB (%)	-1.61	11.00	48.51	-18.52
Metastable	NME (%)	3.55	24.28	124.28	47.44
	NMB (%)	1.32	-9.03	121.61	-46.42

5.5.2 Deliquescence vs. Efflorescence

Due to the hysteresis effect, there is always an issue on what is the appropriate thermodynamic state assumption for RH < 60% (Ansari and Pandis, 2000; Moya et al. 2002). Given that this dataset covers a wide range of RH (19-94%) makes it possible to assess the preferred phase transition path (i.e. deliquescence or efflorescence branch) in Mexico City.

In Figure 5.2 we plot the stable (deliquescence) and metastable (efflorescence) solution predictions of ISORROPIA-II compared to observations for $NH_{4(p)}$ and $NO_{3(p)}$ as a function of RH. The stable state solution of ISORROPIA-II predicts higher concentrations of aerosol ammonium and aerosol nitrate at RH < 50% (which is a typical deliquescence point for the salt mixtures under consideration). This is in agreement with previous studies (Ansari and Pandis, 2000) and is primarily attributed to high concentrations of ammonium nitrate formed in the stable state solution of ISORROPIA II through the reaction $NH_{3(g)} + HNO_{3(g)} \leftrightarrow NH_4NO_{3(s)}$. At low RH (<50%), the stable state solution predicts a solid phase consisting mainly of $(NH_4)_2SO_4$ and NH_4NO_3. The metastable state solution assumes an aqueous supersaturated solution throughout the whole RH regime; hence no solid NH_4NO_3 is allowed to form, which for RH < 50% predicts less $NO_{3(p)}$ and $NH_{4(p)}$ at compared to the stable solution. At higher RH solid NH_4NO_3 dissolves and both solutions become identical. The fact that the deliquescent path is consistent with the observations suggests that the particles do not exhibit hysteresis; this may be a result of the presence of insoluble mineral dust which could facilitate nucleation of salts out of supersaturation aqueous solutions.

The difference between stable and metastable solutions predictions shown in Figure 5.2

are quantified in Table 5.3; NME and NMB are computed only for data with RH < 50%. For aerosol ammonium, although the NME for the two solutions of ISORROPIA II is essentially the same, the opposite sign in NMB (Table 5.3), indicates an overprediction (+11%) of ammonium by the stable state and an underprediction (-9%) by the metastable solution. The systematic overprediction of ammonium by the stable solution (seen in Figure 5.1) may partially reflect measurement uncertainty, which is analyzed in detail in section 5.5.3. For aerosol nitrate, the NME and NMB between predictions and observations is significantly larger when using the metastable solution of ISORROPIA II compared to the stable state solution (for RH < 50%), indicating the potential existence of deliquescence branch aerosols in Mexico City.

5.5.3 Sensitivity of Model Predictions to Aerosol Precursors

In this section we explore the sensitivity of predictions to aerosol precursor concentrations to a) assess the importance of measurement uncertainty on predictions, and, b) assess the sensitivity of $PM_{2.5}$ to changes in emitted precursors. The sensitivity is assessed by perturbing the input concentrations of total ammonia (TA), total nitrate (TN), total sulfate (TS), crustals and Na are perturbed by ±20% (approximately the PILS measurement uncertainty); results are shown in Table 5.4. As seen in Table 5.4, a 20% increase in TS does not improve the agreement between predictions and observations; in fact, a slight increase of the NME was found for ammonia and nitrate. Since the MOUDI data showed ~40% (on average) higher TS than the PILS (not shown), we further perturb TS by 40%, but NME does not decrease (67.9% for $NH_{4(p)}$ and 27.8% for $NO_{3(p)}$). A +20% perturbation in crustals and sodium concentrations slightly improved predictions of

$NH_{3(g)}$ and $NH_{4(p)}$ compared to the base case, and slightly decreased the observed overprediction of Figure 5.1b; this is because crustals and sodium are available to neutralize sulfates, thus less sulfate is available to bind with ammonia to form $(NH_4)_2SO_4$ which decreases the predicted $NH_{4(p)}$ concentration and increases the amount of free ammonia in the gas phase. In fact, the MOUDI impactor data suggest that Ca, Mg and Na are much higher (approximately 4 times) than obtained with the PILS. Increasing crustals and sodium by a factor of 4 was found to significantly decrease the systematic error between predictions and measurements for particulate ammonium (NMB = 13.6%) and improve predictions for $NH_{3(g)}$ (mean predicted value = 17.42 μg m^{-3}) and $NH_{4(p)}$ (mean predicted value = 2.55 μg m^{-3}) implying that for this dataset, PILS may not account for all the crustals present.

In Figure 5.3 we plot the predicted change (%) in $PM_{2.5}$ nitrate as a function of RH when a 20% decrease in input concentrations of TA, TS and TN is applied. The nitrate response to sulfate is negligible, Δx=0.36%, (Figure 5.3, Table 5.4) because TA concentrations are substantially in excess, and, thus a 20% change in TS is not enough to affect the formation of ammonium nitrate. In an ammonia-limited environment, a reduction in sulfate would increase aerosol nitrate as ammonia is freed and reacts with nitric acid. As seen in Figure 3, nitrate predictions are sensitive to changes in TA only for RH < 60%. Reducing TA reduces the amount of NH_4NO_3 formed. Aerosol nitrate predictions are more directly influenced by reductions in TN as shown in Figure 5.3 and Table 5.4 (Δx=-22.8%), and is in agreement with Takahama et al., (2004). The sensitivity of aerosol nitrate is RH-dependent as the partitioning of NO_3 strongly depends on the amount of aerosol water.

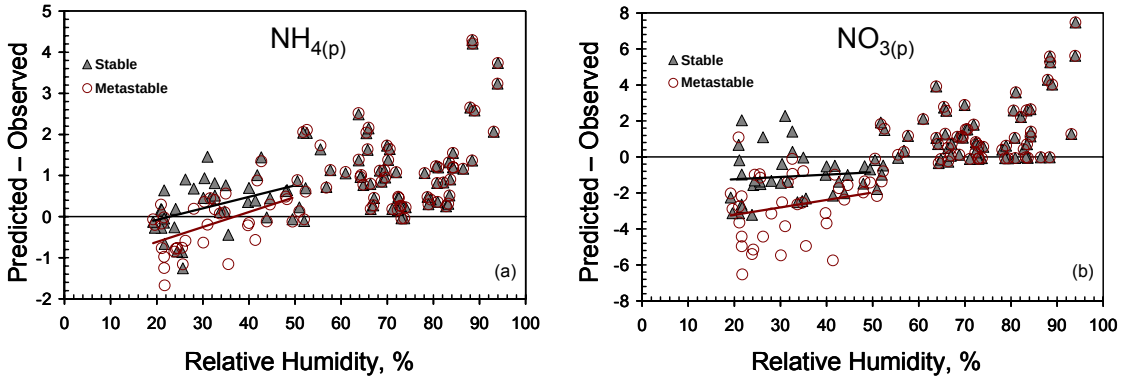

Figure 5.2: Difference (μg m^{-3}) between predicted and observed concentrations of aerosol ammonium (a), and, nitrate (b), as a function of RH using the stable (deliquescence) and metastable (efflorescence) solutions of ISORROPIA-II.

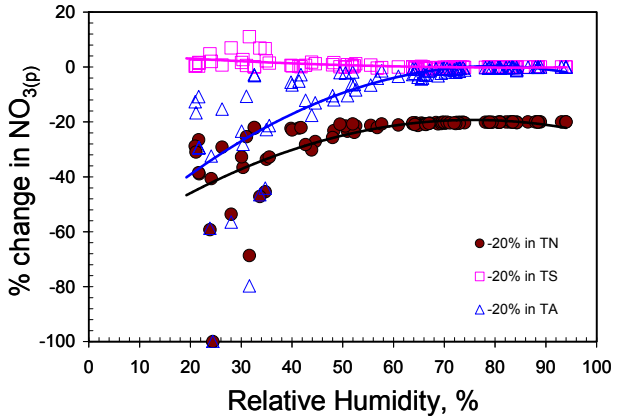

Figure 5.3: Response of aerosol nitrate predictions of ISORROPIA-II (stable solution; forward mode) to a -20% change in TA, TS and TN as a function of RH. All data (CF=0 – CF=3) are used in the dataset.

Table 5.4: Sensitivity of volatile species to aerosol precursor concentrations

Statistics		$NH_{3(g)}$	$NH_{4(p)}$	$HNO_{3(g)}$	$NO_{3(p)}$	$HCl_{(g)}$	$Cl_{(p)}$
base case	mean observed (μg m^{-3})	17.73	2.24	1.81	5.37	-	0.25
	mean predicted (μg m^{-3})	16.89	3.08	1.38	5.80	0.03	0.22
	NME (%)	5.31	41.96	80.86	27.20	-	15.57
	NMB (%)	-4.70	37.14	-23.80	8.01	-	-15.57
(+20%) TS	mean predicted (μg m^{-3})	16.57	3.40	1.40	5.78	0.03	0.22
	NME (%)	6.91	54.56	81.86	27.54	-	15.47
	NMB (%)	-6.52	51.53	-22.52	7.58	-	-15.47
	Δx^* (%)	-1.91	10.50	1.68	-0.40	-	0.12
(-20%) TS	mean predicted (μg m^{-3})	17.21	2.76	1.36	5.82	0.04	0.21
	NME (%)	3.99	31.50	79.87	26.87	-	15.70
	NMB (%)	-2.91	22.95	-24.95	8.39	-	-15.70
	Δx^* (%)	1.88	-10.34	-1.50	0.36	-	-0.15
(+20%) TN	mean predicted (μg m^{-3})	16.53	3.44	1.46	7.15	0.03	0.22
	NME (%)	7.11	56.20	83.92	41.06	-	15.32
	NMB (%)	-6.75	53.36	-18.98	33.11	-	-15.32
	Δx^* (%)	-2.16	11.83	6.33	23.24	-	0.29
(-20%) TN	mean predicted (μg m^{-3})	17.25	2.72	1.26	4.48	0.04	0.21
	NME (%)	4.09	32.32	77.02	30.47	-	15.91
	NMB (%)	-2.69	21.22	-30.06	-16.61	-	-15.91
	Δx^* (%)	2.11	-11.61	-8.22	-22.80	-	-0.40
(+20%) TA	mean predicted (μg m^{-3})	20.82	3.14	1.15	6.03	0.03	0.22
	NME (%)	17.62	43.29	75.36	25.35	-	14.76
	NMB (%)	17.48	39.93	-36.47	12.27	-	-14.76
	Δx^* (%)	23.27	2.04	-16.63	3.95	-	0.96
(-20%) TA	mean predicted (μg m^{-3})	12.98	2.99	1.69	5.49	0.04	0.21
	NME (%)	26.74	40.26	88.89	29.91	-	16.79
	NMB (%)	-26.74	33.29	-6.40	2.15	-	-16.79
	Δx^* (%)	-23.13	-2.80	22.83	-5.42	-	-1.45
(+20%) Na, Ca, K, Mg	mean predicted (μg m^{-3})	16.94	3.02	1.39	5.77	0.04	0.21
	NME (%)	5.09	40.27	80.44	27.06	-	15.96
	NMB (%)	-4.42	34.97	-22.52	7.57	-	-15.96
	Δx^* (%)	0.29	-1.57	1.68	-0.40	-	-0.47

* Δx denotes the % change of the mean predicted value of each species compared to the base case prediction.

Table 5.5: Effect of crustal treatment on predicted concentrations of ammonium, nitrate and water.

Property	Treatment of crustals	$NH_{4(p)}$	$NO_{3(p)}$	$H_2O_{(liq)}$
Mean Observed (μg m^{-3})		2.24	5.37	-
Mean Predicted (μg m^{-3})	Insoluble	3.18	5.47	13.23
	Equivalent Na	2.77	5.61	13.09
	ISORROPIA-II	2.55	5.86	11.67
NME (NMB), (%)	Insoluble	46.76 (41.53)	31.03 (1.87)	N/A
	Equivalent Na	34.3 (23.3)	28.7 (4.44)	N/A
	ISORROPIA-II	34.04 (13.6)	26.2 (9.2)	N/A

5.5.4 Importance of Explicitly Treating Crustal Species

Often thermodynamic models treat the presence of crustals as mole-equivalent sodium (i.e. $Ca^{2+} = 2Na^{+}$, $Mg^{2+} = 2Na^{+}$, $K^{+} = Na^{+}$) or as insoluble. In this section we examine the impact of these assumptions, versus using full thermodynamics. Table 5.5 displays a summary of this sensitivity test; shown are average concentrations and error metrics for nitrate, ammonium and water with ISORROPIA-II. For all the simulations we used the MOUDI concentrations of crustals and sodium. When Ca, K and Mg are treated as insoluble (unreactive), ISORROPIA-II predicts higher, on average, concentrations of ammonium compared to both the equivalent-Na and explicit treatment, since more sulfate is available to bind with ammonium, and thus the error and bias between predicted and observed ammonium increases for the insoluble approach (Table 5.5). For particulate nitrate, NME is the lowest when crustals are treated explicitly. The changes in NME and NMB among the three crustal treatment approaches are rather small since ammonia is enough to fully neutralize the available nitrate regardless of the treatment of crustals. The difference in nitrate prediction when treating crustals explicitly vs. as equivalent sodium is expected to be large in environments where non-volatile nitrate ($Ca(NO_3)_2$, $Mg(NO_3)_2$, KNO_3) is present in significant amounts (Moya et al., 2002; Jacobson, 1999). In the current dataset, aerosol nitrate is present in the form of ammonium nitrate (due to ammonia-rich environment) and thus replacing crustals with sodium is expected to have a minor effect on predicted nitrate response, primarily from differences in predicted water uptake (Table 5.5). The equivalent Na approach predicts aerosol water content which is higher (by 13.5%) than the one predicted by the explicit treatment of crustals and very close to the insoluble approach (Table 5.5). This is attributed to the formation of salts

with low solubility (e.g., $CaSO_4$) which do not significantly contribute to water uptake. The difference in water content also affects aerosol acidity (i.e. pH) and water soluble species concentration. It should be noted that the differences described in Table 5.5 between the equivalent Na and explicit treatment of crustals are the minimum expected considering the large amounts of ammonia in Mexico City which minimizes the effect of replacing crustals with sodium.

5.6 Conclusions

This study focuses on thermodynamical modeling of aerosols sampled during the MILAGRO 2006 campaign in Mexico City, using high-time (5-min) resolution measurements and a state-of-the-art aerosol equilibrium model, ISORROPIA-II (Fountoukis and Nenes, 2007).

In agreement with observations, ISORROPIA-II predicts a large portion (82.4 ± 10.1 %) of total ammonia partitioning to the gas phase, while most of total nitrate (79.8 ± 25.5%) and chloride (75.3 ± 29.1%) resides in the aerosol phase. The mean observed value for $NH_{3(g)}$ was 17.73 μg m^{-3} and 5.37 μg m^{-3} for $NO_{3(p)}$. An excellent agreement between predicted and observed concentration of $NH_{3(g)}$ was found with a NME of 5.3%. Very good agreement was also found for $NO_{3(p)}$ (NME=27.2%), $NH_{4(p)}$ (NME=37.1%) and $Cl_{(p)}$ (NME=15.5%) concentrations for most of the data. Larger discrepancies were seen in predicted $HNO_{3(g)}$ since uncertainties in the volatile nitrate measurement ($HNO_{3(g)}$ + NH_4NO_3) are magnified by the high sensitivity of $HNO_{3(g)}$ because nitrate partitioned primarily to the aerosol phase. A number of important conclusions arise from this study:

1. Application of ISORROPIA-II is largely successful suggesting that the assumption of thermodynamic equilibrium is appropriate for complex Mexico City aerosols.
2. The timescale of equilibrium ranges between 5 and 20 minutes.
3. At low RH (<50%), the stable state (i.e. deliquescence branch) solution of ISORROPIA-II predicted significantly higher concentrations of aerosol nitrate compared to the metastable (i.e. efflorescence) solution. The NME and NMB between predictions and observations for aerosol nitrate were found to be significantly larger when using the metastable solution indicating that the deliquescence branch appropriately describes aerosols in Mexico City at RH below 50%. This can serve as an important constraint for three dimensional air quality models that simulate ambient particle concentrations under conditions characteristic of Mexico City.
4. The volatile fraction of $PM_{2.5}$ was found to be mostly sensitive to changes in TN. This suggests that in an ammonia-rich environment, (such as Mexico City) a combined reduction in TS and TN appears to be a more promising strategy for $PM_{2.5}$ control, rather than reducing ammonia emissions.
5. Treating crustal species as "equivalent sodium" or insoluble (rather than explicitly) in the thermodynamic equilibrium calculations has an important impact on predicted aerosol water uptake, nitrate and ammonium, despite the ammonia-rich environment of Mexico City. This suggests that comprehensive thermodynamic calculations are required to predict the partitioning and phase state of aerosols in the presence of dust.

6. Concentrations of gas phase chloride were most likely low in Mexico City (mean predicted value for $HCl_{(g)}$=0.03 μg m^{-3}), a consequence of having large excess of $NH_{3(g)}$ which tends to drive Cl^- into the aerosol

5.7 Acknowledgements

This work was supported by the National Oceanic and Atmospheric Administration under contract NMRAC000-5-04017, the EPA under contract X83234201 and ATM-0513035.

5.8 References

Amundson, N.R., Caboussat, A., He, J.W., Martynenko, A.V., Savarin, V.B., Seinfeld, J.H., and Yoo, K.Y.: A new inorganic atmospheric aerosol phase equilibrium model (UHAERO), Atmos. Chem. Phys., 6, 975-992, 2006.

Ansari, A.S., and Pandis, S.N.: The effect of metastable equilibrium states on the partitioning of nitrate between the gas and aerosol phases, Atmos. Environ., 34, 157-168, 2000.

Ansari, A.S., and Pandis, S.N.: Prediction of multicomponent inorganic atmospheric aerosol behavior, Atmos. Environ., 33, 745-757, 1999a.

Ansari, A.S., and Pandis, S.N.: An analysis of four models predicting the partitioning of semivolatile inorganic aerosol components, Aerosol Sci. Technol., 31, 129-153, 1999b.

Capaldo, K.P., Pilinis, C., and Pandis, S.N.: A computationally efficient hybrid approach for dynamic gas/aerosol transfer in air quality models, Atmos. Environ., 34, 3617-3627, 2000.

Cruz, C.N., Dassios, K.G., and Pandis, S.N.: The effect of dioctyl phthalate films on the ammonium nitrate aerosol evaporation rate, Atmos. Environ., 34, 3897-3905, 2000.

Dassios, K.G., and Pandis, S.N.: The mass accommodation coefficient of ammonium nitrate aerosol, Atmos. Environ., 33, 2993-3003, 1999.

Day, D.A., Wooldridge, P.J., Dillon, M., Thornton, J.A., and Cohen, R.C.: A Thermal dissociation-laser induced fluorescence instrument for in-situ detection of NO2, peroxy(acyl)nitrates, alkyl nitrates, and HNO3., J. Geophys. Res., 107(D6), 10.1029/2001JD000779, 2002.

Doran, J.C., Arnott, W.P., Barnard, J.C., Cary, R., Coulter, R., Fast, J. D., Kassianov, E.I., Kleinman, L., Laulainen, N.S., Martin, T., Paredes-Miranda, G., Pekour, M.S., Shaw, W.J., Smith, D.F., Springston, S.R., Yu, X.-Y., The T1-T2 study: evolution of aerosol properties downwind of Mexico City, Atmos. Chem. Phys., 7, 1585-1598, 2007.

Farmer, D.K., Wooldridge, P.J., and Cohen, R.C.: Thermal-dissociation laser induced fluorescence (TD-LIF) as a new technique for measurement of HNO_3, ΣAlkyl nitrates, Σperoxy nitrates, and NO2 eddy covariance fluxes, Atmos. Chem. Phys., 6, 3471-3486, 2006.

Fast, J.D., de Foy, B., Acevedo Rosas, F., Caetano, E., Carmichael, G., Emmons, L., McKenna, D., Mena, M., Skamarock, W., Tie, X., Coulter, R.L., Barnard, J.C., Wiedinmyer, C., Madronich, S.: A meteorological overview of the MILAGRO field campaigns, Atmos. Chem. and Phys. Discuss., Vol. 7, 2037-2089, 2007.

Fischer, M.L., Vanreken, T.M., Coffey, M.T., Wood, E., Herndon, S.C., Littlejohn, D., Hannigan, J.W.: Measurements of ammonia at the T1 site during MILAGRO 2006, in preparation.

Fountoukis, C., and Nenes, A.: ISORROPIA II: A computationally efficient thermodynamic equilibrium model for K^+-Ca^{2+}-Mg^{2+}-NH_4^+-Na^+-SO_4^{2-}-NO_3^--Cl^--H_2O aerosols, Atmos. Chem. Phys. Discuss., 7, 1893-1939, 2007.

Fountoukis, C., Sullivan, A., Weber, R., VanReken, T., Fischer, M., Matías, E., Moya, M., Farmer, D., Cohen, R., and Nenes, A.: Thermodynamic characterization of Mexico City Aerosol during MILAGRO 2006, Atmos. Chem. Phys., in review, 2007.

Jacobson, M.Z.: Studying the effect of calcium and magnesium on size-distributed nitrate and ammonium with EQUISOLV II, Atmos. Environ., 33, 3635-3649, 1999.

Heitzenberg, J.: Fine particles in the global troposphere: a review, Tellus 41B, 149–160, 1989.

Malm, W.C., Sisler, J.F., Huffman, D., Eldred, R.A., and Cahill, T.A.: Spatial and seasonal trends in particle concentration and optical extinction in the United States, J. Geophys. Res., 99, 1347-1370, 1994.

Marple, V.A., Rubow, K.L., Behm, S.M.: A micro-orifice uniform deposit impactor (MOUDI): description, calibration, and use, Aerosol Sci. and Technol., 14, 434-446, 1991.

Meng, Z.Y., Seinfeld, J.H., Saxena, P., and Kim, Y.P.: Atmospheric gas - aerosol equilibrium IV. Thermodynamics of carbonates, Aerosol Sci. Technol., 23, 131-154, 1995.

Meng, Z., and Seinfeld, J.H.: Time scales to achieve atmospheric gas aerosol equilibrium for volatile species, Atmos. Environ., 30, 2889-2900, 1996.

Moya, M., Pandis, S.N., and Jacobson, M.Z.: Is the size distribution of urban aerosols determined by thermodynamic equilibrium? An application to Southern California, Atmos. Environ., 36, 2349-2365, 2002.

Moya, M., Ansari, A.S., and Pandis, S.N.: Partitioning of nitrate and ammonium between the gas and particulate phases during the 1997 IMADA-AVER study in Mexico City, Atmos. Environ., 35, 1791-1804, 2001.

Nenes, A., Pandis, S.N., and Pilinis, C.: ISORROPIA: A new thermodynamic equilibrium model for multiphase multicomponent inorganic aerosols, Aquatic Geochemistry, 4, 123-152, 1998.

Nenes, A., Pilinis, C., and Pandis, S.N.: Continued development and testing of a new thermodynamic aerosol module for urban and regional air quality models, Atmos. Environ., 33, 1553-1560, 1999.

Orsini, D.A., Ma, Y., Sullivan, A., Sierau, B., Baumann, K., and Weber, R.J.: Refinements to the particle-into-liquid sampler (PILS) for ground and airborne measurements of water soluble aerosol composition, Atmos. Environ., (37), 1243-

1259, 2003.

Pilinis, C., Capaldo, K.P, Nenes, A., Pandis, S.N.: MADM – A New Multicomponent Aerosol Dynamics Model, Aerosol Sci. Technol., 32 (5), 482-502, 2002.

Pinder, R.W., Adams, P.J., Pandis, S.N.: Ammonia emission controls as a cost-effective strategy for reducing atmospheric particulate matter in the eastern United States, Environ. Sci. Technol., 41, 380-386, 2007.

Potukuchi, S., and Wexler, A.S.: Identifying solid-aqueous phase transitions in atmospheric aerosols - I. Neutral-acidity solutions, Atmos. Environ., 29, 1663-1676, 1995.

San Martini F.M., West J.J., de Foy B., Molina L.T., Molina M.J., Sosa G., McRae G.J.: Modeling inorganic aerosols and their response to changes in precursor concentration in Mexico City, Journal of the air & waste management association, 55 (6), 803-815, 2005.

Takahama, S., Wittig, A.E., Vayenas, D.V., Davidson, C.I., and Pandis, S.N.: Modeling the diurnal variation of nitrate during the Pittsburgh Air Quality Study, J. Geophys. Res., 109, D16S06, doi:10.1029/2003JD004149, 2004.

Wexler, A.S., and S.L. Clegg, Atmospheric aerosol models for systems including the ions H^+, NH_4^+, Na^+, SO_4^{2-}, NO_3^-, Cl^-, Br^-, and H_2O, J. Geophys. Res., 107, 4207, doi:10.1029/2001JD000451, 2002.

Wexler, A.S., and Seinfeld, J.H.: Second - generation inorganic aerosol model, Atmos. Environ., 25A, 2731-2748, 1991.

Wexler, A.S., and Seinfeld, J.H.: Analysis of aerosol ammonium nitrate: departures from equilibrium during SCAQS, Atmos. Environ., 26A, 579-591, 1992.

Yu, S., Dennis, R., Roselle, S., Nenes, A., Walker, J., Eder, B., Schere, K., Swall, J., and Robarge, W.: An assessment of the ability of three-dimensional air quality models with current thermodynamic equilibrium models to predict aerosol NO_3^-, J. Geophys. Res., 110, D07S13, doi:10.1029/2004JD004718, 2005.

Zhang, Y., Seigneur, C., Seinfeld, J.H., Jacobson, M., Clegg, S.L., and Binkowski, F.S.: A comparative review of inorganic aerosol thermodynamic equilibrium models: similarities, differences, and their likely causes, Atmos. Environ., 34, 117-137, 2000.

Zhang, J., Chameides, W.L., Weber, R., Cass, G., Orsini, D., Edgerton, E.S., Jongejan, P., and Slanina, J.: An evaluation of the thermodynamic equilibrium assumption for fine particulate composition: Nitrate and ammonium during the 1999 Atlanta Supersite Experiment, J. Geophys. Res., 107, 8414, doi:10.1029/2001JD001592, 2003.

CHAPTER 6

INCORPORATING AN AEROSOL EQUILIBRIUM MODEL INTO A THREE DIMENSIONAL AIR QUALITY MODEL[I]

6.1 Abstract

The impact of including crustal species in equilibrium calculations within a three dimensional air quality model is studied. A state-of-the-art aerosol equilibrium model, ISORROPIA-II, which explicitly treats the thermodynamics of K^+-Ca^{2+}-Mg^{2+}-NH_4^+-Na^+-SO_4^{2-}-HSO_4^--NO_3^--Cl^--H_2O aerosols is incorporated into the Community Multiscale Air Quality (CMAQ) and the effect of crustal species, when treated a) as insoluble (i.e. neglecting the presence of crustals), b) as mole - equivalent sodium (i.e. $Ca^{2+} = 2Na^+$, $Mg^{2+} = 2Na^+$, $K^+ = Na^+$), and, c) explicitly, was explored. A significant change in aerosol water (-19.8%) and ammonium (-27.5%) concentrations was predicted by the explicit treatment of crustals even though crustals (Ca^{2+}, K^+, M^{2+}) contributed, on average, only a few percent of the total $PM_{2.5}$ mass highlighting the need for comprehensive thermodynamic calculations in the presence of crustal species. The results were also compared against measurements made at the Jefferson Street Southeastern Aerosol Research and Characterization study (SEARCH) monitoring site an urban location in Atlanta, GA during the period of 12-20 June, 2005. Both the explicit and the equivalent

[I] Under preparation for submission to Atmospheric Environment: Fountoukis, C., Hu, Y., Russell, A., and Nenes, A.: Sensitivity of Inorganic Aerosols within an Air Quality Model: Including Crustal Species in Equilibrium Calculations, Atmos. Environ., in preparation, 2007.

sodium treatment of crustals in CMAQ decrease the error for aerosol nitrate but increase it for ammonium suggesting that additional species (e.g. organic acids) may be required to be incorporated into future equilibrium modeling efforts in addition to crustal species. The addition of crustal species in ISORROPIA does not considerably increase the CPU time required by CMAQ.

6.2 Introduction

A large fraction of atmospheric aerosols consists of inorganic species which mainly include ammonium (NH_4^+), sulfate (SO_4^{2-}), and nitrate (NO_3^-). Depending on the location, sodium (Na^+) and chloride (Cl^-) may also be found in atmospheric particle composition as well as crustal species, such as Ca^{2+}, K^+, Mg^{2+} which are a major component of dust. Air quality models have been extensively used in recent years to simulate ambient fine particle concentrations. A major challenge for three dimensional air quality models is the consideration of thermodynamic equilibrium calculations for inorganic species. A thermodynamic equilibrium model is an essential component of every air quality model that needs an accurate prediction of the partitioning of semivolatile species between the gas and aerosol phase. Performing thermodynamic equilibrium calculations for aerosol systems is a demanding computational task (e.g., Nenes et al., 1998, 1999) because aqueous aerosol solutions are strongly non-ideal and require the use of activity coefficients which may substantially increase the computational burden for a 3-D model. Therefore, both speed and accuracy are very important issues for equilibrium modules included in 3-D air quality models.

Aerosol equilibrium models have been widely developed in the past two decades. Some

recent examples include SCAPE2 (Meng et al., 1995), GFEMN (Ansari and Pandis, 1999a,b), AIM2 (Wexler and Clegg, 2002), UHAERO (Amundson et al., 2006) and ISORROPIA-II (Fountoukis and Nenes, 2007). Main differences between equilibrium models include, the method used to solve equilibrium problems, the type of input they can accept, their computational speed and the chemical species that they can treat.

Often, equilibrium models neglect the presence of some species (e.g. the crustal species Ca^{2+}, K^{+}, Mg^{2+}) for simplicity and computational speed. It has been shown, however, that the consideration of crustal material in a thermodynamic equilibrium framework can be important in modeling the partitioning of semivolatile inorganic aerosols, especially in areas where dust is significantly present. Ansari and Pandis (1999b) found a 14% improvement in agreement between predictions and observations for $PM_{2.5}$ nitrate when considering crustals in the modeling framework (SCAPE2). Jacobson (1999) studied the effect of Ca^{2+} and Mg^{2+} on predicted nitrate and ammonium for RH > 60% in different regions of Los Angeles using EQUISOLV II and found predictions being significantly affected when removing these species from the equilibrium calculations. Moya et al., (2001) found a 5% improvement in predicted nitrate (compared to measurements from Mexico City) when considering crustals in the modeling framework (SCAPE2). By treating crustals as "mole-equivalent" sodium (using ISORROPIA), nitrate predictions remained practically unchanged provided that Ca^{2+} was a relatively small fraction of aerosol dry mass. Moya et al., (2002) showed that the treatment of crustal species as equivalent concentration of sodium may introduce errors in predicting aerosol behavior when concentrations of crustals are high. San Martini et al., (2005) found (using ISORROPIA) that the estimated response of inorganic PM to changes in precursor

concentrations can be affected when including crustal species (as equivalent Na). Fountoukis et al. (2007), using ISORROPIA-II, showed that including crustal species reduces the error for ammonium and nitrate compared to measurements (MILAGRO 2006 campaign) while a significant change was also found in the aerosol water uptake response.

Although the previous studies have thoroughly investigated the effect of crustal species on predictions of various equilibrium models, the impact of these changes on a 3-D model's predictions is yet unknown. In this study we test the sensitivity of the Community Multiscale Air Quality (CMAQ) model's predictions to the presence of crustal species. A state-of-the-art aerosol equilibrium model, ISORROPIA-II, which explicitly treats the thermodynamics of K^+-Ca^{2+}-Mg^{2+}-NH_4^+-Na^+-SO_4^{2-}-HSO_4^--NO_3^--Cl^--H_2O aerosols, is incorporated into CMAQ and the effect of crustal species, when treated a) as insoluble (i.e. neglecting the presence of crustals), b) as mole - equivalent sodium (i.e. $Ca^{2+} = 2Na^+$, $Mg^{2+} = 2Na^+$, $K^+ = Na^+$), and, c) explicitly, is investigated. CMAQ is used to simulate atmospheric conditions over the Atlanta area in the United States. Finally, the computational time needed by CMAQ and ISORROPIA-II are reported.

6.3 Aerosol Thermodynamic Equilibrium Modeling: Description of ISORROPIA-II

ISORROPIA-II (Fountoukis and Nenes, 2007) simulates the thermodynamic partitioning of semivolatile inorganics between the gas and aerosol phase. The possible species for each phase are shown below:

Gas phase: NH_3, HNO_3, HCl, H_2O

Liquid phase: NH_4^+, Na^+, H^+, Cl^-, NO_3^-, SO_4^{2-}, $HNO_{3(aq)}$, $NH_{3(aq)}$, $HCl_{(aq)}$, HSO_4^-,

OH^-, H_2O, Ca^{2+}, K^+, Mg^{2+}

Solid phase: $(NH_4)_2SO_4$, NH_4HSO_4, $(NH_4)_3H(SO_4)_2$, NH_4NO_3, NH_4Cl, NaCl, $NaNO_3$, $NaHSO_4$, Na_2SO_4, $CaSO_4$, $Ca(NO_3)_2$, $CaCl_2$, K_2SO_4, $KHSO_4$, KNO_3, KCl, $MgSO_4$, $Mg(NO_3)_2$, $MgCl_2$

ISORROPIA-II determines the number of species and equilibrium reactions by the relative abundance of each aerosol precursor (NH_3, Na, Ca, K, Mg, HNO_3, HCl, H_2SO_4) and the ambient relative humidity and temperature. The following ratios determine the major species potentially present:

$$R_1 = \frac{\left[NH_4^+\right]+\left[Ca^{2+}\right]+\left[K^+\right]+\left[Mg^{2+}\right]+\left[Na^+\right]}{\left[SO_4^{-2}\right]}$$

$$R_2 = \frac{\left[Ca^{2+}\right]+\left[K^+\right]+\left[Mg^{2+}\right]+\left[Na^+\right]}{\left[SO_4^{-2}\right]}$$

$$R_3 = \frac{\left[Ca^{2+}\right]+\left[K^+\right]+\left[Mg^{2+}\right]}{\left[SO_4^{-2}\right]}$$

where $\left[X\right]$ denotes the concentration of an aerosol precursor X (mol m^{-3} of air).

ISORROPIA II solves two classes of problems:

c) Forward (or "closed") problems, in which known quantities are *T*, *RH* and the total (gas + aerosol) concentrations of NH_3, H_2SO_4, Na, HCl, HNO_3, Ca, K, and Mg.

d) Reverse (or "open") problems, in which known quantities are *T*, *RH* and the precursor concentrations of NH_3, H_2SO_4, Na, HCl, HNO_3, Ca, K, and Mg in the aerosol phase.

The model also offers the option of solving for two types of aerosol behavior; the "stable" state (or deliquescence branch) and, the "metastable" state (or efflorescence branch) solution. In the stable branch salts are assumed to precipitate once the aqueous phase becomes saturated with respect to them, while in the metastable the aerosol is composed only of an aqueous phase which can be supersaturated with respect to dissolved salts (no solids are assumed to form). Other important feature of the model include i) the choice of using precalculated tables of binary activity coefficients and water activities of pure salt solutions, which decreases computational cost, ii) a simplified treatment of mutual deliquescence of multicomponent salt particle solutions which lowers the deliquescence point of the aerosol phase, iii) an updated water activity database from the output of the AIM model (http://www.hpc1.uea.ac.uk/~e770/aim.html), and, iv) an optimized activity coefficient calculation algorithm for increased computational speed. Depending on the three sulfate ratios and the relative humidity, ISORROPIA II solves the appropriate set of equilibrium equations and together with mass conservation, electroneutrality, water activity equations and activity coefficient calculations, the final concentrations at thermodynamic equilibrium are obtained.

6.4 Air Quality Modeling: Description of CMAQ and application to Atlanta, GA

The U.S. Environmental Protection Agency's Models-3/CMAQ model system (Byun and Ching, 1999) is used (version 4.5) in this study to predict PM concentration of species. The model includes meteorological fields from the fifth Generation Pennsylvania State/National Center for Atmospheric Research Mesoscale Meteorological Model (MM5) (Grell et al. 1994). Processes performed in the CMAQ model include emissions,

advection, dispersion, gas and aqueous phase chemistry, aerosol nucleation, condensation, coagulation, dry and wet deposition and cloud processing. Emissions inputs of gas-phase SO_2, CO, NO, NO_2, NH_3, volatile organic compounds (VOCs) and $PM_{2.5}$ are from the 1999 EPA National Emissions Inventory (NEI99 version 1) (http://www.epa.gov/ttn/chief/). The model domain includes the continental United States with a horizontal grid of 178 × 124 32 km grid cells and 21 layers in the vertical resolution from the surface to ~100mb.

CMAQ was applied to measurements made at the Jefferson Street Southeastern Aerosol Research and Characterization study (SEARCH) monitoring site (Hansen et al., 2003), an urban location in Atlanta, GA during the period of 12-20 June, 2005. A detailed description of the methods and instruments used is given elsewhere (http://www.atmospheric-research.com; Smith et al., 2005; Stolzenburg et al., 2005; Hansen et al., 2003). Data from the first three days of simulations were disregarded to mitigate the effect of initial conditions on the model results. For all the simulations in this study the "forward" mode and metastable state of ISORROPIA-II is used in CMAQ. The simulations were performed on a 2x AMD Opteron SE Model 285 (2.6 GHz), 16 GB of RAM, dual core processor running Linux 2.6.9. The code was compiled with PGF90 version 6.1.

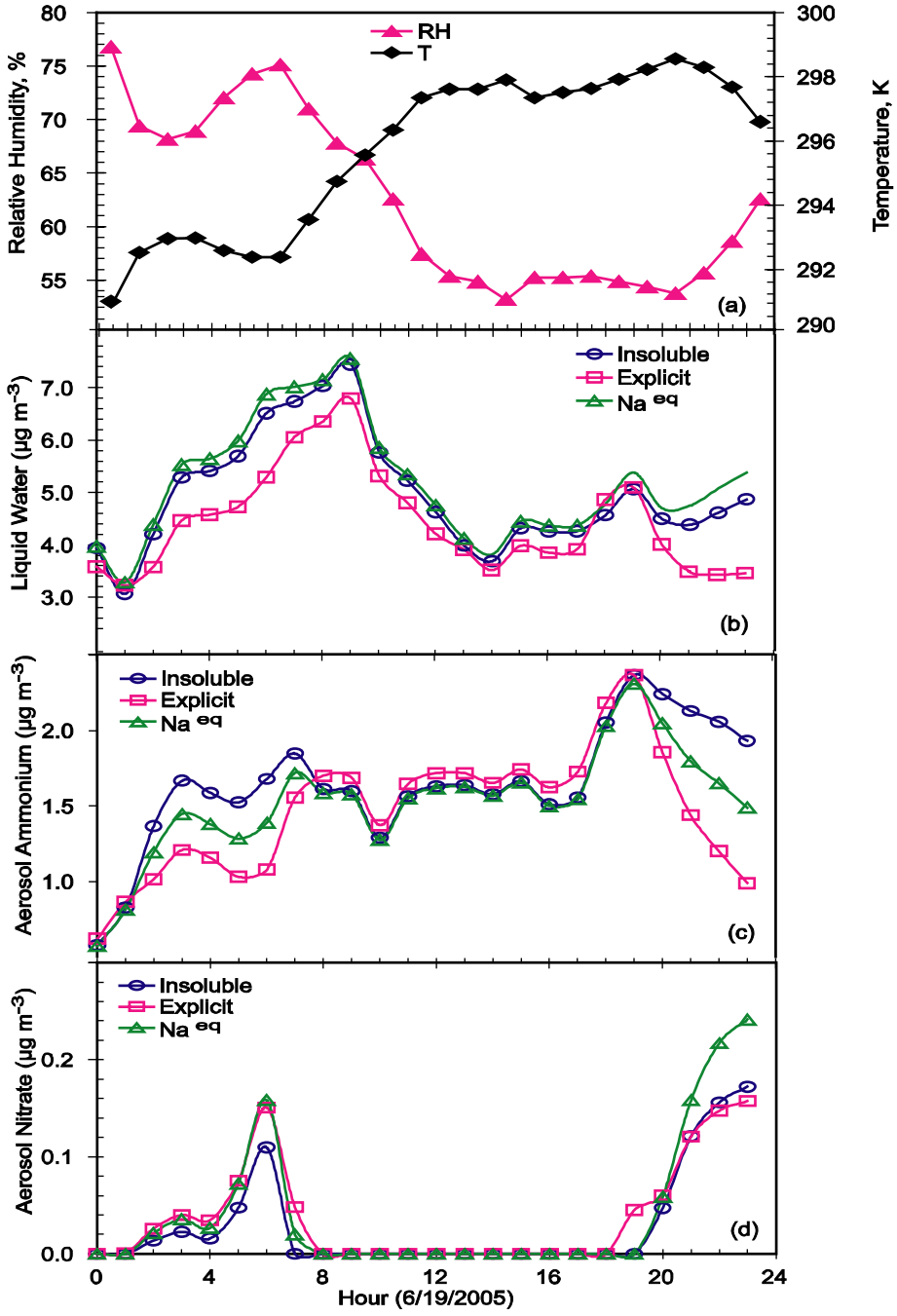

Figure 6.1: Diurnal profile of observed relative humidity and temperature (a), and predicted (by CMAQ) aerosol water content (b), aerosol ammonium (c) and aerosol nitrate (d) over Atlanta, GA for 19 June 2005. CMAQ was run three times: when crustals are treated (in ISORROPIA) as insoluble, as equivalent sodium, and explicitly.

6.5 Results and Discussion

In order to study the effect of crustal species (Ca, K, Mg) on aerosol water uptake and the partitioning of semivolatile inorganic species, CMAQ was run three times corresponding to three different versions of the ISORROPIA equilibrium model. In the first (base case) run, crustal species are assumed insoluble, not interacting with other species. In the second run ISORROPIA-II is used which explicitly treats the thermodynamics of crustal species $Ca^{2+}/K^{+}/Mg^{2+}$ in addition to the $NH_4/Na/SO_4/HSO_4/NO_3/Cl/H_2O$ aerosol system. In the third run crustals are treated as mole - equivalent sodium (i.e. $Ca^{2+} = 2Na^{+}$, $Mg^{2+} = 2Na^{+}$, $K^{+} = Na^{+}$) in ISORROPIA-II.

Figure 6.1a shows the diurnal profile of 19 June 2005 for observed relative humidity and temperature, and Figure 6.1b - d show predictions of CMAQ (for the same day) for aerosol liquid water content, ammonium and nitrate respectively, for the three runs described above. The relative humidity and temperature profiles are anti-correlated indicating no significant mixing of air masses for that day. Aerosol liquid water (Figure 6.1b) decreases during midday following the decrease of RH and increase of temperature. The water content predicted by CMAQ using ISORROPIA-II (i.e. explicit treatment of crustals) is clearly less than the one predicted by the base case run or the Na^{eq} approach during the whole day. The difference in water uptake is larger during early morning (midnight – 8a.m.) and night (8p.m. –midnight) when the RH (and water) is increased. This is largely because of the formation of insoluble species (e.g. $CaSO_4$) predicted by ISORROPIA-II which do not contribute to water uptake. The Na^{eq} approach, on the other hand, predicts a mixture of salts of Na and NH_4 with SO_4, which are more water soluble, and thus the predicted water content is higher (and close to the base case run).

Interestingly, aerosol ammonium (Figure 6.1c) predicted by ISORROPIA-II is slightly higher during midday (when RH drops) and significantly lower during early morning and night (when RH increases) compared to the base case and Na^{eq} run. During early morning and night, water content is high enough to deliquesce a large portion of salts. When crustals are present (ISORROPIA-II) sulfate will preferentially be neutralized by crustals and thus ammonium is shifted to the gas phase decreasing the amount of aerosol ammonium.

The same is true for Na in the Na^{eq} approach, where crustals are converted to sodium which neutralizes sulfate and shifts ammonium to the gas phase. The Na^{eq} approach predicts more aerosol ammonium than ISORROPIA-II during the early morning and night due to higher amount of predicted water (Figure 6.1b). When RH drops (during midday) and deliquescence of salts is limited, the partitioning of ammonia is controlled by the reaction $NH_{3(aq)} + H_2O_{(aq)} \leftrightarrow NH^+_{4(aq)} + OH^-_{(aq)}$. Since ISORROPIA-II predicts more "free" ammonia (due to neutralization of sulfates by crustals) it also predicts slightly more aerosol NH_4^+ through the above reaction. Aerosol nitrate (Figure 6.1d) was, on average, present in small amounts. During midday, (when RH is low) nitrate is present in the gas phase, while when RH is increased, water is enough to dissolve most of the gas phase nitrate with small differences between the three runs.

The diurnal trend described in Figure 6.1 for RH, T and species concentration predictions was found to be very similar for all 6 days (15-20 June 2005) of our simulation runs. Figures 6.2 and 6.3 show aerosol water and ammonium, respectively, predicted by CMAQ when crustals are treated in ISORROPIA as insoluble (x-axis) and explicitly (y-axis) for the period between 15 and 20 June 2005 (hourly averages). During midday

CMAQ, with the explicit treatment of crustals, predicts water content very close to the insoluble approach while during early morning and night it significantly underpredicts the amount of aerosol water for all 6 days of simulations for the reasons described in Figure 6.1b. In agreement with Figure 1c, the amount of aerosol ammonium predicted by the explicit treatment of crustals is slightly higher than the insoluble approach during midday, while during early morning and night it is significantly lower throughout the 6-day period. On average, the explicit treatment of crustals resulted in a -27.5% change in predicted aerosol ammonium and -19.8% in aerosol water content. These changes in aerosol water and ammonium concentrations are very important considering that crustals (Ca^{2+}, K^{+}, M^{2+}) contributed, on average, only a few percent (~6%) of the total $PM_{2.5}$ mass during the 6-day period of measurements.

Observed and predicted concentrations of species over Atlanta, GA for the period 15-20 June 2005 are shown in Table 6.1. Both the explicit and the Na^{eq} treatment of crustals in CMAQ decrease the error for aerosol nitrate but increase it for ammonium. The error in sulfate remains essentially the same while aerosol water is significantly changed. The explicit treatment of crustals within CMAQ reduces the amount of ammonium partitioning in the particulate phase. This is because ammonium, being the weakest among cations (Na^{+}, Ca^{2+}, K^{+}, Mg^{2+}), is shifted to the gas phase due to an excess of cations with respect to SO_4^{2-}, NO_3^{-} and Cl^{-}. A possible reason for the underprediction (-32.5%) of aerosol ammonium by the explicit treatment of crustals compared to the observations is a presence of organic acids which keeps ammonium in the aerosol phase. This has been found to be the case in previous studies (Trebs et al. 2005; Metzger et al. 2006) indicating a need for including organic acids in current thermodynamic equilibrium

models in addition to crustal species. All three runs predict the same amount of sulfate, which is expected since sulfate, being non-volatile, resides completely in the aerosol phase, and thus the amount of it depends on processes other than thermodynamic partitioning (e.g. chemistry).

The total CPU time needed by CMAQ as well as the time required by the equilibrium model is given in Table 6.2. Less than 10% of the total CPU time is devoted to either ISORROPIA or ISORROPIA-II.

ISORROPIA-II slightly increases the computational cost for CMAQ (by ~9%). This is expected since 10 new equilibrium reactions have been added for the new salts in ISORROPIA-II which require additional equilibrium calculations. It should be noted that this is the maximum expected difference in CPU time considering that the metastable state solution of ISORROPIA (and ISORROPI-II) is used in CMAQ. The metastable solution, which always assumes a liquid solution, requires calculation of activity coefficients at any RH which increases computational burden. If stable solution is used instead, the computational costs required by the two versions are expected to be very close to each other especially when RH is low (during midday) and the aerosol dries up. Considering a large number of species incorporated, ISORROPIA-II is a fast and computational efficient module suitable for use in large scale air quality models.

Table 6.1: Mean observed and predicted concentration of species (in μg m^{-3}) over Atlanta, GA for the period 15-20 June 2005. Values in parentheses show the % errors

		Mean predicted (CMAQ)		
$PM_{2.5}$ species	Mean observed	Insoluble	Explicit	Na^{eq}
NH_4	1.72	1.43 (-16.8)	1.16 (-32.5)	1.27 (-26.1)
NO_3	0.43	0.17 (-60.4)	0.20 (-53.4)	0.23 (-46.5)
SO_4	5.33	4.97 (-6.7)	4.97 (-6.7)	4.97 (-6.7)
H_2O	-	3.60	3.08	3.82

Table 6.2: CPU times required for the simulation period 15-20 June 2005

Equilibrium model (EQM)	CPU_{CMAQ} (s)	CPU_{EQM} (s)	t_{EQM}/t_{CMAQ} (%)
ISORROPIA	1306	63	4.8
ISORROPIA-II	1432	109	7.6

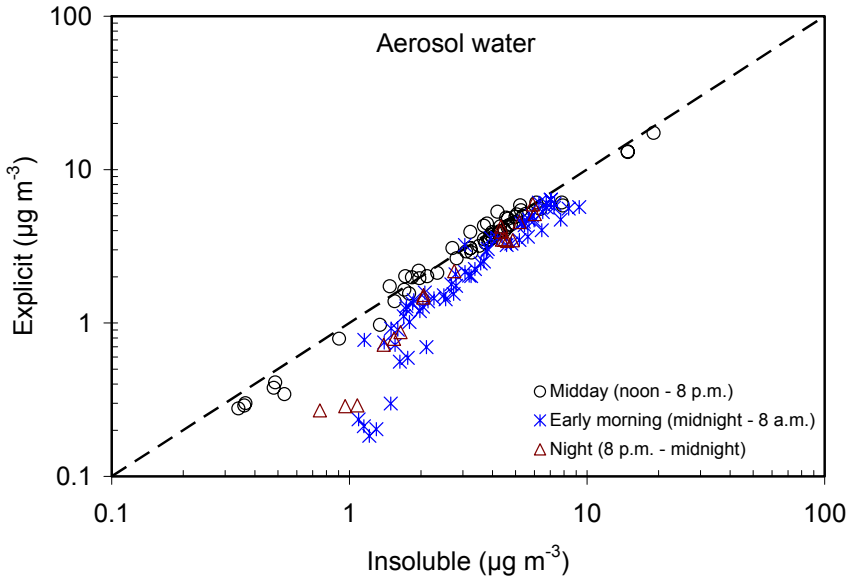

Figure 6.2: Aerosol water predicted by CMAQ when crustals are treated in ISORROPIA as insoluble (x-axis) and explicitly (y-axis) for the period 15-20 June 2005.

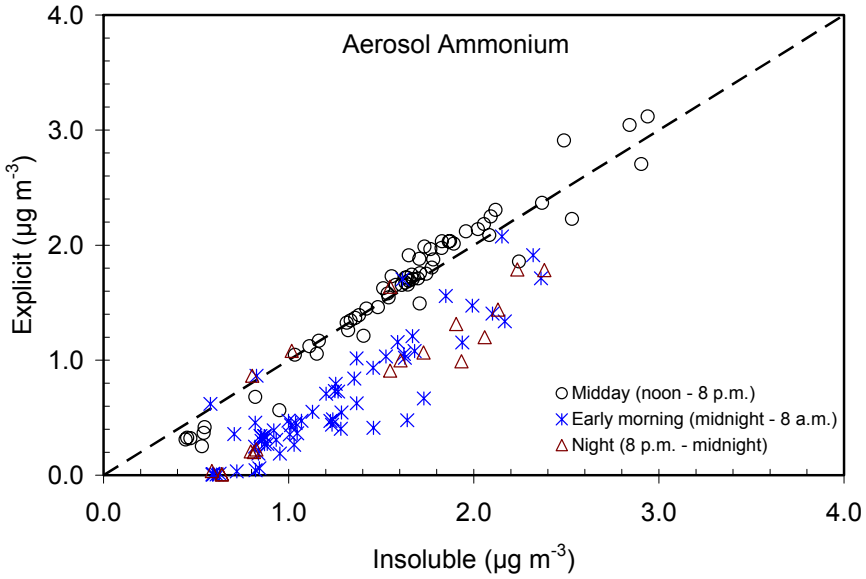

Figure 6.3: Aerosol ammonium predicted by CMAQ when crustals are treated in ISORROPIA as insoluble (x-axis) and explicitly (y-axis) for the period 15-20 June 2005.

6.6 Conclusions

In this paper the impact of including crustal species in equilibrium calculations within the Community Multiscale Air Quality (CMAQ) model is studied. A state-of-the-art aerosol equilibrium model, ISORROPIA-II, which explicitly treats the thermodynamics of K^+-Ca^{2+}-Mg^{2+}-NH_4^+-Na^+-SO_4^{2-}-HSO_4^--NO_3^--Cl^--H_2O aerosols, is incorporated into CMAQ and the effect of crustal species, when treated a) as insoluble (i.e. neglecting the presence of crustals), b) as mole - equivalent sodium (i.e. $Ca^{2+} = 2Na^+$, $Mg^{2+} = 2Na^+$, $K^+ = Na^+$), and, c) explicitly, was investigated. On average, the explicit treatment of crustals resulted in a -27.5% change in predicted aerosol ammonium and -19.8% in aerosol water content mainly due to formation of species exhibiting limited solubility in water (i.e. CaSO4). Considering that crustals (Ca^{2+}, K^+, M^{2+}) contributed, on average, only a few percent of the total $PM_{2.5}$ mass, these changes in aerosol water and ammonium concentrations highlight the importance of comprehensive thermodynamic calculations in the presence of crustal species. The results were also compared against measurements made at the Jefferson Street Southeastern Aerosol Research and Characterization study (SEARCH) monitoring site an urban location in Atlanta, GA during the period of 12-20 June, 2005. Both the explicit and the Na^{eq} treatment of crustals in CMAQ decrease the error for aerosol nitrate but increase it for ammonium suggesting that additional species (e.g. organic acids) may be required to be incorporated into equilibrium calculations in addition to crustal species. The CPU time required by CMAQ when ISORROPIA-II is included is comparable to that when ISORROPIA is used. Considering the large number of species incorporated, this makes ISORROPIA-II a fast and computational efficient module suitable for use in large scale air quality models.

6.7 Acknowledgements

This work was supported by the National Oceanic and Atmospheric Administration under contract NMRAC000-5-04017.

6.8 References

Amundson, N.R., Caboussat, A., He, J.W., Martynenko, A.V., Savarin, V.B., Seinfeld, J.H., and Yoo, K.Y.: A new inorganic atmospheric aerosol phase equilibrium model (UHAERO), Atmos. Chem. Phys., 6, 975-992, 2006.

Ansari, A.S., and Pandis, S.N.: Prediction of multicomponent inorganic atmospheric aerosol behavior, Atmos. Environ., 33, 745-757, 1999a.

Ansari, A.S., and Pandis, S.N.: An analysis of four models predicting the partitioning of semivolatile inorganic aerosol components, Aerosol Sci. Technol., 31, 129-153, 1999b.

Byun, D.W., and Ching J.K.S.: Science algorithms of the EPA Models-3 community multiscale air quality (CMAQ) modeling system, Rep. USA EPA/600/R-99/030, Environ. Protect. Ag., Washington, D.C., 1999.

Fountoukis, C., and Nenes, A.: ISORROPIA II: A computationally efficient thermodynamic equilibrium model for K^+-Ca^{2+}-Mg^{2+}-NH_4^+-Na^+-SO_4^{2-}-NO_3^--Cl^--H_2O aerosols, Atmos. Chem. Phys. Discuss., 7, 1893-1939, 2007.

Fountoukis, C., Sullivan, A., Weber, R., VanReken, T., Fischer, M., Matías, E., Moya, M., Farmer, D., Cohen, R., and Nenes, A.: Thermodynamic characterization of Mexico City Aerosol during MILAGRO 2006, Atmos. Chem. Phys., in review, 2007.

Grell, G.A., Dudhia, J., and Stauffer, D.R.: A description of the fifth generation Penn State/NCAR mesoscale model (MM5), Rep. NCAR/TN- 389+STR, 138 pp., Natl. Cent. for Atmos. Res., Boulder, Colo., 1994.

Hansen, D.A., Edgerton, E.S., Hartsell, B.E., Jansen, J.J., Kandasamy, N., Hidy, G.M., and Blanchard, C.L.: The southeastern aerosol research and characterization study: part 1-Overview, J. Air Waste Management Assoc., 53, 1460-1471, 2003.

Jacobson, M.Z.: Studying the effect of calcium and magnesium on size-distributed nitrate and ammonium with EQUISOLV II, Atmos. Environ., 33, 3635–3649, 1999b.

Meng, Z.Y., Seinfeld, J.H., Saxena, P., and Kim, Y.P.: Atmospheric gas - aerosol equilibrium IV. Thermodynamics of carbonates, Aerosol Sci. Technol., 23, 131-154, 1995.

Metzger, S., Mihalopoulos, N., and Lelieveld, J.: Importance of mineral cations and organics in gas-aerosol partitioning of reactive nitrogen compounds: case study based on MINOS results, Atmos. Chem. Phys., 6, 2549–2567, 2006.

Moya, M., Pandis, S.N., and Jacobson, M.Z.: Is the size distribution of urban aerosols determined by thermodynamic equilibrium? An application to Southern California, Atmos. Environ., 36, 2349-2365, 2002.

Moya, M., Ansari, A.S., and Pandis, S.N.: Partitioning of nitrate and ammonium between the gas and particulate phases during the 1997 IMADA-AVER study in Mexico City, Atmos. Environ., 35, 1791-1804, 2001.

Nenes, A., Pandis, S.N., and Pilinis, C.: ISORROPIA: A new thermodynamic equilibrium model for multiphase multicomponent inorganic aerosols, Aquatic Geochemistry, 4, 123–152, 1998.

Nenes, A., Pilinis, C., and Pandis, S.N.: Continued development and testing of a new thermodynamic aerosol module for urban and regional air quality models, Atmos. Environ., 33, 1553-1560, 1999.

San Martini F.M., West J.J., de Foy B., Molina L.T., Molina M.J., Sosa G., McRae G.J.: Modeling inorganic aerosols and their response to changes in precursor concentration in Mexico City, Journal of the air & waste management association, 55 (6), 803-815, 2005.

Smith, J.N., Moore, K.F., Eisele, F.L., Voisin, D., Ghimire, A.K., Sakurai, H., and

McMurry, P.H.: Chemical composition of atmospheric nanoparticles during nucleation events in Atlanta, J. Geophys. Res., 110, D22S03, doi:10.1029/2005JD005912, 2005.

Stolzenburg, M.R., McMurry, P.H., Sakurai, H., Smith, J.N., Mauldin III, R.L., Eisele, F.L., and Clement, C.F.: Growth rates of freshly nucleated atmospheric particles in Atlanta, J. Geophys. Res., 110, D22S05, doi:10.1029/2005JD005935, 2005.

Trebs, I., Metzger, S., Meixner, F.X., Helas, G., Hoffer, A., Andreae, M.O., Moura, M.A.L., da Silva (Jr.), R.S., Slanina, J., Rudich, Y., Falkovich, A., Artaxo, P.: The NH_4^+-NO_3^--Cl^--SO_4^{2-}-H_2O system and its gas phase precursors at a rural site in the Amazon Basin: How relevant are crustal species and soluble organic compounds?, J Geophys. Res., 110 (D07303), doi:10.1029/2004JD005478, 2005.

Wexler, A.S., and S.L. Clegg, Atmospheric aerosol models for systems including the ions H^+, NH_4^+, Na^+, SO_4^{2-}, NO_3^-, Cl^-, Br^-, and H_2O, J. Geophys. Res., 107, 4207, doi:10.1029/2001JD000451, 2002.

CHAPTER 7

SUMMARY AND CONCLUSIONS

The motivation of this work is to improve understanding of aerosol – water interactions both in subsaturated and supersaturated atmospheric conditions. In Chapter 2 we study aerosol-cloud-climate interactions through a state of the art cloud droplet formation parameterization. We appropriately modified the parameterization to *i)* allow for a lognormal representation of aerosol size distribution, and, *ii)* include a size-dependant mass transfer coefficient for the growth of water droplets which explicitly includes the accommodation coefficient. To address this, an average value of the water vapor diffusivity is introduced in the parameterization. Two methods were explored for determining the upper and lower bound of the droplet diameter needed for calculating the average water vapor diffusivity. The most accurate employs an empirical correlation derived from numerical parcel simulation. Predictions of the modified NS parameterization are compared against detailed cloud parcel model simulations for a wide variety of aerosol activation conditions. The modified NS parameterization closely tracks the parcel model simulations, even for low values of the accommodation coefficient, without any increase in computational cost. This work offers a much needed rigorous and computationally inexpensive framework for directly linking complex chemical effects on aerosol activation in global climate models.

In Chapter 3 the new aerosol activation parameterization was tested against observations

from highly polluted clouds. We analyzed 27 cumuliform and stratiform clouds sampled aboard the CIRPAS Twin Otter during the 2004 ICARTT (International Consortium for Atmospheric Research on Transport and Transformation). A unique feature of the dataset is the sampling of highly polluted clouds within the vicinity of power plant plumes. *In-situ* observations of aerosol size distribution, chemical composition and updraft velocity were input to *i*) a detailed adiabatic cloud parcel model (Nenes *et al.*, 2001; Nenes *et al.*, 2002), and, *ii*) the modified NS parameterization (Fountoukis and Nenes, 2005; Nenes and Seinfeld, 2003); predicted droplet number is then compared with the observations. Remarkable closure was achieved (on average to within 10%) for parcel model and parameterization. The error in predicted cloud droplet concentration was found to correlate mostly with updraft velocity. Aerosol number also correlated with droplet error for clouds affected by power plant plumes (which is thought to stem from spatial variability of the aerosol not considered in the closure). Finally, we assess the sensitivity of droplet closure to "chemical effects". Cloud droplet number closure is excellent even for the highly polluted clouds downwind of power plant plumes. Droplet number error does not correlate with background pollution level, only with updraft velocity and aerosol mixing state. A highly variable aerosol does not necessarily imply a highly variable N_d concentration. The clouds in this study often do not respond to aerosol variations because they take place primarily at small particle sizes, and cloud s_{max} is not high enough to activate them. Any droplet variability that does arise is inherently less than the CCN variability it originated from (Sotiropoulou *et al.*, 2006). Usage of average updraft velocity is appropriate for calculating cloud droplet number. The water vapor uptake coefficient ranges between 0.03 and 1.0. Optimum closure (for which average N_d error is

minimal and its standard deviation is within droplet measurement uncertainty) is obtained when the water vapor uptake coefficient is about 0.06. This agrees with values obtained from previous closure studies for polluted stratocumulus (Meskhidze *et al.*, 2005) and marine cumulus clouds (Conant *et al.*, 2004). On average, organic species do not seem to influence activation through contribution of solute and surface tension depression. Optimal cloud droplet closure is obtained if the CCN are approximated by a combination of soluble inorganics and partially-soluble organics (less than 1 g kg^{-1} water assuming a molar volume of 66 cm^3 mol^{-1} and a Van't Hoff factor of 1). The cloud droplet activation parameterization used in this study (Nenes and Seinfeld, 2003; Fountoukis and Nenes 2005) has performed as well as the detailed cloud parcel model. Excellent performance has also been reported by Meskhidze *et al.*, (2005). Together, both studies suggest that the parameterization can robustly be used in GCM assessments of the aerosol indirect effect. Distinguishing the "chemical effects" on the cloud droplet spectrum requires the observational uncertainty to be of order 10%. All the above conclusions can serve as much needed constraints for the parameterization of aerosol-cloud interactions in the North America. Future *in-situ* studies will determine the robustness of our findings.

Aerosol – water interactions in ambient relative humidities less than 100% were studied using a thermodynamic equilibrium model for inorganic aerosol and a three dimensional air quality model. In Chapter 4, a new model, ISORROPIA-II, is developed which treats the thermodynamics of K^+-Ca^{2+}-Mg^{2+}-NH_4^+-Na^+-SO_4^{2-}-NO_3^--Cl^--H_2O aerosol systems. A comprehensive evaluation was conducted against the thermodynamic model SCAPE2 in terms of composition predicted and computational speed for a wide variety of aerosol conditions that cover typical urban, remote continental, marine and non-urban continental

environments. The overall predictions of aerosol water, total PM and concentration of semi-volatile species were generally comparable between the two models under most conditions. For aerosol water content and total PM mass the two models agreed within approximately 13%. The normalized mean error for total aerosol nitrate predictions was 16% while for aerosol chloride and ammonium concentration the agreement was within 2 – 6%. Small discrepancies were found to exist between the two models under certain conditions, primarily for relative humidities between 40 and 70%. These discrepancies are mainly attributed to the solution dynamics treatment of water uptake in mutual deliquescence regions and the association of non-volatile cations with sulfate, nitrate and chloride. For all cases examined, ISORROPIA II is more than an order of magnitude faster than SCAPE2, showing robust and rapid convergence for all conditions examined, making it one of the most computationally efficient and comprehensive inorganic thermodynamic equilibrium modules available.

In Chapter 5 the new equilibrium model was used to thermodynamically characterize aerosols measured at a highly polluted area. This study focuses on thermodynamical modeling of aerosols sampled during the MILAGRO 2006 campaign in Mexico City, using high-time (5-min) resolution measurements and a state-of-the-art aerosol equilibrium model, ISORROPIA-II (Fountoukis and Nenes, 2007). In agreement with observations, ISORROPIA-II predicts a large portion (82.4 ± 10.1 %) of total ammonia partitioning to the gas phase, while most of total nitrate (79.8 ± 25.5%) and chloride (85.3 ± 29.1%) resides in the aerosol phase. The mean observed value for $NH_{3(g)}$ was 17.73 μg m^{-3} and 5.37 μg m^{-3} for $NO_{3(p)}$. An excellent agreement between predicted and observed concentration of $NH_{3(g)}$ was found with a NME of 5.3%. Very good agreement was also

found for $NO_{3(p)}$ (NME=27.2%), $NH_{4(p)}$ (NME=37.1%) and $Cl_{(p)}$ (NME=15.5%) concentrations for most of the data. Larger discrepancies were seen in predicted $HNO_{3(g)}$ since uncertainties in the volatile nitrate measurement ($HNO_{3(g)}$ + NH_4NO_3) are magnified by the high sensitivity of $HNO_{3(g)}$ because nitrate partitioned primarily to the aerosol phase. Application of ISORROPIA-II is largely successful suggesting that the assumption of thermodynamic equilibrium is appropriate for complex Mexico City aerosols. The timescale of equilibrium ranges between 5 and 20 minutes. At low RH (<50%), the stable state (i.e. deliquescence branch) solution of ISORROPIA-II predicted significantly higher concentrations of aerosol nitrate compared to the metastable (i.e. efflorescence) solution. The NME and NMB between predictions and observations for aerosol nitrate were found to be significantly larger when using the metastable solution indicating that the deliquescence branch appropriately describes aerosols in Mexico City at RH below 50%. This can serve as an important constraint for three dimensional air quality models that simulate ambient particle concentrations under conditions characteristic of Mexico City. The volatile fraction of $PM_{2.5}$ was found to be mostly sensitive to changes in TN. This suggests that in an ammonia-rich environment, (such as Mexico City) a combined reduction in TS and TN appears to be a more promising strategy for $PM_{2.5}$ control, rather than reducing ammonia emissions. Treating crustal species as "equivalent sodium" or insoluble (rather than explicitly) in the thermodynamic equilibrium calculations has an important impact on predicted aerosol water uptake, nitrate and ammonium, despite the ammonia-rich environment of Mexico City. This suggests that comprehensive thermodynamic calculations are required to predict the partitioning and phase state of aerosols in the presence of dust. Concentrations of gas

phase chloride in were most likely low in Mexico City (mean predicted value for $HCl_{(g)}$=0.03 μg m^{-3}), a consequence of having large excess of $NH_{3(g)}$ which tends to drive Cl^- into the aerosol.

The impact of including crustal species (Ca^{2+}, K^+, M^{2+}) in equilibrium calculations within a three dimensional air quality model was studied in Chapter 6. A state-of-the-art aerosol equilibrium model, ISORROPIA-II, which explicitly treats the thermodynamics of K^+-Ca^{2+}-Mg^{2+}-NH_4^+-Na^+-SO_4^{2-}-HSO_4^--NO_3^--Cl^--H_2O aerosols, is incorporated into CMAQ and the effect of crustal species, when treated a) as insoluble (i.e. neglecting the presence of crustals), b) as mole - equivalent sodium (i.e. Ca^{2+} = $2Na^+$, Mg^{2+} = $2Na^+$, K^+ = Na^+), and, c) explicitly, was investigated. On average, the explicit treatment of crustals resulted in a -27.5% change in predicted aerosol ammonium and -19.8% in aerosol water content mainly due to formation of species exhibiting limited solubility in water (i.e. CaSO4). Considering that crustals (Ca^{2+}, K^+, M^{2+}) contributed, on average, only a few percent of the total $PM_{2.5}$ mass, these changes in aerosol water and ammonium concentrations highlight the importance of comprehensive thermodynamic calculations in the presence of crustal species. The results were also compared against measurements made at the Jefferson Street Southeastern Aerosol Research and Characterization study (SEARCH) monitoring site an urban location in Atlanta, GA during the period of 12-20 June, 2005. Both the explicit and the Na^{eq} treatment of crustals in CMAQ decrease the error for aerosol nitrate but increase it for ammonium suggesting that additional species (e.g. organic acids) may be required to be incorporated into equilibrium calculations in addition to crustal species. The CPU time required by CMAQ when ISORROPIA-II is included is comparable to that when ISORROPIA is used.